SpaceOAR© hydrogel optimization and management for rectal sparing in prostate cancer patients

by

D. Owen Paetkau
B.Sc., Thompson Rivers University, 2017

A Thesis Submitted in Partial Fulfillment of the
Requirements for the Degree of

MASTER OF SCIENCE

in the Department of Physics and Astronomy

SpaceOAR© hydrogel optimization and management for rectal sparing in prostate cancer patients

by

D. Owen Paetkau
B.Sc., Thompson Rivers University, 2017

Supervisory Committee

Dr. Isabelle M. Gagne, Co-Supervisor
(Department of Physics and Astronomy)

Dr. Magdalena Bazalova-Carter, Co-Supervisor
(Department of Physics and Astronomy)

Supervisory Committee

Dr. Isabelle M. Gagne, Co-Supervisor
(Department of Physics and Astronomy)

Dr. Magdalena Bazalova-Carter, Co-Supervisor
(Department of Physics and Astronomy)

Abstract

External beam radiation therapy for prostate cancer can result in urinary, sexual, and rectal side effects, often impairing quality of life. A polyethylene glycol-based product, SpaceOAR © hydrogel (SOH), implanted into the connective tissue between prostate gland and rectum can significantly reduce the dose received by the rectum and hence risk of rectal toxicity. The optimal way to manage the hydrogel and rectal structures for plan optimization is therefore of interest.

A retrospective planning study was completed with 13 patients to examine optimal planning and treatment methods. Computerized tomography (CT) scans were taken pre- and post-SOH implant. Six hypofractionated (60 Gy in 20 fractions) treatment plans were produced per patient using either a structure of rectum plus the hydrogel, termed composite rectum wall (CRW), or rectal wall (RW) as the inverse optimization structure and intensity modulated radiotherapy (IMRT) or volumetric modulated arc therapy (VMAT) as the treatment technique. Dose-volume histogram metrics were compared between plans to determine which optimization structure and treatment technique offered the maximum rectal dose sparing. RW structures offered a statistically significant decrease in rectal dose over CRW structures, whereas the treatment technique (IMRT vs VMAT) did not significantly affect the rectal dose. However, there was improvement seen in bladder and penile bulb dose when VMAT was used as a treatment technique over IMRT. Overall, treatment plans using the RW optimization structure offered the lowest rectal dose while VMAT treatment technique offered the lowest bladder and penile bulb dose. These treatment techniques and

optimization structures have now been implemented at BC Cancer - Victoria based on this retrospective study.

SOH implant has been shown not to be equally effective in all patients. Determining *a priori* patients in which the implant will offer most benefit allows for effective management of SOH resources. Several factors have been shown to be correlated to reduction in rectal dose including distance between rectum and planning treatment volume (PTV), volume of rectum in the PTV and change in rectum volume pre- to post-SOH. Several of these factors along with other pre-SOH CT metrics were found via multiple linear regression models to predict reduction of rectal dose using data from 21 patients who received SOH implant. Two high rectal dose metrics were modeled, change in the relative volume receiving 55 Gy (ΔRV55Gy) and change in the partial high dose integral (ΔHDI), integrating over the dose-volume histogram (DVH) from 55 Gy to 60 Gy. Models were also produced to predict pre-SOH RV55Gy (Pre-RV55). These models offered R^2 between 0.57 and 0.87 with statistical significance in each model. Applying a 3.5% lower limit on pre-SOH RV55Gy removed one third of patients as implant candidates. This may offer a clinically useful tool in deciding which patients should receive SOH implant given limited resources. Predictive models, nomograms and a workflow diagram were produced for clinical management of SOH implant.

Contents

List of Tables

List of Figures

Acknowledgements

I would like to thank my supervisory committee for all the time spent discussing rectal dose. I would especially like to thank Isabelle Gagne for all her support through weekly meetings and Abraham Alexander for his feedback. Thank you to the radiation oncology team working to implement SpaceOAR © Hydrogel at BC Cancer - Victoria. It was a pleasure to be a part of such a professional, enthusiastic team. Thanks to everyone else at BC Cancer - Victoria and to the medical physics group at University of Victoria. This community has been welcoming and fulfilling to be a part of. I look forward to continuing to develop professionally with all of you.

I am thankful for my dad, Mark, for inspiring me to continue to explore and appreciate physics. To my mom, Nicola, for teaching me how to work hard and how to have fun. To my girlfriend, Leigh McNamara, for listening to the roadblocks and continuous rants throughout my research. Thank you, I appreciate you.

I would also like to acknowledge the University of Victoria Vikes Men's ultimate team. This community helped keep me motivated after long weeks with the countless practices and tournaments. I was proud to be a member of this team and for the opportunity to represent University of Victoria at USAU Nationals in Milwaukee, WI and Round Rock, TX.

Additional thanks go to Island Prostate Center for providing funding to BC Cancer - Victoria for SpaceOAR ©Hydrogel units. This work has been partially supported by an Alexander Graham Bell Canada Graduate Scholarship from the Natural Sciences and Engineering Research Council of Canada (NSERC).

Chapter 1

Introduction

A recent estimate by the Canadian Cancer Society predicts that about 1 in 2 Canadians will be diagnosed with cancer in their lifetime and 1 of 4 will die of the disease. Prostate cancer is the leading diagnosis site excluding skin in Canadian men with over 20 000 new cases in 2017.[1] Prostate cancer is treated with three major techniques: surgery, chemotherapy and radiotherapy. Radiation therapy (RT) may be used in conjunction with surgery or chemotherapy or as a standalone treatment to provide targeted radiation damage. Due to its effectiveness in tumour control, approximately half of all cancer patients receive a course of RT.[2] Advances in RT, such as intensity modulated radiotherapy (IMRT) or volumetric modulated arc therapy (VMAT), produce more conformal radiation distributions to improve tumour control while reducing radiation to the surrounding organs at risk (OAR).[3,4] A pre-RT supportive implant, called SpaceOAR © Hydrogel (SOH), is being clinically implemented at BC Cancer - Victoria to reduce rectal normal tissue complications in prostate cancer RT. The aim of this work is to optimize the implementation of SOH as a clinical treatment option at BC Cancer - Victoria by comparing modulated treatment techniques and structures in treatment planning optimization. In addition, predictive models were developed to determine *a priori* the effectiveness of SOH in reducing rectal dose in any given patient. This chapter will offer an overview of radiotherapy, the SOH technology and describe the scope of the presented thesis.

1.1 Radiation Therapy

Radiation therapy, or radiotherapy, is the targeted use of mostly highly energetic photons to destroy cancerous lesions. Radiotherapy may be used as a stand alone treatment or in conjunction with chemotherapy or surgery. Chemotherapy is a less local approach offering cell kill through identifying characteristics associated with cancerous cells. Chemotherapy is commonly used in conjunction with radiotherapy to provide targeting agents or radiosensitizers to the tumour volume increasing the effect or radiation damage within the cell. Surgery is a targeted approach to cancer treatment removing the gross volume of a solid tumour. Post-operative radiotherapy treatment is often used to remove local and regional residual disease.

Radiation damage through high energy photons increases the incidence of cell death within the region irradiated. Radiotherapy photons within the MeV range interact in the patient through a series of photon interactions with molecules and electrons. These electrons are emitted with some transferred energy causing further interactions with molecules creating a cascading chain reaction. This cascade effect continues until the photon and electron energies have been depleted or the particle has been scattered away. As electron energy begins to decrease, the speed of the electrons decreases in turn increasing the probability of particle interactions at a localized region near the end of the electron track. This produces a cluster of ionizations which can break bonds between molecules. This effect causes double strand breaks within DNA in the cellular nucleus causing irreparable damage, often resulting in cell death. Radiation damage can be described using absorbed dose in units of gray (Gy) defined as absorbed energy per unit mass. Radiotherapy targets tumour volumes, however the same radiation damage may occur in healthy irradiated tissue causing normal tissue complications.

Research on the relationship between dose of radiation and cell survival revealed that fractionated dose often offers a more effective method to deliver tumour cell kill compared to single dose.[5] Fractionation is the delivery of small doses of radiation over several days to produce a larger total dose to the cancerous cells. The interaction between irradiation of healthy and tumour cells is a complicated process which is modeled through the tumour control probability (TCP) and normal tissue complication probability (NTCP) models.[6] However, fractionation provides healthy cells recovery time prior to the following fraction and therefore reduces OAR normal tissue complications. Standard fractionation is 2 Gy per fraction with secondary fractionation

schemes such as hyperfractionation (less than 2 Gy per fraction) or hypofractionation (greater than 2 Gy per fraction) employed to offer clinical benefit for tumour control, normal tissue complications and patient convenience. Prostate cancer hypofractionation treatments have shown to be non-inferior to standard fractionation in terms of tumour control and genitourinary and gastrointestinal toxicities.[7–9] BC Cancer - Victoria has adopted hypofractionated clinical prescriptions of 73.65 Gy in 28 fractions and 60 Gy in 20 fractions for treatment of prostate cancer.

Figure 1.1: Varian TrueBeam STx linear accelerator at BC Cancer - Victoria with gantry and patient couch used for external beam radiotherapy treatment.

Major improvements in EBRT dose shaping occurred with the development of collimation. The first of these improvements was three-dimensional conformal radiotherapy (3D-CRT) which used multi-leaf collimators to produce geometric shaping to fit the desired target volume offering a large improvement over previous cut-out collimation. The same multi-leaf collimators were then moved in a step and shoot or a moving window fashion to modulate the fluence of the beam creating a technique called intensity modulated radiotherapy (IMRT). 3DCRT and IMRT techniques are delivered using a static gantry set-up at several gantry positions.[10] Additional improvements allowed for a continuous arc of radiation to be delivered to the patient termed volumetric modulated arc therapy (VMAT) with fluence being modulated through photon dose rate and gantry speed variations.[11] In modern cancer centers, both IMRT and VMAT techniques are often used to treat patients.[12] The linac shown in Figure 1.1 is a Varian TrueBeam Stereotactic Treatment (STx) residing at BC Cancer - Victoria with the ability to deliver IMRT and VMAT to patients with localized prostate cancer. These radiation delivery techniques are often combined with imag-

ing to create image guided radiotherapy (IGRT) allowing for more accurate patient positioning.[13]

1.2 Delivery of Radiation Therapy

Patient treatment with radiation began the year after the discovery of X-rays in 1895.[5] By the 20th century, studies reported an increased use of radiation in medicine to treat cancer. Initially, skin cancers were most often treated due to the low penetration depth of the x-rays produced. Depth of the treated lesions increased as produced photon energy increased.[13,14] The field continued to grow with the addition of superficial, orthovoltage, Cobalt teletherapy and MeV linacs.

Modern radiotherapy treatment is delivered using external beam therapy (EBRT) machines or through radionuclide implants. Superficial and orthovoltage therapy use low energy x-rays produced from X-ray tubes to treat skin lesions at shallow depths. Gross tumour volumes deep within tissue are treated with high energy photons produced by linacs. Alternatively, radionuclides are permanently or temporarily implanted allowing for radioactive decay products to destroy cancerous lesions. These modern radiotherapy techniques are capable of curing many cancer sites, but may also be used in conjunction with surgery or chemotherapy to further improve the therapeutic ratio. Additionally, palliative radiotherapy is often used to improve patient quality of life (QOL) during end-of-life care.

Figure 1.2: CT scan of patient pelvic anatomy with no contours (left), and contours (right) from a prostate cancer 60 Gy in 20 fraction treatment planning protocol.

Teletherapy courses begin by imaging the patient anatomy for treatment planning

and simulation of radiation dose which require electron density information available from a computed tomography (CT) scan. The patient is immobilized to allow for consistent anatomy position through radiotherapy treatment. In the context of prostate cancer, patients are also given a specific bladder and bowel protocol that they must adhere to prior to planning CT and all subsequent treatments to ensure consistency in rectal and bladder volumes. The CT scan is imported into a treatment planning software where OAR and target structures can be delineated (see Figure 1.2) and dose calculations can be performed. The final step before beginning the course of treatment is development of a treatment plan. Fixed beams (IMRT) or arcs (VMAT) are positioned around the patient based on a planning target volume (PTV). Inverse treatment planning is completed by varying optimization objectives set on structures until site specific plan evaluation goals are achieved. A successful treatment plan provides both specific dose coverage of the clinical target volume (CTV) and PTV while meeting OAR dose-volume objectives.

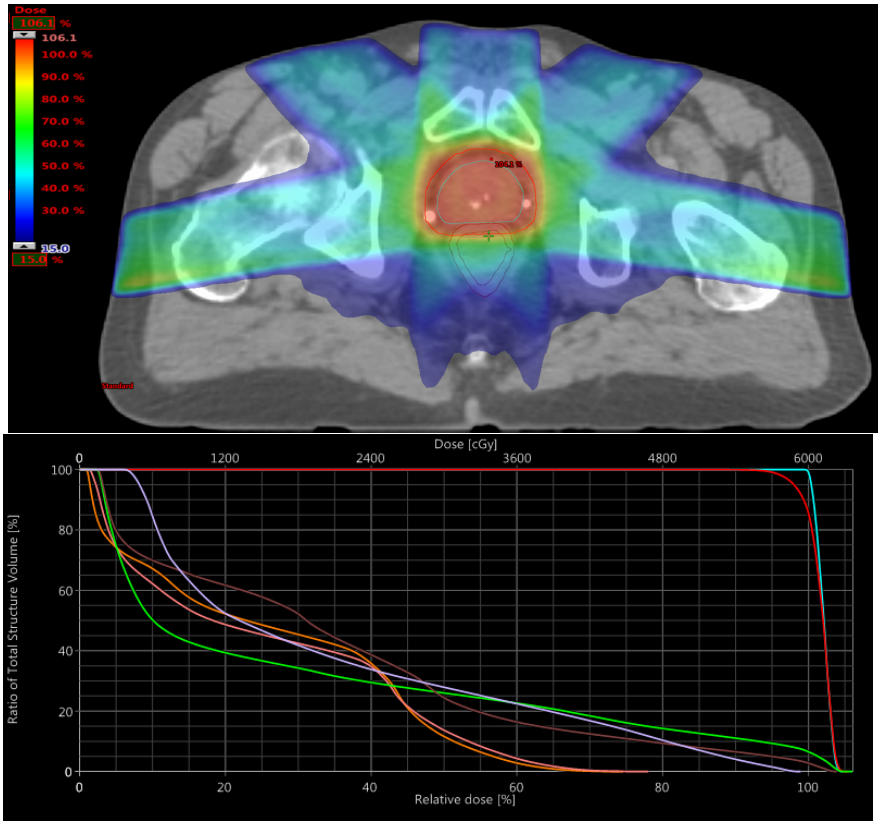

Figure 1.3: Prostate cancer IMRT treatment plan depicting simulated dose distribution (top) and DVH (bottom) for prostate cancer treatment plan. The DVH colours correspond to the coloured contours seen in Figure 2.

OAR dose-volume objectives are based on clinical trials relating dose to normal tissue complications with many results being collected and reported as QUANTEC data.[15] These objectives are maximum dose-volume relationships, for example, the volume of an OAR receiving 37 Gy may not exceed 50% of the OAR volume. Dose-volume objectives can be compiled to produce a clinical protocol consisting of plan evaluation objectives for each OAR and targets for a given treatment site. Figure 1.3 depicts a DVH and dose distribution for prostate cancer treatment in which the prostate has been completely covered while dose decreases moving away from the PTV allowing for reduced dose to OAR such as the rectum and bladder. A treatment plan may not achieve all OAR plan evaluation objectives and PTV coverage and radiation oncologists need to make compromises between target coverage and OAR dose-volume objectives.

Treatment planning provides simulated dose distributions and as such dose delivered may vary from planning dose distribution. Quality assurance (QA) is performed on both the algorithms used for simulation and linacs delivering radiotherapy to minimize discrepancies. Additionally, improvements are made to dose calculation algorithms to improve the accuracy of treatment planning software. The planning dose distributions can be described using dose volume histogram (DVH) analysis for each OAR, creating metrics which relate dose to OAR side effects.

1.3 SpaceOAR Hydrogel

For intermediate risk prostate cancer patients, the CTV consists of the prostate and 1 cm of the seminal vesicles (SV).[16] The planning target volume (PTV) is a geometric volume designed to address planning and setup uncertainties and is created by adding margins to the CTV. OAR include the rectum, bladder, penile bulb, and femoral heads. Irradiation of these OARs lead to a large variety of side effects associated with bowel, urinary[17] and sexual functions.[18] These side effects can be attributed to DVH characteristics. Studies have shown that the rectum is the dose-limiting organ in prostate radiotherapy.[7,19] High dose to a portion of the rectal volume results in high probability of rectal complications, including the volume of the rectum receiving 70 Gy (RV70Gy) >25% which has been correlated with Grade 2 or higher rectal complications.[20,21] Due to the proximity of prostate and rectum, a portion of the rectum often lies within the PTV resulting in a high dose to that small region of the rectum as seen in the contoured CT scan in Figure 1.2. Reducing the amount

of rectum in the PTV by creating space between the prostate and the rectum may result in a lower incidence of rectal complications.

Various techniques have been used to produce prostate-rectum space including polyethylene-glycol (PEG) hydrogels, hyaluronic acid spacers, collagen spacing and biodegradeable endorectal balloons.[22–25] These spacers produced varied results of reduced rectal dose with the endorectal balloon[24] and PEG spacers[25] offering the best rectal sparing. However, PEG spacers have more consistently been shown to create peri-rectal space, improve stability of rectal position[25] and require a single procedure prior to RT making them a more convenient option for patient treatment.[26]

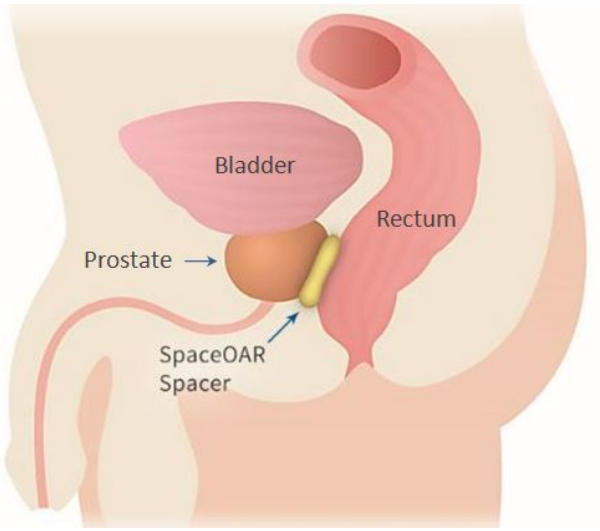

Figure 1.4: Artist rendition of pelvic anatomy with SpaceOAR hydrogel insert between the prostate and rectum. Taken from Augmenix Inc.[27]

Augmenix Inc. has produced a commercially available PEG spacer termed SpaceOAR © hydrogel (SOH). SOH is implanted transperineally (Figure 1.4), often during the implant of gold fiducial markers, and maintains its structure for 3 months during the course of radiotherapy before being absorbed by the body after 6 months.[28,29] Prior to clinical trials, the effectiveness of SOH to reduce rectal dose in prostate cancer EBRT treatment was studied on cadavers.[25]

Recent clinical studies have indicated SOH improves bowel, urinary and sexual QOL in prostate cancer patients[30,31] with the improved bowel QOL being correlated with a reduction of rectal dose.[30,32–36] Several studies, including Mariados et al. and Song et al., showed a reduction of RV70Gy by more than 25% post-SOH implant.[32,33,37] Many other studies indicate a decrease of rectal dose between pre- and

post-SOH treatment plans.[34,38–40] Figure 1.5 summarizes the rectal dose reduction from pre- to post-SOH treatment plans observed in five studies. In many cases, the volume of the rectum receiving 100% of the prescription dose was reduced to 0% as the rectum was moved away from the prostate. SOH has been shown to effectively reduce rectal dose and the associated rectal complications involved with prostate cancer EBRT. Rectal dose-volume reduction in SOH published studies was around 10% for doses below 85% relative prescription dose and around 5% for doses above 85% (Figure 1.5).

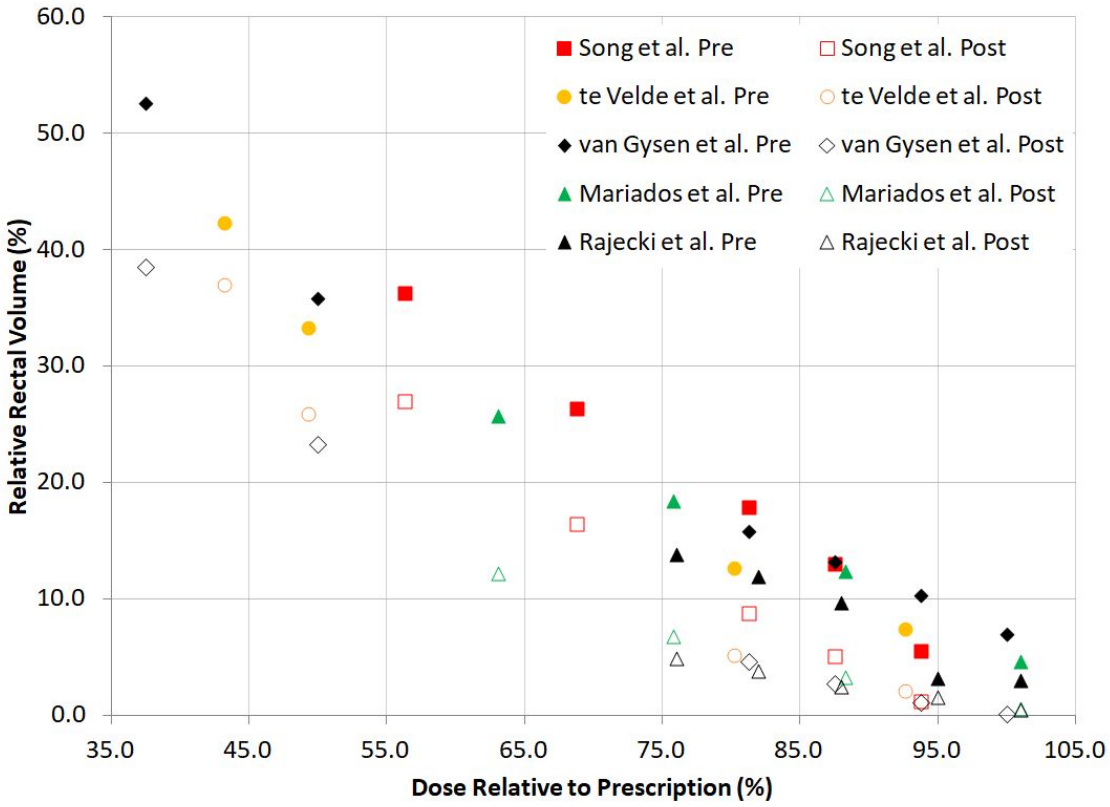

Figure 1.5: Reduced DVH metrics for relative rectal volume with application of SOH through five studies.[32,33,38–40]

1.4 Thesis Scope

In November 2017, five patients at BC Cancer - Victoria received the SpaceOAR© hydrogel implant marketed by Augmenix thanks to funding from Island Prostate Center. An institutional research ethics board approved a retrospective planning

study of SOH. Two treatment plans were produced on pre-SOH CT scans while four treatment plans were produced on post-SOH CT scans for each patient allowing for effective evaluation of the dose reduction due to SOH.

By February 2019, twenty-two patients had received SOH implant producing DVH data required for two studies. The first study used an initial patient pool of thirteen patients to compare and contrast the rectal wall (RW) and composite rectal wall (CRW) optimization structures and IMRT and VMAT treatment techniques in terms of rectal dose sparing requiring six treatment plans to be produced per patient. The second study examined treatment plans from twenty-two patients for correlation between pre-SOH anatomy and rectal dose reduction. A predictive model of rectal dose reduction was produced using anatomical features from the pre-SOH CT scan. Both studies were performed to optimize the effectiveness of SOH implant.

In this thesis, Chapter 2 will offer background information on radiotherapy and SOH implant techniques. This includes particle interactions in the context of both radiotherapy and medical imaging. Additionally, the contouring of critical OAR structures and the inverse optimization treatment planning method will be discussed in detail.

Chapter 3 will discuss the rectal dose reduction available in the application of composite rectal and rectal wall optimization structures and IMRT and VMAT treatment techniques for SOH based, hypofractionated prostate radiotherapy. These results will be put in perspective by comparing to results from a number of clinical trials. Results will offer guidelines to clinicians creating 60 Gy in 20 fraction protocols for prostate EBRT with SOH implant.

Chapter 4 will present a predictive model of the decrease in rectal dose from pre-SOH to post-SOH treatment plans. SOH implant is an expensive treatment option and as such, sufficient rectal dose reduction should be expected for a patient to receive a pre-RT supportive implant. Patient anatomy information available on the pre-SOH CT scan were used as predictors of change in RV55Gy (ΔRV55) and high dose integral from 55 to 60 Gy of the rectal DVH (ΔHDI). The models will aid in clinical decision making to offer SOH as an additional treatment option for prostate EBRT patients.

Chapter 5 will summarize the preferred optimization structure and treatment technique for prostate EBRT with SOH and present models and factors which predict the reduction in rectal dose. Additionally, a suggestion of future direction will be presented along with concerns or considerations about the presented work.

Chapter 2

Background

2.1 Particle Interactions

Radiotherapy treatment is often performed with photons, electrons or both. The particle interaction process in the body is important to characterize to ensure accurate simulation of particle interactions took place within treatment planning softwares. In photon radiotherapy, the photon enters the tissue and imparts energy to electrons through a series of interactions. The electrons then travel through the tissue depositing energy through charged particle interactions such as Coulomb effect and Bremsstrahlung, or braking, radiation. The photon and electron interactions in tissue are described below.

2.1.1 Photon Interactions

Photon interactions are the first step of energy deposition in photon radiotherapy. There are several different mechanisms of photon interaction, with each occurring at an energy dependent probability. This interaction probability has been described by the mass attenuation coefficient of a given material. Figure 2.4 indicates the mass attenuation coefficients for water and lead as it varies with energy. The four interactions of interest are photoelectric effect, coherent/incoherent scattering, and pair production. Each of these interactions have a region in which they are dominant processes, with radiotherapy treatment generally delivered in photon energies ranging from 0.1 - 20 MeV. Characterizing the interactions will aid in describing radiation damage to tissue.

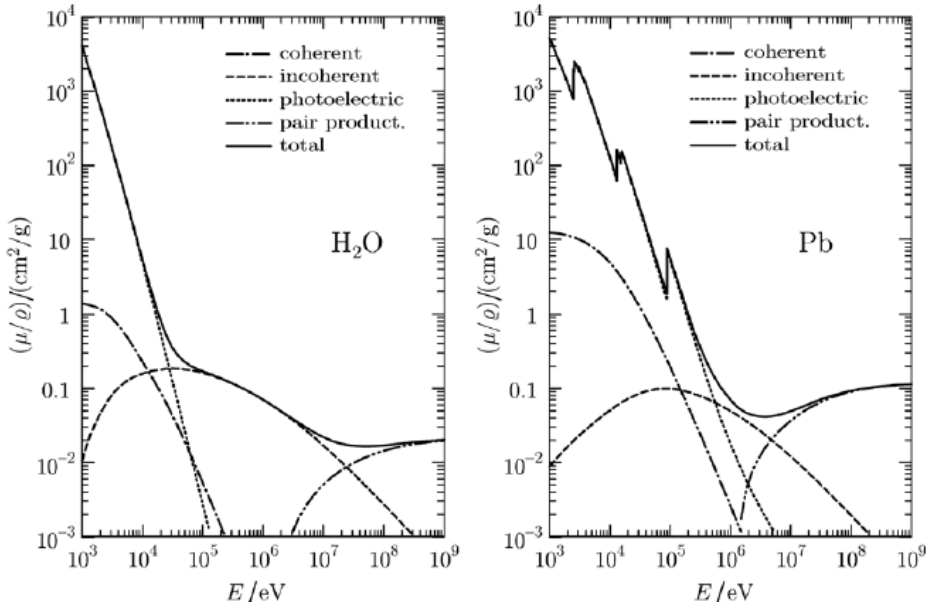

Figure 2.1: Mass attenuation coefficient for water (left) and lead (right) describing dominant regions of photoelectric effect, pair production, coherent and incoherent scattering. Taken from Salvat et al.[41]

2.1.1.1 Photoelectric Effect

Photoelectric effect is the dominant photon interaction for energies below one electron rest energy, 0.511 MeV. The photoelectric effect describes the emission of bound electrons once excited by a photon. This excitation of an electron requires a minimum energy to occur dependent on the binding energy of the electron shell. The energy transferred to the excited electron is described as follows:

$$E_{tr} = h\nu - B \tag{2.1}$$

In this case, $h\nu$ describes the energy of the incident photon and B is the binding energy of the electron orbit. This binding energy depends on both the material, and the shell of the excited electron which is generally an inner electron orbit.

2.1.1.2 Coherent & Incoherent Scattering

Coherent and incoherent scattering occur when a photon interacts with a target electron. Coherent scattering, also known as Rayleigh scattering, results in a change in direction of the photon emitted with no loss of energy. A photon interacts with an outer shell electron, is absorbed and subsequently re-emitted in a new direction,

effectively scattering the incident photon. The cross section of this interaction varies with the atomic number of the absorber (Z) and the energy of the incident photon ($h\nu$).

$$\sigma_R = \frac{Z}{(h\nu)^2} \tag{2.2}$$

Coherent scattering is not a dominant process at any energy, with contributions given in the region of photoelectric effect. As such, coherent scattering is not a major interaction at therapeutic radiation energies.

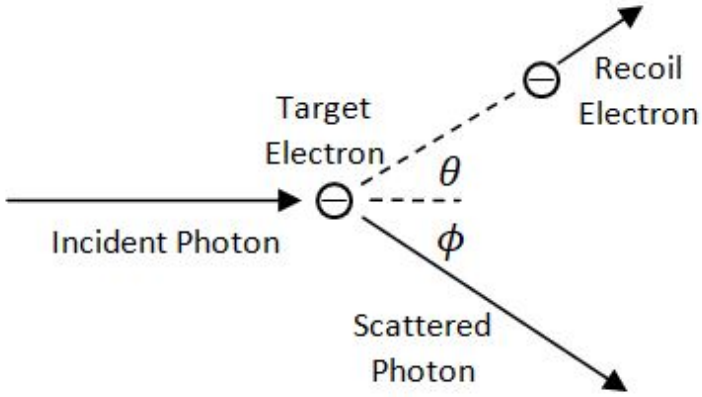

Figure 2.2: Compton scattering effect.

Meanwhile, incoherent, or Compton, scattering is the dominant effect at therapeutic energies causing the majority of energy transfer due to photons. This describes the process in which a photon strikes and transfers energy to a target electron. The resulting electron and scattered photon are emitted at two separate angles with scattered photon energy as follows:

$$E_{\gamma'} = \frac{E_\gamma}{1 + \frac{E_\gamma}{m_o c^2}(1 - \cos\theta)} \tag{2.3}$$

The scattered photon energy, $E_{\gamma'}$, is dependent on the incident photon energy, E_γ, and the electron rest energy, $m_o c^2$. This process is dominant between 0.1-10 MeV.

2.1.1.3 Pair Production

Pair production is a photon interaction process which begins to occur at energies higher than 1.022 MeV, or two times the electron rest energy. This process occurs

when a photon near a nucleus produces an electron-positron pair, releasing the 1.022 MeV activation energy required to produce the pair as seen in Figure 2.3. The pair are emitted at symmetrical angles, with each receiving half of the transferred energy. Total energy transferred from the pair production interaction can be described as follows:

$$E_{tr} = h\nu - 1.022MeV \tag{2.4}$$

where, $h\nu$ is the incident photon energy. Once the energy has been transferred, the electron and the positron particles move freely away from the interaction site.

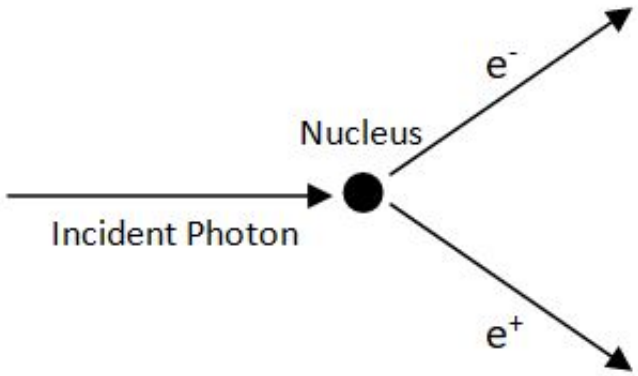

Figure 2.3: Pair production interaction producing an electron-positron particle pair.

2.1.1.4 Characteristic X-Rays & Auger Electrons

Characteristic x-rays may be emitted after a photon has interacted with a bound electron. These x-rays, whose energy are highly element dependent, are emitted when an electron moves from a highly bound state to a lower bound state within the atom. This process often occurs through photon interactions in which a photon expels a lower shell electron, such as a K-shell electron. A higher shell electron, such as an L-shell electron, may then move to the lower state emitting a photon. This photon may subsequently interact with an additional electron, ejecting it from the atom. The ejected electrons have been termed Auger electrons.

2.1.2 Electron Interactions

Electron interactions can be described as general charged particle (CP) interactions which may also apply to positron interactions. These interactions occur with the use of electron beams, or after photons have released electrons from bound states. These CP interactions are described using stopping powers, which is a CP counterpart of mass attenuation coefficients. The mass stopping power is related to the mean energy lost by CP over a unit distance. It can be used to describe three types of interactions: soft and hard collisions when the particle is outside the nucleus of the atom and bremsstrahlung radiation emission when the charged particle is within the radius of the atom. The total stopping power expression is a combination of both collisional and radiative stopping powers which describe these interactions (see Figure 2.5).

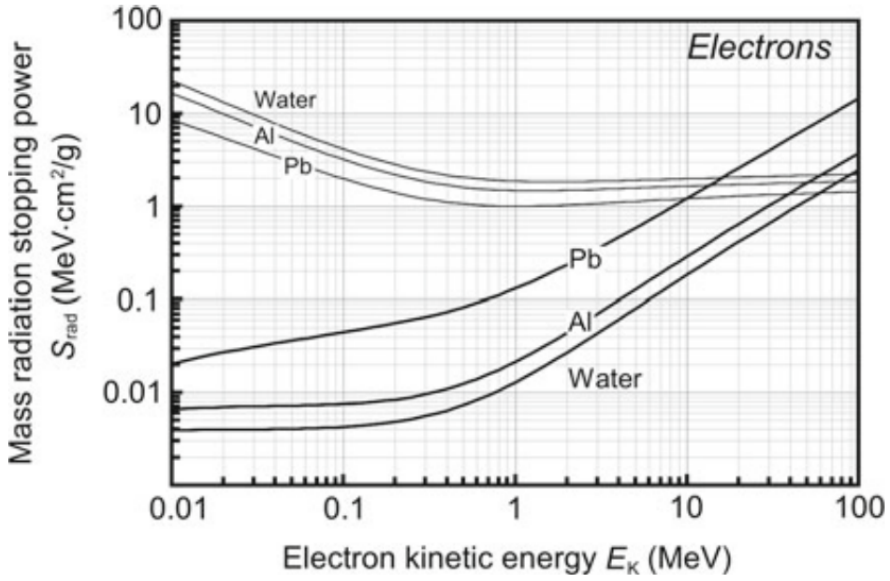

Figure 2.4: Collisional (top) and radiative (bottom) stopping powers for lead, aluminum and water. Taken from Podgorsak.[42]

2.1.2.1 Soft & Hard Collisions

Collisions between CP may occur when electrons interact closely with an atom and its electron cloud as depicted by Figure 2.5. Hard collisions characterize an electron emitted from the atom when the electron is a distance of approximately one atomic radius (ie., b $\sim$ a) away from the nucleus. The incident electron collides and expels an

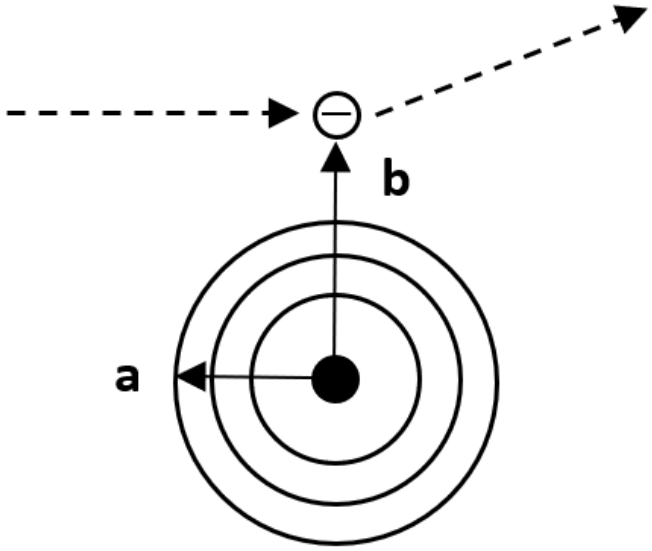

Figure 2.5: Image of charged particles interacting with nucleus where **a** is the atom radius and **b** is the distance to the interacting CP.

electron from its bound state after transferring energy. A characteristic x-ray for the atom is then produced as a higher shell electron fills the space produced in the hard collision. The x-ray is dissipated through photon interactions and the two electrons exit the electron cloud. A soft collision occurs when an electron is outside the radius of the atom (ie., b » a) which results in small transfer of energy to nearby electrons due to Coulomb forces between the CP and the whole atom. This interaction is the most probably type of interaction between a CP and an atom.

Soft and hard collisions can be described through the collisional stopping power expression. The following expression can be used for both positrons and electrons with slight variations in functional form.[43]

$$\left(\frac{S}{\rho}\right)_{col} = \left(\frac{2\pi r_e^2 m_o c^2}{\beta^2}\right)\left(\frac{ZN_A}{A}\right)\left[ln\left(\frac{T^2}{I}\right) + ln(1+\frac{\tau}{2} + F^{\mp}(\tau) - \delta\right] \tag{2.5}$$

The variables include the kinetic energy of the electron, T, the rest energy of the electron, $m_o c^2$, ratio of kinetic to rest energy, $\tau = \frac{T}{m_o c^2}$, the ratio of electron speed and speed of light, β, atomic number of the target atom, Z, atomic mass of target atom, A, Avagadro's number, N_A, and the mean excitation energy of the

medium. The collisional stopping power for electrons and positrons varies only by the functional form expression, $F^{\mp}(\tau)$. The functional expressions for electrons and positrons respectively are expressed below in Equation 2.6. Note that the forms are related to β and τ.

$$F^{-}(\tau) = (1-\beta^2)\left[1 + \frac{\tau^2}{8} - (2\tau+1)ln2\right] \tag{2.6a}$$

$$F^{+}(\tau) = 2ln2 - \frac{\beta^2}{12}\left[23 + \frac{14}{\tau+2} + \frac{10}{(\tau+2)^2} + \frac{4}{(\tau+2)^3}\right] \tag{2.6b}$$

The above forms can be used to describe the stopping power of electrons (Eq. 2.6a) and positrons (Eq. 2.6b), approximating energy lost through soft and hard collision interactions.

2.1.2.2 Bremsstrahlung Radiation

A CP passing through the radius of an atom (ie., b $\ll$ a) may either be deflected only or lose nearly all energy through inelastic radiative interactions. Loss of energy through radiative interactions can be described by the radiative stopping power:

$$\left(\frac{S}{\rho}\right)_{rad} = \left(\frac{\rho^2}{m_o c^2}\right)\left(\frac{Z^2 N_A}{137A}\right)(T + m_o c^2)B_{rad} \tag{2.7}$$

The rate of radiative energy loss is related to density, ρ, and atomic number, Z, of the material and subsequently the kinetic energy, T, of the incoming CP. This radiative loss is quite common in radiotherapy and is emitted after an electron experiences a strong deceleration due to Coulomb interactions.[43] The change in direction causes radiation emission termed bremsstrahlung, or braking, radiation. Brehmsstrahlung interactions produce photons within x-ray tubes or linacs but also occur within tissues causing large changes in CP direction.

2.2 Medical Imaging

Medical imaging is employed in many steps of the radiotherapy process. This includes imaging for diagnosis, for treatment planning and for patient alignment in radiotherapy. Modalities such as positron emission tomography, computed tomography (CT), and magnetic resonance (MR) imaging are used throughout radiotherapy. CT and

MRI are common modalities in diagnosis, planning and treatment of prostate cancer. The basics of CT and MRI will be discussed below.

2.2.1 Computed Tomography Scan

CT scans are commonly used for treatment planning and image guidance in radiotherapy. The contrasting electron density between soft tissue and bone along with Hounsfield units used for dose simulation make it an effective imaging modality for treatment planning. These images are produced by directing x-rays through the patient and detecting them on the other side. The energy deposited can be determined through a reconstruction algorithm and related to a gray scale via Hounsfield units to produce an image.

The x-rays are produced through an x-ray tube by accelerating electrons towards an anode using magnetic steering coils. The tungsten anode rotates allowing for target area to cool after high rate of electron interactions. The high energy electrons interact with tungsten and emit photons through bremsstrahlung radiation. Photons are emitted through an opening near the x-ray tube anode. Most commercially available CT scanner x-ray tubes produce photons with peak energies between 80-140 kV. The total photon beam is collimated using pre-patient collimators to reduce the lower energy penumbra. Additional filtering removes low energy photons without sufficient energy to escape the patient.

Photons then pass through the patient with energy attenuation corresponding to linear attenuation coefficients of the material through which they pass.[44] Photons with energy 80-140 kV in soft tissue hold a Compton scattering cross section much higher than the photoelectric cross section as seen in Figure 2.6. As such, CT images of soft tissue indicate physical properties for which Compton scattering is dependent on electron density as follows:

$$\mu_{Compton} \propto \rho N \frac{Z}{A} \tag{2.8}$$

where $\mu_{Compton}$ is linear attenuation coefficient for Compton scattering, ρ is mass density of the tissue, N is Avagadro's number and A is the atomic mass. This varying cross section within soft tissue, bone and other materials of interest may be leveraged to produce contrast between materials. This difference can be converted to a gray scale value within CT images. Hounsfield units (HUs) are the gray scale representation of this attenuation coefficient of materials.

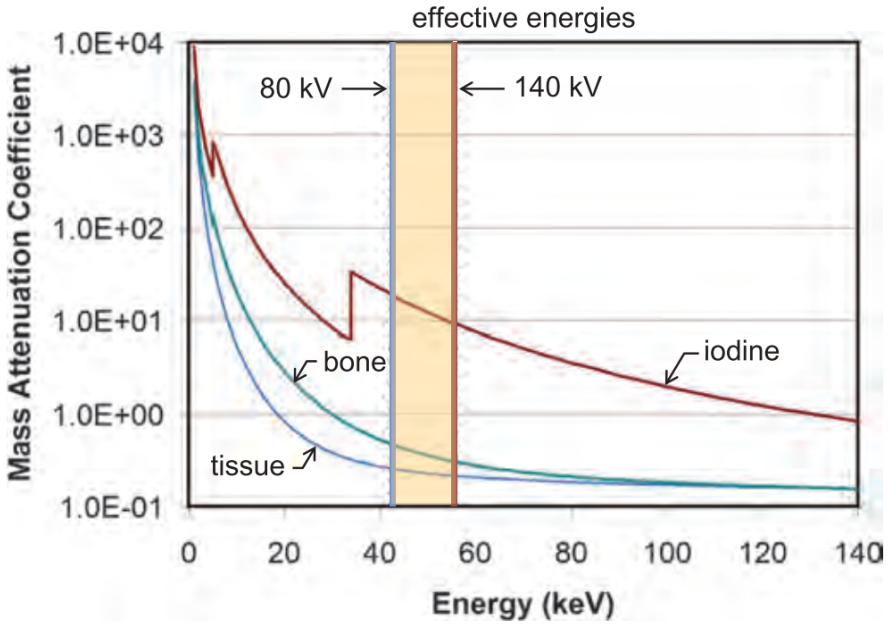

Figure 2.6: Differences in mass attenuation coefficients of materials produces contrast within the energy range of interest for CT scans. Figure taken from Bushberg et al.[44]

$$HU\ (x,y,z) = 1000\frac{(\mu(x,y,z) - \mu_w)}{\mu_w} \tag{2.9}$$

where $\mu(x,y,z)$ and μ_w are linear attenuation coefficients of materials of interest and water respectively. Within this scale, water is a Hounsfield unit of 0 HU, air is -1000 HU, soft-tissues lie between -30 and +220 HU and tissue with iodinated contrast agents may run up to +3000 HU.

After being attenuated by tissues within the body, remaining photons are detected through solid state detectors consisting of a scintillator and a photodiode.[44] Each discrete detector, j, returns a signal which may be described through the form or linear attenuation coefficients:

$$I_j = g_j I_o e^{-(\mu_1+\mu_2+...+\mu_n)t} \tag{2.10}$$

where I_j is signal at detector element j, g_j is the gain of the detector, I_o is the initial signal, t is the thickness of material and μ_n is the linear attenuation coefficient of materials through which the photons passed. This signal can be compared to a reference signal outside the patient field of view. This returns a ratio, $\beta = g_r/g_j$, where g_r is the reference gain and g_j is the gain of the detector of interest. Therefore

the projection measurement can be extracted from comparing signals and gains of the detectors:

$$P_j = \ln\left(\frac{I_r}{\beta I_j}\right) = t(\mu_1 + \mu_2 + ... + \mu_n) \tag{2.11}$$

where I_r is the signal from a reference detector and μ_n are the attenuation coefficients of the material through which the photons pass. Thus, the projection signal after pre-processing corresponds to the sum of the linear attenuation coefficients along the ray through which the photons pass. Reconstruction methods may be performed on the signals collected from all detectors within the array to produce a CT image.

Detectors in a CT array are highly pixelated to increase the resolution of photon detection. Current CT scanning techniques rotate the x-ray source through a 360^o rotation while detectors are placed throughout the circular path. This reduces ring artifacts due to damaged pixels if a single detector were used to detect photons. Signal to noise ratio in CT images is highly dependent on either the number of photons passing through the patient which can be increased through an increased x-ray current or the slice thickness. Increasing slice thickness on a CT scan will improve signal to noise ratio, but may result in lower resolution images between slices.

CT images are produced using an image reconstruction algorithm to combine the projection data.[44] The two main reconstruction algorithm families are iterative reconstruction and back projection algorithms. Iterative reconstruction algorithms begin with an expected image, often a guess or constant image. The iterative process updates the image by making slight adjustments and comparing the expected projections to the measured projection data. An error matrix is then produced based on the difference between projections. This error matrix is used to guide the next iteration. This process continues until noise has been reduced within the image. Iterative reconstruction methods are computationally intensive and are currently not commonplace in a clinical setting. However, iterative reconstruction algorithms offer lower noise images while delivering a lower radiation dose. As such, iterative reconstruction algorithms may become commonplace in clinical applications.

Most current clinical CT scans apply a filtered back projection algorithm to produce CT images. A back projection algorithm is applied to produce an image from the detector data by back projecting data along the path of the projection. A simple back projection can be produced from evaluating an inequality expression.[45] This is not an effective method for clinical CT reconstruction but may act as an effective

model to understand the algorithm. In clinical filtered backprojection algorithms, each projection is convolved with a kernel to remove radial blurring seen in simple backprojection methods prior to back projection. Filtering kernels filter specific features in CT scans, producing a more useful image.

2.2.2 Magnetic Resonance Imaging

Magnetic resonance imaging takes advantage of the density of magnetic nuclei (ie., protons) within material.[46] Applying a magnetic field to these nuclei causes the tissue to become magnetized in the longitudinal direction. This magnetization may be flipped into the transverse plane by applying a 90 degree radiofrequency (RF) pulse to the magnetized tissue. Both longitudinal and transverse magnetizations have a characteristic which may be adjusted to display different types of image contrast.

The transition from longitudinal magnetization to transverse magnetization is know as *excitation* due to the unstable nature of the transverse magnetization or *saturation* as the longitudinal magnetization was destroyed. After the RF pulse, the longitudinal magnetization begins to recover while the transverse magnetization begins to decay. The rate of recovery and decay can be described by the longitudinal relaxation time, T1, and transverse decay time, T2, respectively. Tissues will have varied T1 and T2 times resulting in contrast between the materials.

MR images are acquired through repeating an imaging cycle consisting of RF pulses controlled through two time parameters.[46] The first parameter is the time of repetition (TR) which describes the time interval between saturation and excitation and describes when a 90 degree RF pulse will be applied. This produces contrast in T1, T2 or proton density (PD) range as seen in Figure 2.7. The second parameter is the time of echo (TE) which is the interval between beginning of transverse relaxation and when the magnetization is measured to produce image contrast. At this point, the magnetization signal is measured through a 180 degree echo pulse. This method of MR image acquisition is the conventional spin-echo method, one of the two major MR acquisition method families. The other, gradient echo, applies a slightly different process to create the echo event at the end of each imaging cycle.

The two time parameters, TR and TE, can be varied to produce a series of imaging protocols to produce different contrast between tissues. This contrast comes from T1 or T2 characteristic times or from PD contrast. T1 contrast is developed during the longitudinal magnetization phase, T2 contrast is present during the transverse

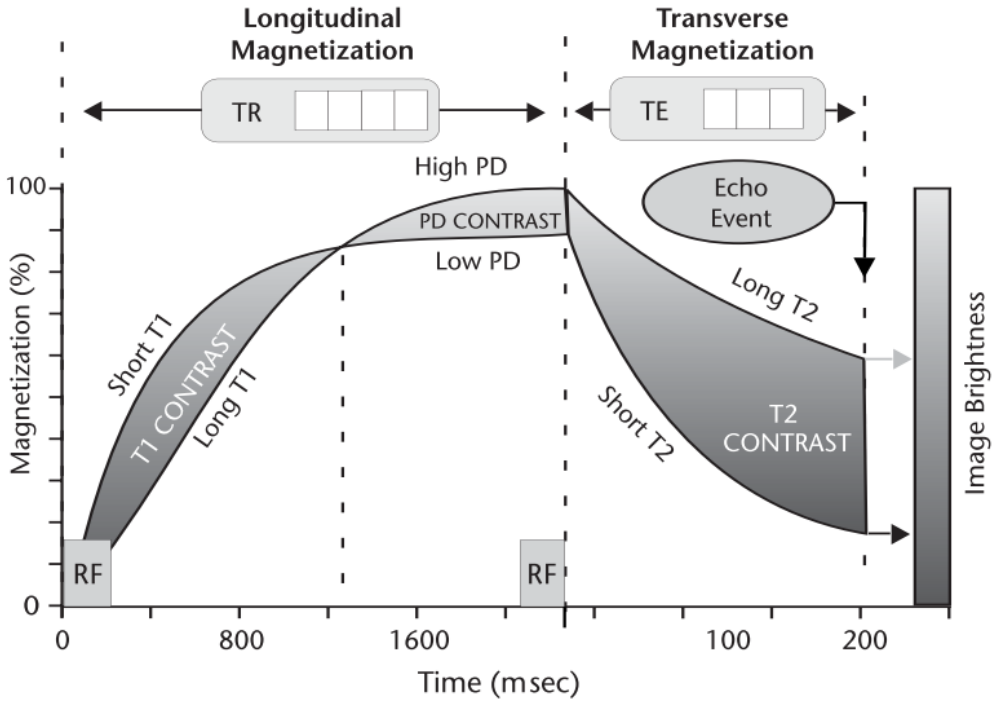

Figure 2.7: Sequence of magnetic resonance (MR) pulses for image acquisition. Taken from Sprawls.[46]

magnetization phase while PD contrast is always present but may be overshadowed by either T1 or T2 contrasts as noted in Figure 2.7.

2.2.2.1 T1 Weighted Contrast

T1 contrast leverages difference between longitudinal magnetization relaxation times of tissues by implementing a TR which optimizes the difference.[46] A short T1 will recover more quickly compared to a long T1 as shown in Figure 2.8. The TR selects a time to readout the signal by applying an RF pulse, at which point a T1 contrast image may be produced. This cycle is repeated multiple times to produce an MR image.

After the initial saturation pulse, all tissues appear dark. As time passes, the image becomes brighter or more intense. The final intensity of the image depends on TR and the T1 contrast required for the MR image. Increasing TR increases the signal intensity, but may reduce effects seen from T1 contrast to a point at which the longitudinal magnetization is completely recovered. Selection of an appropriate TR

value will ensure contrast between tissues of interest.

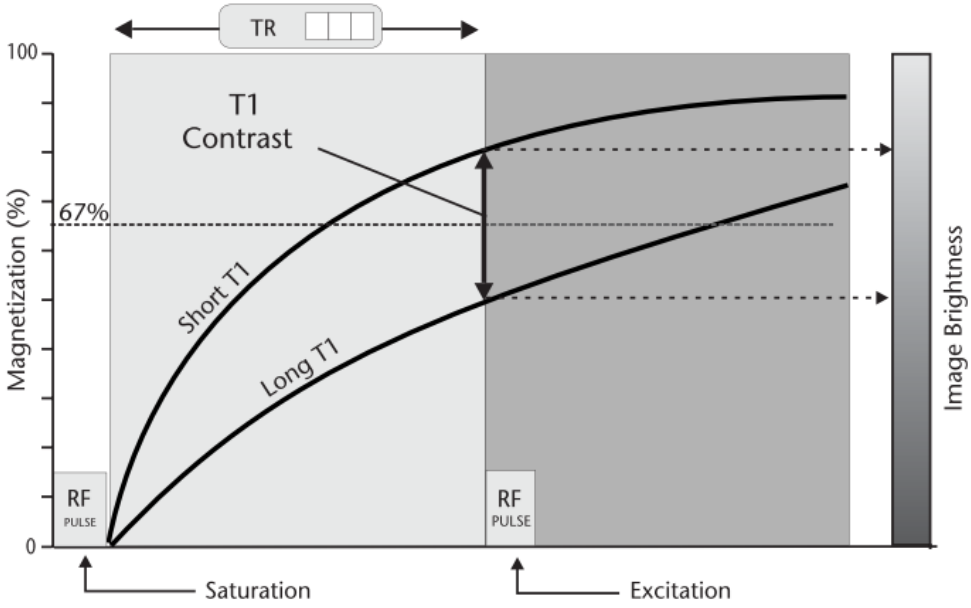

Figure 2.8: T1 weighted MRI imaging. Taken from Sprawls.[46]

2.2.2.2 Proton Density (PD) Contrast

The proton density within tissue determines the maximum achievable magnetization.[46] As such, contrast occurs near the end of the longitudinal relaxation as the magnetization nears a maximum. PD contrast may be present earlier in the cycle, however T1 contrast is dominant at this point. The difference between T1 and PD contrast is that T1 employs the rate of relaxation to create contrast while PD employs the maximum achievable magnetization of the tissue to produce the contrast.

Generally, T1 contrast is dominant in early portion of relaxation curve while PD contrast becomes dominant near the end as seen in Figure 2.9. To overcome T1 contrast and achieve PD contrast, a long TR time must be used for the MR sequence. Complete relaxation occurs when TR is approximately three times T1 of the tissues of interest at which proton density contrast begins. Selection of a TR within this region allows for sufficient contrast. At this point, high proton density tissues will appear lighter compared to low density tissues.

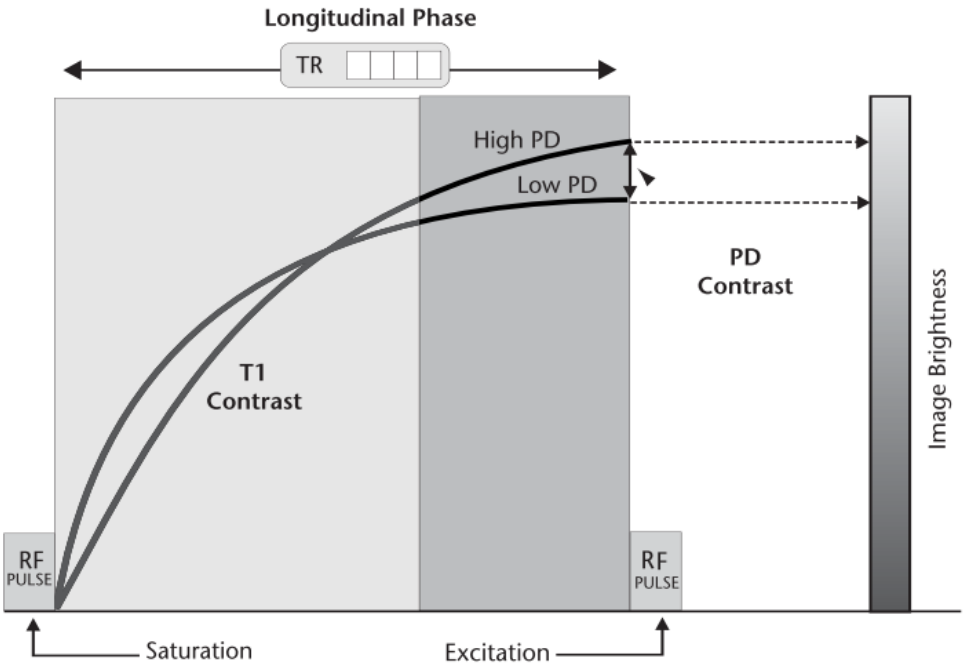

Figure 2.9: Proton density weighted MRI imaging. Taken from Sprawls.[46]

2.2.2.3 T2 Weighted Contrast

Both T1 and PD contrast were available within the longitudinal magnetization phase however, T2 contrast occurs during the transverse magnetization.[46] Similar to T1 contrast, within the transverse magnetization, tissues will have different decay rates, or T2 values. After an RF pulse to induce excitation, there is initially PD contrast from the longitudinal magnetization. The T2 contrast begins to present as time passes and transverse magnetization begins to relax as seen in Figure 2.10. The image is read out using an echo event, with the TE selected by the operator to optimize T2 contrast.

Maximum T2 contrast occurs at long TE times, however TE times too large cause the transverse magnetization to decay to a point where there is minimal magnetization. As such, a compromise must be made between T2 contrast and signal intensity. The brightness of specific tissues depends on TE time selected, however generally the long T2 tissues will appear light while short T2 tissues will appear dark.

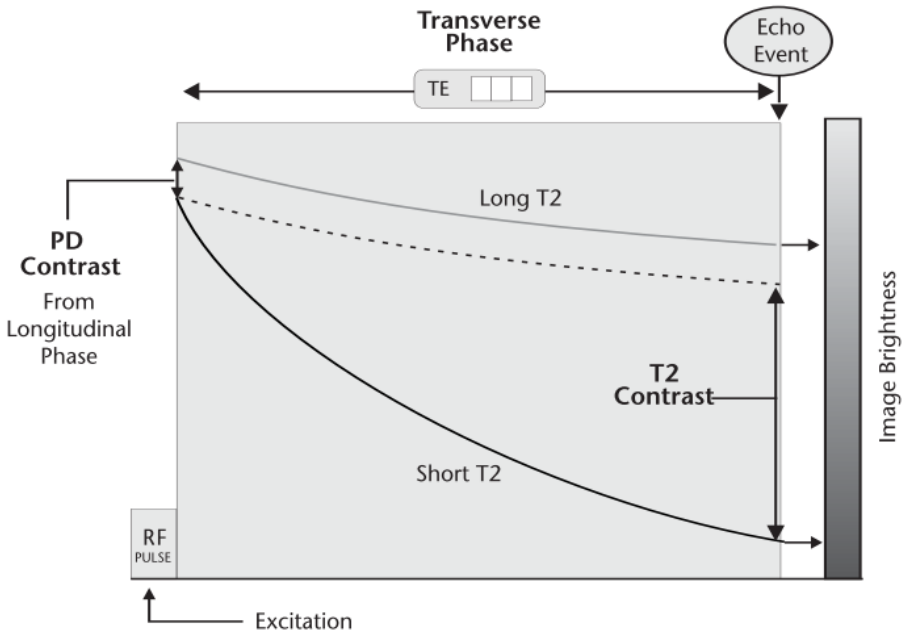

Figure 2.10: T2 weighted MRI imaging. Taken from Sprawls.[46]

2.3 SpaceOAR Hydrogel Implant

SpaceOAR© Hydrogel (SOH) is a polyethylene glycol (PEG) hydrogel spacer with applications in prostate cancer radiotherapy treatment to reduce rectal dose.[32,33,38–40,47,48] High rectal dose in prostate cancer radiotherapy is due to high overlap of PTV and rectum in treatment planning. Increasing the distance between prostate and rectum, using a technique such as SOH, has been shown to reduce the rectal dose.[49] SOH is placed between the rectal wall and Denonvilliers' fascia in the perirectal fat.[50] Hydrodissection of the perirectal fat creates space for SOH. Two fluids, Precursor and Accelerator, are injected through an 18-gauge (18G) needle implant and reacts to produce SOH in situ. Augmenix Inc. provides a Y-connector system to facilitate the combination of the Precursor and Accelerator fluids required to produce a PEG hydrogel within tissue. At BC Cancer - Victoria, SOH is injected post fiducial marker implant.

PEG is a polymer containing hydroxyl functional groups along the carbon backbone which act as electron donors, forming hydrogen bonds with other available hydrophobic compounds.[51] This compound offers many beneficial characteristics including biocompatibility, odorless, nonirritating, rapid solidification, and low cost creating an effective compound for implant. The hydroxyl functional groups on PEG

allow for cross-linking with each other creating a 3D, hydrophilic polymer network retaining a large amount of water and forming a gel-like matrix, termed hydrogel. PEG hydrogels are soluble in water and liquefy through hydrolysis in situ before being absorbed and cleaned through renal filtration, leaving the body within 6 months of implant.[50]

The Precursor and Accelerator are solutions which form the PEG hydrogel through chemical reaction. Precursor solution is composed of trilysine buffer solution along with PEG powder while the Accelerator solution is a salt buffer solution.[50] The two solutions cross-link to form a PEG hydrogel when mixed through the Y-connector, creating a solid structure in situ. This mechanism behind SOH creates a simple, effective method of creating perirectal space.

Patients receive specific bowel and bladder preparation instructions prior to the hydrogel/fiducial implant. A fleet enema is prescribed for both the night before and the morning of the procedure. Patients are asked to drink 750 mL of water within 15 minutes, 45 minutes prior to the pre-SOH CT scan and are then asked to empty the bladder prior to hydrogel and fiducial insertion.

Patients receiving SOH implants are placed in dorsal lithotomy position with stirrups used to keep knees bent at 90 degrees. The pelvic region is prepared using chlorhexidine producing aseptic skin and a local anesthetic is injected through the perineum to anesthetize the surrounding region. A transrectal ultrasound (TRUS) probe is positioned in the rectum to allow for visual guidance of the 18G, 15 cm needle. Clear image guidance, without artifacts, is critical to ensure the needle does not breach the prostate capsule or rectal wall. After positioning the TRUS, the needle can be attached to a syringe filled with saline solution and primed. Subsequently, the needle is slowly inserted 1-2 cm above the anal opening and advanced at a 10-15% downwards angle, while maintaining a visual through the ultrasound probe. Small puffs of saline may be used to verify the needle position prior to hydrodissection. Once the needle has reached the perirectal fat between rectal wall and Denonvilliers' fascia (seen in Figure 2.11), the 10 mL saline solution is injected, performing hydrodissection of the perirectal fat creating space for the SOH injection. The empty syringe is then removed from needle, and the Y-connector with Precursor and Accelerator liquids is attached while maintaining the needle position in the hydrodissected tissue. Steps are taken to ensure the TRUS probe is maintained in the correct position. Precursor and Accelerator are combined by slowly, consistently emptying the entire syringe in one continuous motion over a span of 8-10 seconds to produce a uniform gel distribu-

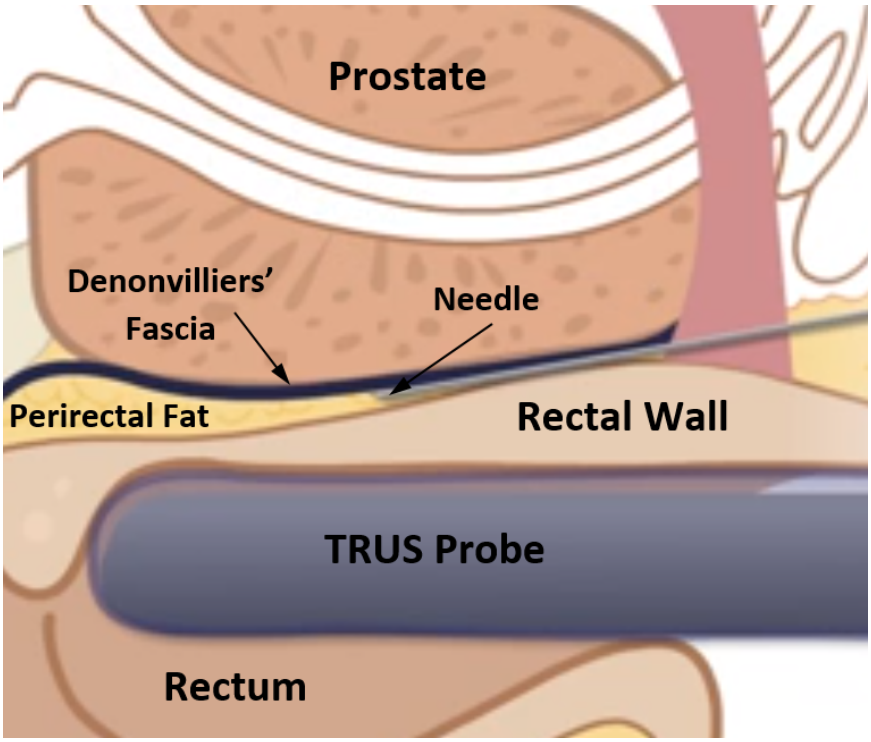

Figure 2.11: Clinical set-up for SOH implant with the use of a transrectal ultrasound probe for image guidance of the 18G needle into the perirectal fat. Image adapted from SpaceOAR© system instructions for use.[52]

tion.[28] This places the SOH into the perirectal space created through hydrodissection producing around 1 cm of separation between prostate and rectum.

There are several errors through implant process which would cause non-optimal placement of SOH due to needle insertion and probe placement. TRUS probe placement in rectal cavity can act as a mold for SOH to form around, and as such incorrect placement will result in errors. The factors affecting SOH placement include probe angle and height as seen in Figure 2.12 with TRUS probe pushing the hydrogel incorrectly in many cases. Additionally, needle position may result in a non-uniform distribution if needle is inserted away from the midline position. Other factors that might affect SOH implant include abnormal patient anatomy, injection speed and perirectal fibrosis.[28]

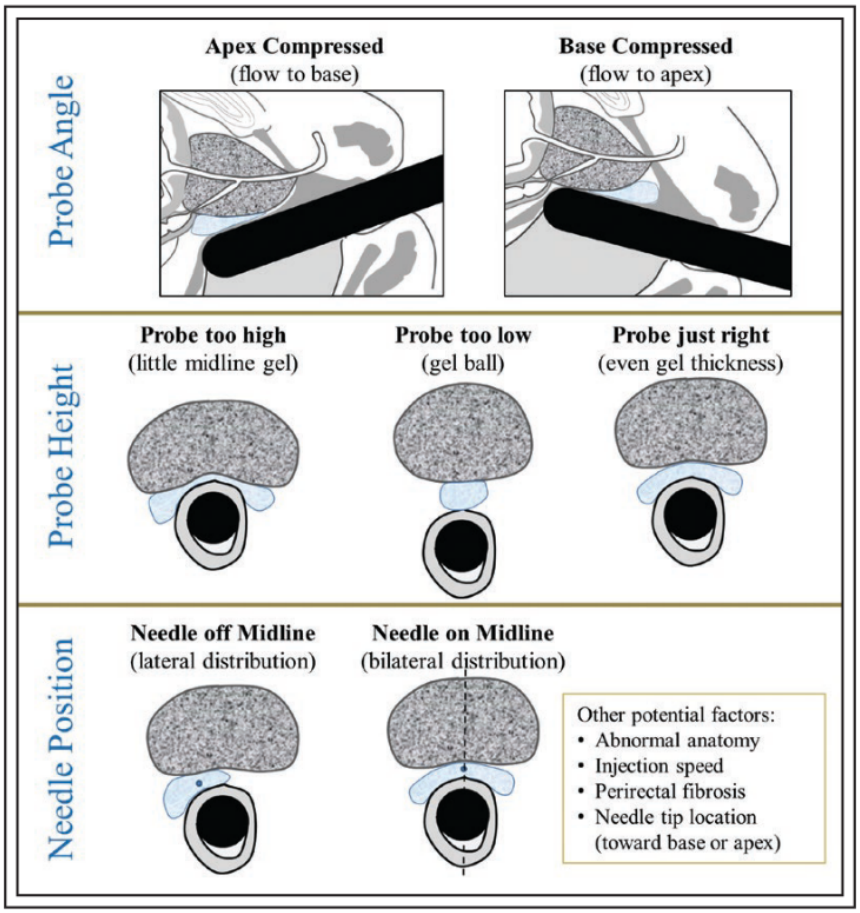

Figure 2.12: Errors due to TRUS positioning and needle injection site through process of SOH system implant. Figure taken from Montoya et al.[28]

2.4 Prostate Cancer Organs at Risk

The prostate gland is surrounded by a number of organs at risk (OAR) that must have restricted dose during radiotherapy to reduce bowel, urinary and sexual complications. Contours of interest during radiotherapy planning include rectum, bladder, penile bulb, prostate and femoral head with the addition of the SOH in patients receiving the implant. Many of these organs are essential to the functions of reproductive, genitourinary (GU) and gastrointestinal (GI) systems as seen in Figure 2.13. Manual, semi-automatic and automatic tools in Eclipse contouring workstation are used to contour these organs prior to treatment planning. Specific guidelines were used to contour both targets and OARs in this study.

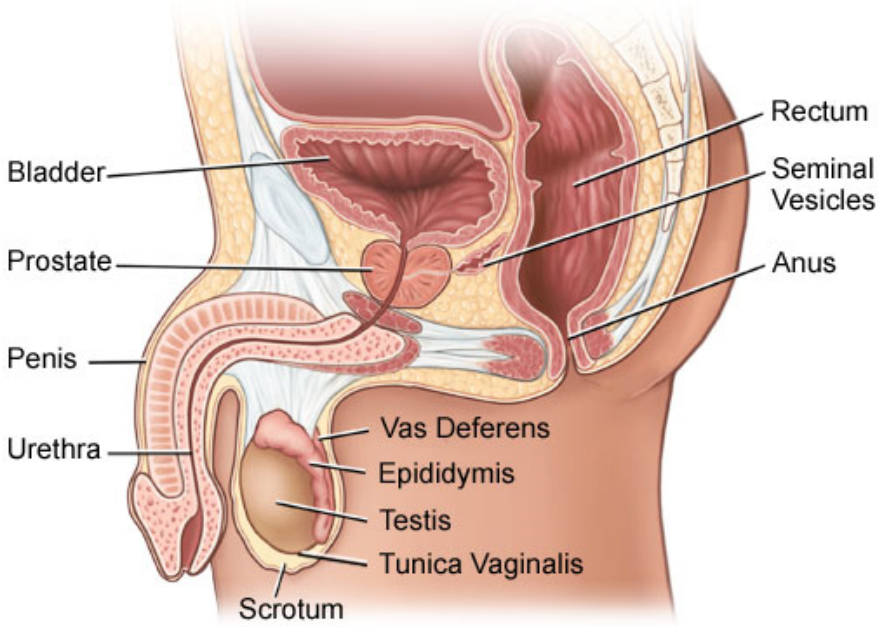

Figure 2.13: Male pelvic anatomy describing organs at risk in prostate cancer radiotherapy. Taken from University of Chicago.[53]

2.4.1 Contours of Interest

Prostate cancer OARs in this retrospective study have been contoured in a method similar to other SOH dosimetric studies to enable effective comparisons. CTV was contoured as the prostate plus 1 cm of seminal vesicles as per the definition of intermediate risk for prostate cancer.[16] Penile bulb was contoured as the bulbous spongiosum below the urogenital diaphragm and proximal to the penile shaft. Each femoral head was contoured separately from the top of the femoral head to the lesser trochanter. Rectum and bladder contours vary depending on the protocol used, and as such many structures were produced for this work.

Rectum and bladder structures were contoured using several methods outlined in dosimetric studies. SOH dosimetric studies followed the convention of contouring rectum as a solid organ from ischial tuberosities to rectosigmoid junction with cranial-caudal length kept consistent from pre- to post-SOH and the bladder as a solid organ. Meanwhile, BC Cancer - Victoria 60 Gy in 20 fractions planning protocol based on PROFIT and CHHiP studies for hypofractionated prostate cancer treatment[8,9] require additional rectum and bladder wall structures contoured to 17.5 mm above the superior PTV slice and below the inferior PTV slice. Rectal wall (RW) and

bladder wall (BW) structures were extracted using an inner wall margin of 3 mm.

Complete organ structures have been used as avoidance structures in the optimization and evaluation of plans in many SOH dosimetric studies.[32,33,38–40] However, chronic rectal toxicity has been linked to metrics pulled from rectal wall (RW) structures with a higher correlation compared to entire rectum.[54,55] As a result, studies such as PROFIT and CHHiP have begun to use RW as plan evaluation objective for rectal structure. Physically, rectal tissue was encompassed in RW structure while material contained within rectum was gas or material waiting to be excreted from the body with a similar trend seen in the bladder. Therefore, BC Cancer - Victoria has adopted the use of wall structures for both bladder and rectal optimization objectives and plan evaluation objectives of 60 Gy in 20 fractions hypofractionated prostate radiotherapy planning.

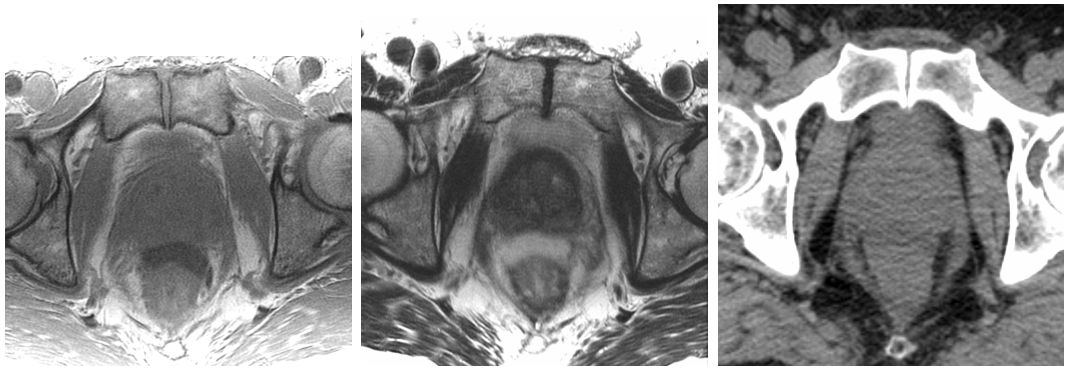

Figure 2.14: Three images of the same slice with T1 weighted MRI (left), T2 weighted MRI (middle) and with CT (right).

Post-SOH implant scans required the SOH to be contoured for OAR purposes and to guide contouring of the rectum. This contour was difficult to perform on CT scans due to lack of contrast between SOH and surrounding soft tissue (Figure 2.14). An MRI of the patient was taken to aid in contouring of this structure. CT and MRI images were registered together allowing for an effective method to contour the SOH and the rectum. However, there was time for organ motion between CT and MRI offering a source of error for SOH and rectum contouring. Additionally, variation between contours created by radiation oncologists provided additional error for the volume of organs studied.

Studies have explored the inter- and intra-observer contouring differences, with inter-observer differences from 10-18% in variation among patient contours.[56] As such, a single radiation oncologist created all the contours for each patient within this study

removing the inter-observer variability. However, the same study indicated that there was also some intra-observer variation when producing contours on CT scans. This variation was a mean of 5% across all radiation oncologists while the cranial-caudal length of contours remained consistent in short term intra-observer contouring. This intra-observer variability may have contributed to a difference in trends seen between patients as well as volumes between pre- and post-SOH contours.

2.4.2 Dose-Volume Constraints

All OARs surrounding the prostate have dose-volume dependent complications which reduce patient QOL. Many studies have examined the dose-volume relationship of these complications and as such clinical protocols have been developed on the basis of these studies. The most dose limiting OAR in prostate radiotherapy has been found to be the rectum which may have acute or late toxicity effects such as rectal irritation and bleeding. Meanwhile, the bladder, penile bulb and femoral heads are OARs which have dose specific constraints limiting acute and late toxicity effects such as frequent or urgent urination, erectile dysfunction and femoral neck fractures.

The prostate and the rectum are only separated by peri-rectal space. This proximity often results in overlap of the PTV and the rectum when a margin is applied to the CTV. Studies have shown the rectum to be the most dose-limiting organ in prostate radiotherapy.[7,19] Dose delivered to partial rectum volume often nears the prescription. It is critical to develop dose-volume constraints to reduce acute and late toxicity effects. Many studies have examined dose-volume constraints with consistent results suggesting volumes of high doses were most important in predicting rectal complications.[57] Constraints have been suggested to reduce incidence rate of moderate to severe late bleeding below 5-10%. Consensus has been to apply high (65-78 Gy) and intermediate (40-60 Gy) dose-volume constraints for fractions between 70-80 Gy.[56] The most common high dose-volume constraint has been RV70Gy$<$25% as RV70Gy metric has well documented correlation with Grade 2 or higher rectal complications.[21,58]

GU clinical symptoms are a commonly examined endpoint with many late urinary toxicity endpoints attributed to the effects of radiotherapy including dysuria, frequency, urgency, reduced flow and incontinence.[58] Prostate cancer radiotherapy may result in late GU complications seen in around $\leq$ 10% of patients. Viswanathan et al. provides an in depth overview of radiation dose-volume effects of the bladder in

pelvic radiotherapy treatment.[58] GU symptoms may present due to bladder or urethra damage, with no available distinction by physicians. Post prostatectomy irradiation studies indicate low GU toxicity[59] which may suggest the prostate and the prostatic urethra may cause GU symptoms. Additionally, studies show GU toxicity rates rise in high-dose prostate radiotherapy (>70 Gy) where only partial volume of bladder is treated. Bladder dose-volume modelling is difficult due to variation in bladder filling, resulting in variation of wall volume during treatment.[56] As such,the relationship between bladder dose-volume constraints and urinary toxicities has undergone limited research and QUANTEC publication was unable to provide reliable data for bladder dose-volume constraints.[57]

Penile bulb (PB) dose-volume endpoints have been correlated to the incidence of erectile dysfunction in patients post radiotherapy treatment. However, there have been conflicting results. Fisch et al. found erectile dysfunction develops if PBV70Gy $> 70\%$ after 3D-CRT for studied prescriptions from 65 to 72 Gy under standard fractionation.[60] Meanwhile, Brown et al. offered no conclusive dose-volume constraints[61] while the strongest limiting metric was found to be the mean penile bulb dose.[56,57] A study examined the mean penile bulb dose of patients experiencing erectile dysfunction after a follow up at 2 years post irradiation. Patients were divided into three groups (potent, reduced potency, impotent) and the corresponding average mean penile bulb dose was determined to be 45.5 ± 17.1 Gy, 48 ± 16.1 Gy, and 59.2 ± 13.8 Gy.[62] A strong correlation between incidence of erectile dysfunction and mean penile bulb dose was seen in this study. Further research has shown that a dose constraint of mean penile bulb dose < 52 Gy will greatly reduce risk of impotence.[63]

The final OAR contoured in prostate cancer radiotherapy planning is the femoral heads. No dose-volume relationship studies have been completed to characterize the dose-constraint endpoints within pelvic radiotherapy. Further investigation is required to further qualify this relationship. General endpoints have been suggested due to incidence of femoral neck fractures described by Grigsby et al.[64] Results indicated 4.8% of groin irradiation patients experienced femoral neck fracture with only one case of total femoral neck dose $\leq$50 Gy. Additional work by Bedford et al. recommended a dose-volume constraint of V52 Gy $< 10\%$ for a 70 Gy prescription dose which has been used in further studies.[65]

Many dose-volume constraints from PROFIT[9] study on prostate hypofractionation have been adopted by BC Cancer - Victoria for 60 Gy in 20 fractions hypofractionated prostate radiotherapy. These dose-volume constraints include rectal wall

dose constraints of D30% < 46 Gy and D50% < 37 Gy, bladder wall constraints of D30% < 46 Gy and D50% < 37 Gy and femoral head constraints of D5% < 43 Gy. All of the above constraints have been adopted from previous studies with rectum constraints following the high and intermediate dose constraints with similar constraints applied to the bladder.[56] Additionally, the 52 Gy dose endpoint seen in the femoral heads was reduced to 43 Gy in the hypofractionated regime with a stricter partial volume constraint included. A penile bulb dose-volume constraint was not provided in the PROFIT study however a constraint of PBV41.66Gy < 50% has been adopted by BC Cancer - Victoria for the hypofractionated regime.

2.5 Eclipse TPS Inverse Optimization

Inverse optimization problems have been studied for various applications, including the inverse optimization treatment planning problem to produce beam fluences. In each of these applications, some optimal decision variables are set. Each variable has an associated weight and cost function relating to the importance and difficulty in achieving the optimal objective.[66] Total cost function is minimized until a stable solution is found. This solution may not meet all requirements, as there exists a large solution space. In radiotherapy treatment planning, each contour of interest is designated with an optimization objective to be met and an associated weight. The distance of the DVH from the optimization objectives and the objective weights are related to the cost function. There is a large solution space available through radiotherapy treatment planning which may provide variation in treatment plans.

Inverse optimization treatment planning is the process of working backwards from a dose prescription and dose-volume constraints, termed optimization objectives, to find the beam fluence which achieves the plan evaluation objectives. Eclipse TPS optimizing algorithm applies a simple pencil beam to determine the beam fluence. Eclipse TPS IMRT algorithm applies fluence based optimization to produce an optimal distribution while VMAT algorithm is fluence and aperture based. Both inverse optimization algorithms optimize the cost function to reduce the pencil beam simulated dose and produce optimal fluence or fluence and aperture positions. Subsequently, an intermediate dose calculation with the analytical anisotropic algorithm (AAA) more effectively accounts for inhomogeneity effects during the optimization stage. These algorithms are not fully deterministic, and as such the same optimization objectives may result in different dose distributions.

2.5.1 IMRT Optimization in Eclipse

Eclipse TPS employs the dose volume optimizer (DVO) algorithm to optimize beam intensity modulation for IMRT treatment plans.[67] This optimization algorithm determines the optimal field shape and intensity through iteratively varying the dose distribution until optimization objectives are met.

Initially, the DVO fits fluence projections to the target within a 5 mm margin expanded symmetrically around the isocenter. This describes the region in which the fluence may be edited or modulated through the algorithm. Fluences are then incremented beginning at zero or at a fluence from a previous optimization. At each iteration, the dose is calculated from the optimized fluence.

Cost functions are developed from the optimization objectives at each point within the volume of interest. These cost functions are back projected to the fluences at each point to produce a gradient evaluated during the optimization process.

2.5.2 VMAT Optimization in Eclipse

Eclipse TPS employs the progressive resolution optimizer (PRO) algorithm to produce VMAT plans through optimization of dynamic multileaf collimators, variable dose rate and variable gantry speeds.[67] A constant number of control points are defined along the arc to represent the VMAT fields. The optimization occurs using the multi-resolution approach with a varied number of dose calculation segments. Initially, a low number of segments are used and the number of segments is increased throughout the optimization to improve the resolution of the calculation.

Within each multi-resolution level there is a varied number of steps of the optimization process. Each of these steps allows for small discontinuities within the dose distribution and the size of these discontinuities decreases with each subsequent step. At each step boundary, the distribution must lie within specific discontinuity levels which may cause a spike in the cost function as the optimization process moves between steps.

Initially, the MLC shapes conform to the target and dose rates are equal through all dose calculation segments. Through the beginning steps of multi-resolution optimization, larger changes are made to optimize the leaf patterns and fluences with the size of these adjustments decreasing throughout the optimization. The multi-resolution optimization results in dose calculation segments which are 2-4 degrees apart with the total number of segments depending on the span of the arc.

The fluence through MLCs at a control point within the dose calculation segment is used to calculate the segment dose. From the optimized fluence, leaf motion is modelled by interpolating leaf positions between control points. The angular resolution of dose calculations improves as the number of dose calculation segments increases.

2.5.3 Dose Calculations

There are many available dose calculation algorithms available in Eclipse TPS with the analytical anisotropic algorithm (AAA) being applied for the work presented in this thesis. This algorithm converts Hounsfield units from a CT scan to relative electron density using a calibration curve specific to individual CT units. AAA algorithms are used to produce dose distributions from beam fluence. This process occurs to produce an intermediate dose distribution and a final dose distribution.

The intermediate dose distribution is calculated partway through the optimization process in both DVO and PRO. This dose calculation aids in accounting for inhomogeneities not fully accounted for during the optimization stage. From this distribution, the algorithms calculate the difference between the intermediate dose and initial optimization results and compensates in consequent iterations of optimizations. Once an intermediate dose distribution has been calculated, the optimization continues until the final dose distribution.

Both intermediate and final dose calculations apply the AAA algorithm to calculate the dose distribution. The AAA algorithm calculates the total dose distribution through a superposition of dose deposition of primary photon, secondary photon and electron contamination sources.[68] The primary photon source is modeled as photon interactions on the target. Beam hardening by a flattening filter is taken into account by decreasing mean photon beam energy with distance from the central axis. The secondary photon source models photons produced through flattening filter, primary and secondary collimation of the linac. This source is produced as a convolution of the primary fluence and a Gaussian with width proportional to the photon source with no off-axis variation accounted. Electron source models electrons created by Compton interaction within the linac through an energy deposition function and two Gaussians. These dose deposition matrices are then convolved with Monte Carlo scatter kernels produced from photon and electron interactions. The resulting matrix is scaled by the electron density matrix from a CT scan to produce a three-dimensional dose distribution.

2.5.4 BC Cancer - Victoria Prostate Protocol

In an attempt to maintain consistent treatment plans, the optimization objectives and weighting have been well documented for each treatment site. Prostate cancer treatment planning applies objectives to rectum, bladder, penile bulb, femoral heads, PTV and CTV to ensure coverage while reducing dose to OARs. Each of these structures have optimization objectives along with plan evaluation objectives. BC Cancer - Victoria have adopted a series of optimization objectives and plan evaluation objectives based on dose constraints/limits. The optimization objectives, seen in Table 2.1 and used for this study, have been adopted from PROFIT[9] studies for hypofractionated prostate radiotherapy. These optimization objectives are set lower than the OAR dose constraints to ensure that the plan evaluation objectives are met. The rectal wall objectives were varied on a patient by patient basis to ensure maximum rectal sparing. RW objectives seen in Table 2.1 were the starting objectives based on the BC Cancer - Victoria protocol. In addition to OAR objectives, normal tissue objectives (NTO) were set to ensure all other tissue receives minimal dose.

Structure	**Limit**	**Volume (%)**	Dose (cGy)	**Priority**
PTV	upper	0	6000	100
	lower	100	6000	120
CTV (*IMRT*)	lower	100	6000	110
CTV (*VMAT*)	lower	100	6050	110
Bladder Wall	upper	40	3700	50
	upper	20	4600	70
Rectal Wall	upper	40	3700	50
	upper	20	4600	70
Lt Femoral Head	upper	0	4300	50
Rt Femoral Head	upper	0	4300	50
Penile Bulb	upper	45	4166	70

Table 2.1: Optimization objectives set for IMRT and VMAT treatment planning.

Chapter 3

Maximizing rectal dose sparing with hydrogel: a retrospective planning study

This chapter was taken, largely, from "Maximizing rectal dose sparing with hydrogel: a retrospective planning study" published in the Journal of Applied Clinical Medical Physics by Paetkau et al.[69] Sections comparing complete and wall rectum and bladder structures for optimization objectives were added to Materials and Methods, Results and Discussion sections.

3.1 Introduction

Prostate cancer is the most common non-cutaneous malignancy in Canadian men, representing 21% of new cancer cases and 10% of cancer deaths in men in 2017.[1] Standard treatment options for localized disease include surgery, external beam radiotherapy (EBRT) and brachytherapy, with many men opting for EBRT. Potential toxicities of EBRT can include rectal, urinary and sexual dysfunction due to the proximity of the rectum, bladder and penile bulb/neurovascular bundles to the prostate.[19] The rectum is the dose-limiting organ in prostate cancer external beam irradiation due to its proximity to the prostate, with the anterior rectal wall often falling within the planning target volume.[17,20,54,70,71] In recent years a number of products have been developed to spare the rectum during radiotherapy. One such innovation is SpaceOAR© hydrogel (SOH), a polyethylene glycol-based product, that is injected

between the rectum and the prostate to displace the prostate away from the rectum. The physical shift of the rectum allows a greater proportion of the organ to be spared high dose and, in a randomized trial, has resulted in reduced rectal toxicity and improved quality of life (QOL).[30,32–36]

The SOH has been shown to reduce the rectal dose in patients receiving both volumetric modulated arc therapy (VMAT)[34,38,40] and intensity modulated radiotherapy (IMRT).[32–34,36,39] Studies have compared VMAT and IMRT treatment techniques in external beam prostate cancer treatment, indicating similar results for prostate coverage. In many studies, the dose to organs at risk (OAR), including the rectum, bladder and penile bulb, was decreased when using VMAT over IMRT.[72,73] However, one planning study shows an exception in which rectal dose was lower with application of IMRT[4] compared to VMAT. The insertion of SOH between the rectum and the prostate may alter dose between treatment techniques. Current SOH studies are split between treatment techniques.

The generation of IMRT or VMAT plans involves an inverse planning optimization, through a series of dosimetric constraints on anatomical structures and regions within a set of radiotherapy planning computed tomography (CT) scans. In previous studies, different definitions of the rectal avoidance structure have been used during optimization to minimize the true rectal organ dose. To date, the rectum avoidance structure, which can be defined as either a solid form or a wall (i.e. rectal wall thickness of 3 mm, excluding the lumen) organ delineated from the anus or bottom of the ischial tuberosities to the rectosigmoid junction, has been commonly employed during optimization in SOH studies.[33,34,38,40] More recently, a fabricated structure, the composite rectum (CR) has been proposed.[39] This structure can be generated by combining the rectum with the hydrogel before extracting a wall structure (i.e. rectum + hydrogel, thickness of 3 mm excluding the lumen). The hydrogel is difficult to contour due to low contrast between rectum and SOH on CT scans, therefore the CR structure may offer a simpler alternative. Additionally, it has been suggested by te Velde et al.[39] that the CR may serve as an alternative rectal organ optimization structure. Optimization with each of these structures offers a varying degree of rectal dose reduction.

The aims of the present study were to firstly evaluate the ideal optimization structure (rectal wall (RW) vs. composite rectum wall (CRW)) in the setting of SOH for hypofractionated EBRT and secondly, to test whether the VMAT technique offers additional rectal sparing compared to IMRT. In this regard, IMRT and VMAT treat-

ment plans for 60 Gy in 20 fractions were generated using anonymized CT datasets from patients with implanted SOH, using RW and CRW in the optimization, and organ at risk (OAR) doses were compared. The treatment plans were examined to determine which combination of optimization structure (RW or CRW) and treatment technique (VMAT or IMRT) resulted in the lowest rectal dose distribution.

3.2 Materials and Methods

3.2.1 Hydrogel implant

The anonymized CT datasets of thirteen prostate cancer patients who were implanted with 10 cc of SpaceOAR hydrogel between the prostate and the rectum were selected for this institutional research ethics board approved retrospective planning study. All patients receiving the SOH also had three to four gold fiducial markers implanted via a trans-perineal technique prior to gel placement. The CT datasets consisted of a pre-SOH and post-SOH planning CT scans for each patient. The pre-SOH planning CT scan was obtained with a comfortably full bladder and empty rectum thirty to sixty minutes prior to implantation of fiducial markers and SOH. Patients were given specific instructions to drink 750 ml of water within 15 minutes, one hour prior to their pre-SOH CT scan and to perform a micro-enema two to three hours prior to their appointment. One week later patients underwent a post-SOH planning CT scan as well as a pelvic MRI with the same bladder and bowel preparation instructions. A T2 weighted MR image was taken to produce contrast between prostate and SOH while a FSPGR (T1 weighted) MR image was taken to provide contrast to the gold fiducial markers and prostate. The MR images were registered to the post-SOH planning CT images by a trained medical physicist, using gold fiducial markers and prostate structures of interest. The majority of the image registration was performed using the prostate and surrounding ligaments, muscle and other soft tissues as major registration structures with the gold fiducial markers used as a guide. The rectum and interface between rectum and prostate were excluded from use as registration structures due to the unstable nature of the rectum. The registered MR images were used to assist with contouring the SOH, rectum and prostate gland.

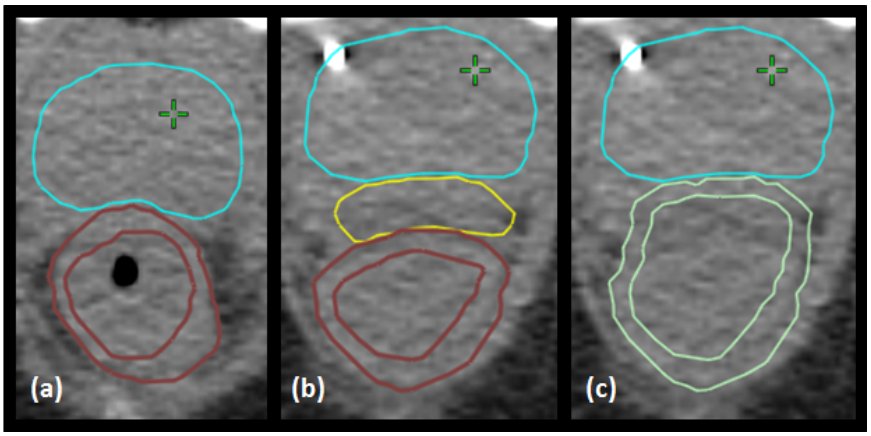

Figure 3.1: Computed tomography scan with clinical target volume (CTV) (light blue) and rectum structures: (a) pre-SpaceOAR hydrogel (SOH) with CTV and rectal wall (RW, brown), (b) post-SOH with CTV, SOH (yellow) and RW, and (c) post-SOH with CTV and composite rectum wall (light green).

3.2.2 Structure of interest contours

A set of target and OARs for optimization and plan evaluation purposes were defined and peer-reviewed by a group of genitourinary radiation oncologists. Clinical target volume (CTV) was defined as the prostate gland and proximal 1 cm of seminal vesicles. The planning target volume (PTV) was defined as the CTV with margins of 7 mm in all directions except for a 5 mm margin in the posterior direction. Rectum was contoured as a solid organ from the rectosigmoid junction to the ischial tuberosities, and the cranial-caudal length was kept consistent from pre- to post-SOH. Composite rectum (CR) was defined as hydrogel plus rectum with manual editing to smooth jagged contours. RW and CRW structures were extracted using an inner wall margin of 3 mm (Figure 3.1). Bladder was contoured with a bladder wall (BW) extracted using an inner wall margin of 3 mm. Femoral heads were contoured separately from the top of femoral head to the lesser trochanter. The penile bulb was contoured as the bulbous spongiosum below the GU diaphragm and proximal to the penile shaft.

3.2.3 Treatment plans

A total of six hypofractionated, 60 Gy in 20 fractions, treatment plans were created for each patient using Eclipse version 13.6 with the final dose calculation performed with the anisotropic analytical algorithm (AAA) version 11.0.31. This included a pre-SOH plan, and two post-SOH plans using either the RW or the CRW as the

optimization structure. These plans were created using both IMRT (dose volume optimizer version 11.0.31) and single arc VMAT (progressive resolution optimizer version 11.0.31) treatment techniques to produce the treatment plans listed in Table 3.1. Most IMRT plans were created using five angle beam arrangements (0^o, 50^o, 100^o, 260^o and 310^o). Two additional beam angles (155^o and 205^o) were added to plans when hot spots in the subcutaneous tissues exceeded planning guidelines with a five beam arrangement. Six additional treatment plans were produced using the full rectum and bladder structures with dosimetric constraints shown in Table 3.3 in order to reproduce planning techniques of other studies. This included a pre-SOH plan, and two post-SOH plans using complete rectum or complete composite rectum as the optimization structure (see Table 3.2).

Treatment Plan	Acronym	Hydrogel	Treatment Technique	Structure
1	Pre_IMRT	No	IMRT	Rectal Wall
2	CRW_IMRT	Yes	IMRT	Composite Rectal Wall
3	RW_IMRT	Yes	IMRT	Rectal Wall
4	Pre_VMAT	No	VMAT	Rectal Wall
5	CRW_VMAT	Yes	VMAT	Composite Rectal Wall
6	RW_VMAT	Yes	VMAT	Rectal Wall

Table 3.1: The six treatment plans created to compare wall optimization structure and treatment technique.

Treatment Plan	Acronym	Hydrogel	Treatment Technique	Structure
1	Pre_IMRT	No	IMRT	Rectum
2	CR_IMRT	Yes	IMRT	Composite Rectum
3	R_IMRT	Yes	IMRT	Rectum
4	Pre_VMAT	No	VMAT	Rectum
5	CR_VMAT	Yes	VMAT	Composite Rectum
6	R_VMAT	Yes	VMAT	Rectum

Table 3.2: The six treatment plans created to compare complete organ optimization structures and treatment techniques.

A plan optimization was deemed successful when the objectives listed in Table 3.3 were met using a plan normalization adjustment of less than $\pm 0.5\%$ following final dose calculation with AAA. Treatment plans which meet all OAR clinical objectives were difficult to produce with no plan normalization adjustment. In a clinical setting, plan normalization may vary up to 5% to meet required goals. Restricting the plan normalization to $\pm 0.5\%$ limited its impact on the treatment plan comparison and ensured the correct balance between target coverage and OAR was achieved mainly during the optimization stage. The small adjustment to plan normalization limited

Structure	Metric (cGy)	Volume
PTV	V5700	$\geq$ 99 %
	V6300	$\leq$ 1.00 cc
CTV	V6000	$\geq$ 99%
RW17.5	V4600	$\leq$ 30%
	V3700	$\leq$ 50%
BW17.5	V4600	$\leq$ 30%
	V3700	$\leq$ 50%
Lt Femoral head	V4300	$\leq$ 2.5%
Rt Femoral head	V4300	$\leq$ 2.5%
Penile Bulb	V4166	$\leq$ 50%

Table 3.3: Planning goals for IMRT and VMAT treatment plans.

the effect of plan normalization on treatment plans, creating a more difficult task for the planner to achieve the clinical goals set in Table 3.3. The clinical objectives, which are routinely utilized at BC Cancer - Victoria for prostate 60 Gy hypofractionated radiotherapy, were adapted from the PROFIT[9] and the CHHiP[8] study dosimetric objectives. The structures RW17.5 and BW17.5 in Table 3.3 were used solely to evaluate the quality of the plans and were contoured from 17.5 mm superiorly to the cranial border of the PTV to 17.5 mm inferiorly to the caudal border of the PTV. All optimizations were performed by a single planner. CRW or RW dose-volume constraints were adjusted during the optimization on a patient by patient basis to produce the lowest rectal dose possible. For the purpose of this study, the rectal volumes receiving 60 Gy, 55 Gy, 50 Gy, 46 Gy and 37 Gy were compared. Pre-SOH and post-SOH CTV, PTV and OAR volumes were also compared along with CTV, PTV and PB mean doses and bladder volumes receiving 60 Gy, 55 Gy, 50 Gy, 46 Gy and 37 Gy.

3.2.4 Statistical Analysis

The statistical testing was done using the non-parametric Wilcoxon signed rank test to compare different plan types as well as observe the change in volume between the pre- and post-SOH CT scans. The tests were two-sided and considered significant at p-value less than 0.01.

3.3 Results

Volume statistics for structures in the pre- and post-SOH CT datasets are summarized in Table 3.4. The majority of structures showed no significant difference between the CT scans with the exception of the PTV which showed a significant difference between pre- and post-SOH volumes ($p = 0.006$). The composite rectum volume was also statistically different from the summed individual rectum and SOH volumes ($p = 0.001$) due to smoothing of the edges of the composite rectum structure.

Structure	Pre-SOH Volume (cc)	Post-SOH Volume (cc)	P-value
CTV	34 ± 7 (25-46)	35 ± 8 (24-49)	0.04
PTV	96 ± 14 (78-120)	102 ± 15 (81-128)	**0.006**
SpaceOAR Hydrogel	-	11 ± 2 (8-12)	-
Bladder	327 ± 197 (154-827)	286 ± 88 (152-431)	0.77
Bladder Wall	73 ± 28 (44-144)	66 ± 13 (43-91)	0.42
Penile Bulb	3 ± 1 (1-4)	2 ± 1 (1-4)	0.60
Rectum	85 ± 35 (45-150)	77 ± 18 (46-103)	0.35
Rectum Wall	36 ± 9 (23-56)	36 ± 5 (28-45)	0.65
Composite Rectum	-	87 ± 19 (58-117)	-
Composite Rectum Wall	-	40 ± 5 (31-47)	-

Table 3.4: Volume information for pre- and post-SOH structures of interest. The volumes were compared using a Wilcoxon signed-rank test. Bold text indicates statistical significance.

Comparisons between all six treatment plans (two pre- and four post-SOH plans) are shown in Table 3.5 while Table 3.6 show the p-values associated with the various treatment plans for the rectal dosimetry. There were no significant differences for mean CTV and PTV coverage with regards to SOH implant, optimization structure and delivery technique. The bladder dose was unaffected by the SOH implant for all five dose levels examined in both IMRT and VMAT plans. Overall, VMAT technique yielded treatment plans with lower bladder dose compared to IMRT, with BV55 Gy, BV50 Gy and BV46 Gy achieving statistical significance ($p < 0.007$). Similarly, the mean penile bulb (PB) dose was found to be unaffected by the SOH implant ($p > 0.24$) while there was statistically significant improvement found in VMAT plans compared to IMRT plans ($p < 0.01$).

Treatment plans produced using full organ structures (ie., R and CR) were compared with treatment plans produced with wall objectives (ie., RW and CRW). Dosi-

metric metrics for the full organ plans are shown in Table 3.7, while Table 3.8 show the p-values of comparison with the two planning approaches. Wall and full structure objectives showed no statistical difference between rectal dose while passing all appropriate plan evaluation objectives with the exception that wall objectives offered a lower RV60Gy ($p < 0.005$) for pre-SOH VMAT treatment plans. Additionally, there was no significant change in bladder dose ($p > 0.05$) and penile bulb ($p > 0.90$) between wall and full organ optimization structures.

Both IMRT and VMAT post-SOH plans resulted in rectal dose-volume reductions of greater than 25% for each metric compared to respective pre-SOH plans. At the prescription dose level, average volume reductions were greater than 80% for all post-SOH plans while they ranged from 28% to 54% at 37 Gy, the lowest dose level evaluated in this study. For both IMRT and VMAT techniques, the use of RW structure in the optimization resulted in significantly lower rectal volumes at doses of 55 Gy, 50 Gy and 46 Gy while there was no significant reduction at the prescription dose level of 60 Gy ($p_{IMRT} = 0.890$, $p_{VMAT} = 0.859$). The use of RW in the optimization compared to CRW did not result in statistically significant reductions in rectal volumes receiving 37 Gy when IMRT ($p=0.019$) was selected as the technique of choice but did result in significant dose reductions for VMAT ($p=0.002$).

3.4 Discussion

SOH has been incorporated into the radiotherapeutic management of prostate cancer in numerous cancer centers as a result of the proven benefits in reducing rectal toxicity and improving QOL.[30,31] Optimal treatment planning techniques are essential to maximize the benefits of SOH. Contoured structures or volumes are used in IMRT or VMAT inverse planning optimization processes to conform dose to the PTV while minimizing the dose to OARs such as the rectum and the bladder. As such, the method in which these optimization structures are contoured and utilized will affect the dosimetric profile of the treatment plan, and therefore the OAR dose. To date, many different optimization structures have been utilized in SOH studies to reduce rectal dose. Rajecki et al.[40] used a control region to shape the dose distribution in the posterior region of the prostate, te Velde et al.[39] chose to contour the SOH and rectal wall together as the CRW to minimize the dose to the true rectum. The SOH is difficult to contour due to low contrast between rectum and SOH on CT scans and as such a registered MR image is required to identify the SOH. This offers new challenges

Plan/Metric	Pre_IMRT	CRW_IMRT	RW_IMRT	Pre_VMAT	CRW_VMAT	RW_VMAT
CTV Mean Dose (%)	102.0 ± 0.7 $(100.5 - 102.9)$	102.4 ± 0.3 $(101.9 - 102.7)$	102.4 ± 0.3 $(102.1 - 102.8)$	102.1 ± 0.2 $(101.8 - 102.6)$	102.1 ± 0.1 $(101.8 - 102.3)$	102.0 ± 0.1 $(101.7 - 102.1)$
PTV Mean Dose (%)	101.6 ± 0.7 $(100.1 - 102.4)$	101.8 ± 0.2 $(101.4 - 102.3)$	101.8 ± 0.2 $(101.5 - 102.1)$	101.7 ± 0.1 $(101.6 - 101.9)$	101.8 ± 0.1 $(101.5 - 101.9)$	101.8 ± 0.2 $(101.5 - 102.3)$
PB Mean Dose (%)	15.2 ± 12.9 $(5.8 - 51.9)$	16.8 ± 16.9 $(5.4 - 66.9)$	16.9 ± 17.0 $(5.7 - 67.7)$	14.0 ± 11.7 $(4.7 - 45.5)$	16.4 ± 17.4 $(5.0 - 68.4)$	16.6 ± 17.3 $(5.0 - 68.0)$
BV60Gy (%)	3.4 ± 1.3 $(1.3 - 5.6)$	3.7 ± 1.5 $(0.9 - 6.8)$	3.6 ± 1.6 $(0.9 - 6.5)$	3.1 ± 1.4 $(1.2 - 6.4)$	3.6 ± 1.6 $(1.0 - 7.4)$	3.6 ± 1.6 $(1.0 - 7.4)$
BV55Gy (%)	6.3 ± 2.9 $(2.1 - 13.5)$	6.6 ± 2.8 $(1.8 - 12.4)$	6.6 ± 2.8 $(1.7 - 12.2)$	5.4 ± 2.4 $(2.0 - 10.7)$	5.9 ± 2.5 $(1.7 - 11.5)$	5.9 ± 2.5 $(1.6 - 11.4)$
BV50Gy (%)	8.4 ± 3.9 $(2.8 - 17.8)$	8.8 ± 3.8 $(2.5 - 16.9)$	8.8 ± 3.7 $(2.4 - 16.7)$	7.3 ± 3.2 $(2.6 - 13.7)$	7.8 ± 3.1 $(2.4 - 14.9)$	7.7 ± 3.2 $(2.2 - 14.7)$
BV46Gy (%)	10.1 ± 4.7 $(3.3 - 20.9)$	10.6 ± 4.6 $(3.2 - 20.9)$	10.7 ± 4.6 $(3.1 - 21.0)$	9.0 ± 3.9 $(3.2 - 16.4)$	9.5 ± 3.7 $(3.1 - 17.9)$	9.4 ± 3.8 $(2.8 - 17.8)$
BV37Gy (%)	15.7 ± 7.6 $(4.7 - 29.8)$	15.8 ± 6.3 $(6.0 - 29.2)$	16.0 ± 6.2 $(5.8 - 29.5)$	14.5 ± 6.8 $(5.0 - 24.8)$	15.2 ± 5.6 $(6.0 - 27.2)$	14.7 ± 5.6 $(5.1 - 26.2)$
RV60Gy (%)	1.1 ± 0.9 $(0.0 - 2.5)$	0.2 ± 0.3 $(0.0 - 0.8)$	0.2 ± 0.4 $(0.0 - 1.4)$	1.6 ± 1.7 $(0.0 - 6.2)$	0.3 ± 0.5 $(0.0 - 1.8)$	0.3 ± 0.4 $(0.0 - 1.3)$
RV55Gy (%)	5.4 ± 4.6 $(0.5 - 16.5)$	1.6 ± 2.4 $(0.0 - 7.8)$	1.2 ± 2.0 $(0.0 - 6.6)$	5.2 ± 4.0 $(0.8 - 13.5)$	1.5 ± 2.1 $(0.0 - 6.7)$	1.1 ± 1.7 $(0.0 - 5.7)$
RV50Gy (%)	8.5 ± 6.6 $(1.3 - 22.8)$	3.3 ± 4.2 $(0.0 - 14.1)$	2.4 ± 3.6 $(0.0 - 11.6)$	8.3 ± 5.4 $(2.4 - 19.0)$	3.1 ± 3.3 $(0.1 - 11.0)$	2.2 ± 3.1 $(0.0 - 9.8)$
RV46Gy (%)	11.0 ± 7.9 $(2.2 - 26.7)$	5.3 ± 5.5 $(0.2 - 18.8)$	3.9 ± 4.9 $(0.1 - 16.3)$	11.2 ± 6.5 $(4.3 - 23.6)$	5.1 ± 4.3 $(0.6 - 14.8)$	3.4 ± 4.3 $(0.1 - 13.4)$
RV37Gy (%)	18.2 ± 10.3 $(5.0 - 35.6)$	12.4 ± 8.0 $(1.7 - 29.1)$	10.3 ± 8.1 $(1.2 - 27.5)$	21.6 ± 8.5 $(11.3 - 37.4)$	15.7 ± 7.3 $(5.4 - 26.9)$	10.4 ± 7.9 $(2.2 - 25.2)$

Table 3.5: DVH metrics of interest for CTV, PTV, PB, bladder and rectum from wall structure optimization objectives planning method. ($Mean \pm Std.Dev.(Min - Max)$)

Treatment Plans		RV60Gy	RV55Gy	RV50Gy	RV46Gy	RV37Gy
Pre_IMRT	**CRW_IMRT**	**0.002**	**0.003**	**0.004**	**0.004**	**0.007**
Pre_IMRT	**RW_IMRT**	**0.002**	**0.002**	**0.002**	**0.002**	**0.002**
CRW_IMRT	**RW_IMRT**	0.890	**0.002**	**0.002**	**0.002**	0.019
Pre_VMAT	**CRW_VMAT**	**0.006**	**0.002**	**0.002**	**0.002**	**0.002**
Pre_VMAT	**RW_VMAT**	**0.003**	**0.002**	**0.002**	**0.002**	**0.002**
CRW_VMAT	**RW_VMAT**	0.859	**0.002**	**0.002**	**0.002**	**0.002**
Pre_IMRT	**Pre_VMAT**	0.917	0.650	0.807	0.650	0.033
CRW_IMRT	**CRW_VMAT**	0.139	0.814	0.917	0.917	0.039
RW_IMRT	**RW_VMAT**	0.091	0.594	0.807	0.553	0.753

Table 3.6: Wilcoxon signed-rank test results comparing treatment plans for rectal DVH metrics. Bold values are statistically significant.

due to organ motion between the CT and MRI as such, the CRW structure offers a simpler contouring process. Finally, numerous studies used the rectum structure to optimize and evaluate the rectal dose.[32,33,38] In the present study, IMRT and VMAT treatment plans were generated using CRW and RW contours. The results of the present study demonstrate that SOH resulted in significant reductions in rectal dose regardless of planning and contouring technique, but that the effect was most marked when optimization was performed with RW contours. Although the VMAT technique

Plan/Metric	Pre_IMRT	CR_IMRT	R_IMRT	Pre_VMAT	CR_VMAT	R_VMAT
CTV Mean (%)	102.2±0.6 (100.4-102.7)	102.3±0.3 (102.1-103.3)	102.4±0.2 (101.9-102.8)	101.9±0.2 (101.8-102.4)	102±0.2 (101.9-102.4)	101.8±0.2 (101.7-102.3)
PTV Mean (%)	101.7±0.5 (100.1-102.1)	101.8±0.2 (101.5-102.1)	101.9±0.1 (101.6-102.2)	101.6±0.1 (101.3-101.8)	101.7±0.2 (101.4-102)	101.7±0.1 (101.6-101.8)
PB Mean (%)	16.3±12.1 (6-51.2)	18.2±15.6 (5.7-64.3)	17.3±15.4 (5.7-63.6)	15.6±13.2 (6-52.9)	18±16.8 (5.6-67.6)	18.4±17.3 (5.5-69)
BV60Gy (%)	3.7±1.9 (1.3-8.8)	3.9±1.7 (1.6-8.9)	3.8±1.9 (1.7-9.6)	3.2±1.2 (1.2-6.3)	3.5±1.3 (1.4-7.3)	3.5±1.4 (1.5-7.6)
BV55Gy (%)	6.4±2.9 (2.1-14.1)	6.7±2.9 (3.1-14.9)	6.4±2.9 (3.2-15.2)	5.4±2.1 (2-10.7)	5.7±2.2 (2.9-12.5)	5.7±2.3 (2.8-12.6)
BV50Gy (%)	8.4±3.8 (2.8-18.2)	8.7±3.6 (4.3-18.9)	8.4±3.5 (4.5-19.1)	7.2±2.8 (2.6-13.9)	7.4±2.9 (4.1-16.2)	7.4±2.9 (4.1-16.4)
BV46Gy (%)	10±4.5 (3.3-21.5)	10.3±4.2 (5.4-22.1)	9.9±4 (5.7-22.1)	8.8±3.5 (3.2-16.8)	8.9±3.4 (5.4-19.4)	9±3.4 (5.2-19.5)
BV37Gy (%)	14.8±7.2 (4.7-30.8)	14.5±5.2 (9.6-28.7)	13.9±5 (9.6-28.7)	13.7±6 (4.9-26.1)	13.5±4.9 (9.7-27.7)	13.4±4.8 (9.1-27.9)
RV60Gy (%)	1.1± 1.8 (0-6.3)	0.1±0.2 (0-0.6)	0.1± 0.2 (0-0.8)	1.7±1.8 (0.1-6.5)	0.1±0.3 (0-1.1)	0.1±0.1 (0-0.3)
RV55Gy (%)	3.9±3.5 (0.5-13.2)	0.7±1.1 (0-4)	0.5±1.1 (0-3.9)	4.3±3.4 (0.9-13.3)	0.8±1 (0-3.8)	0.7±1 (0-3.7)
RV50Gy (%)	6.1±4.9 (1.6-19.3)	1.5±1.9 (0-7.1)	1.3±1.8 (0-6.4)	6.9±4.7 (2.3-18.9)	2.3±1.7 (0.3-6.8)	1.8±2 (0-7.7)
RV46Gy (%)	8±5.9 (2.5-24.3)	2.5±2.6 (0.2-9.7)	2.1±2.4 (0-8.7)	9.6±5.8 (3.9-23.7)	4.9±2.4 (0.8-10)	3.6±3.6 (0-13.1)
RV37Gy (%)	13.2±8.2 (5.2-36.3)	6.9±4.8 (1.9-16.3)	5.8±4.3 (0.3-15.6)	21.8±8.9 (9.6-37.5)	20.1±6 (5.9-26.7)	13.5±9.8 (0-34.8)

Table 3.7: DVH metrics of interest for CTV, PTV, PB, bladder and rectum from full organ optimization objectives planning method. ($Mean \pm Std.Dev.(MinMax)$)

Wall Plans	Full Organ Plans	RV60Gy	RV55Gy	RV50Gy	RV46Gy	RV37Gy
Pre_IMRT	**Pre_IMRT**	0.311	0.116	0.101	0.133	0.075
CRW_IMRT	**CR_IMRT**	0.327	0.480	0.221	0.133	0.173
RW_IMRT	**R_IMRT**	0.866	0.859	0.650	0.917	0.033
Pre_VMAT	**Pre_VMAT**	**0.001**	0.600	0.249	0.249	0.861
CRW_VMAT	**CR_VMAT**	0.038	0.433	0.552	0.075	0.028
RW_VMAT	**R_VMAT**	0.612	0.722	0.382	0.422	0.345

Table 3.8: Wilcoxon signed rank test comparison of treatment plans produced using wall and full organ optimization structures. Bold values are statistically significant.

did not result in significant reductions in rectal dose compared to static field IMRT, it did offer better bladder and penile bulb sparing and conformity of intermediate dose.

Many different dose-fractionation schedules and planning techniques have been utilized for prostate cancer radiotherapy. The pivotal SOH trial by Mariados et al.[32] used an IMRT technique, with a dose of 79.2 Gy in 44 fractions, and rectal doses were evaluated using rectum as a whole solid organ. In the present study, treatment plans were generated using a hypofractionated prescription, 60 Gy in 20 fractions, which has now become a standard option.[9,31,74] The PROFIT protocol has been adopted

clinically by many Canadian centers. This protocol evaluates rectal doses using a RW structure as opposed to the whole organ. As such RW endpoints depicted in Table 3.3 were used in the present study as planning goals for the rectum.

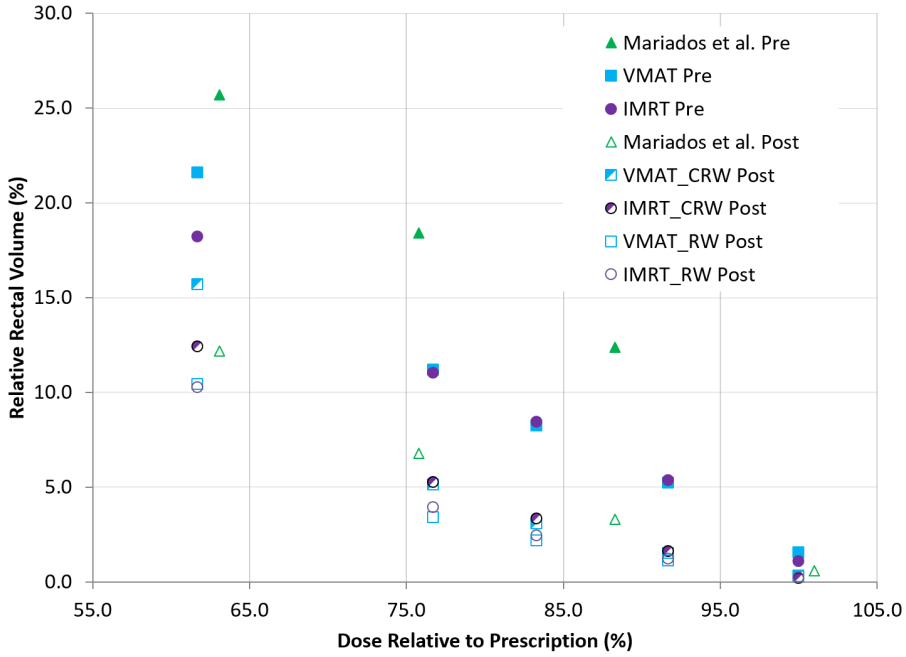

Figure 3.2: Mean rectal dose-volumes for all six treatment plans (Pre_IMRT, Pre_VMAT, CRW_IMRT, CRW_VMAT, RW_IMRT and RW_VMAT) compared to Mariados et al. pivotal trial pre- and post-SpaceOAR © hydrogel (SOH) results.

Figure 3.2 depicts the mean rectal dose-volume results for all six treatment plans generated in this retrospective study in relation to the pre- and post-SOH results obtained in the pivotal SOH trial by Mariados et al. Even though different endpoints, optimization structures, and techniques were used to generate pre- and post-SOH treatment plans in both of these studies, similar gains in rectal sparing were achieved. Gain in rectal sparing of 25% was considered clinically relevant as this gain was seen in RV70Gy between use of three dimensional conformal radiotherapy (3D-CRT) and IMRT for prostate cancer treatment with RV70Gy being linked to high rectal toxicity.[3] Mariados et al. and Song et al.[32,33] observed a 25% reduction in RV70Gy occurring in 95.7% and 97.3% of patients respectively. The corresponding isodose equivalent in the hypofractionated regime is RV55Gy and as such clinically relevant reduction of 25% was seen in 92% (12/13) of patients for RW plans and 85% (11/13) of patients for CRW plans. Furthermore, a 50% reduction of RV55Gy was seen in

85% (11/13) of patients for all post-SOH treatment plans.

The rectal dose in all six wall optimization plans was compared to determine which optimization structure or treatment technique was most effective. The RW optimization structure was shown to result in significantly lower rectal doses than the CRW optimization structure (Table 3.6, Figure 3.2) regardless of planning technique. Although the RW optimization structure was shown to be significantly better for rectal dose, the CRW structure achieved rectal doses similar to those published in other SOH studies such as Mariados et al.[32] (Figure 3.2). This trend followed for all plans with the exception of RV60Gy in both VMAT ($p = 0.859$) and IMRT ($p = 0.890$) plans and RV37Gy in IMRT ($p = 0.019$) plans only. The latter has a p-value which was close to the limit of statistically significant. Meanwhile, the former may be due to the near zero value of RV60Gy metrics in post-SOH treatment plans. In some patients, pre-SOH plans experienced an RV60Gy of zero (IMRT: 6/13, VMAT: 4/13) and as such, there was limited room for improvement of this metric. It is important to note that the CRW structure offered slightly lower RV60Gy in several patients (IMRT: 3/13, VMAT: 5/13) which caused RV60Gy to be inconsistent with the trend seen in other dose metrics. The sparing offered by each respective post-SOH treatment plan was comparable with the reduction seen in many SOH studies.[32,33,38–40]

The six plan types seen in Table 3.1 were reoptimized with full organ rectum and bladder structures as often done in clinical practice. All six wall optimization plans were compared with corresponding full organ optimization plans. There was no statistically significant difference between rectal dose for these two optimization structures with the exception of Pre_VMAT RV60Gy. The two optimization structures produced distributions that appear quite similar from mean, standard deviation and range (Table 3.5 and 3.7) however the wall organ optimization plans had lower RV60Gy in all patients. Additionally, both bladder and penile bulb dose indicated no statistically significant change between plans. The wall optimization structures, such as CRW and RW, offer no significant difference in plans compared to full organ optimization methods as seen in many dosimetric studies.[32,33,40]

Interactions between several optimization objectives is a field that has not been well characterized in inverse optimization planning. Comparing avoidance structures, for example rectal wall and complete rectum, creates a complex interaction between structure optimization objectives. Figure 3.3 compares two plans created with the complete rectum and the rectal wall structures used as optimization objectives respectively. Total dose near PTV remains the same to ensure PTV coverage, while the

dose begins to change near the rectum. A portion of the rectum lies within the PTV and this region has the wall structure dose drop more rapidly (see Pre-IMRT Wall, red profile line). After entering the hollow wall organ, the wall plan has a lower, less aggressive slope while the full organ optimized plan has a larger slope. This change in slope is due to the normal tissue objective becoming dominant in the rectal wall optimized plan while the whole organ objective remains dominant for the full rectum optimized plan, hence the change in slope. Both doses meet around 0.8 cm away from the edge of the PTV where the rectal wall contour begins again. At this point, the two slopes appear similar indicating both are interacting as rectal contour objectives. As seen, the rectal dose curve is difficult to predict due to changing dose avoidance structures used through the optimization process.

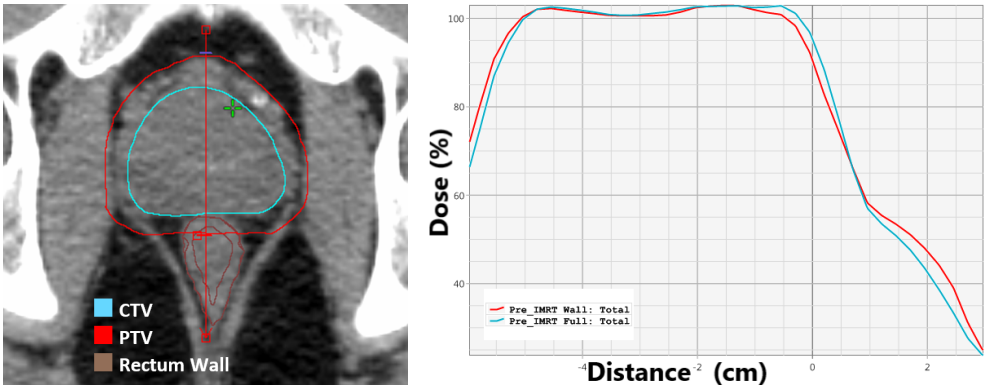

Figure 3.3: Comparison of full rectum (blue) and rectum wall (red) optimization structures. Upper image shows the anatomy information while lower image shows the total dose distribution across the CT scan.

The dose metrics used in the present study were all, except for one, relative to the total volume contoured. For consistency purposes, all target and OAR contours on the anonymized CT datasets were defined and peer-reviewed by a small group of genitourinary radiation oncologists. The contoured volumes, summarized in Table 3.4, indicate no significant difference between pre- and post-SOH implant except for the PTV. Since the PTV was an expansion of the CTV, any differences between pre- and post-SOH CTV were augmented by the application of margins. On average, post-SOH CTV volumes were 35 $\pm$ 8 cc while pre-SOH CTV volumes were 34 $\pm$ 7 cc (p=0.04). The post-SOH CTV volumes were found to be 4.7% larger compared to pre-SOH volumes after an average per patient ratio. The small, but almost statistically significant, difference in the CTV median volume was likely due to a combination of prostate edema from fiducial marker insertion, CTV contouring variation, and differ-

ences in the prostate appearance on the pre- and post-SOH CT scans. The prostate edema effect has been well documented after brachytherapy seed implant.[75] Intra- and inter-observer variability of around 10-18%[56] have been documented for prostate contouring on CT. The pre-SOH CTV structures were based on CT simulation while post-SOH CTV incorporated both CT and MRI offering higher contrast for specific structures.

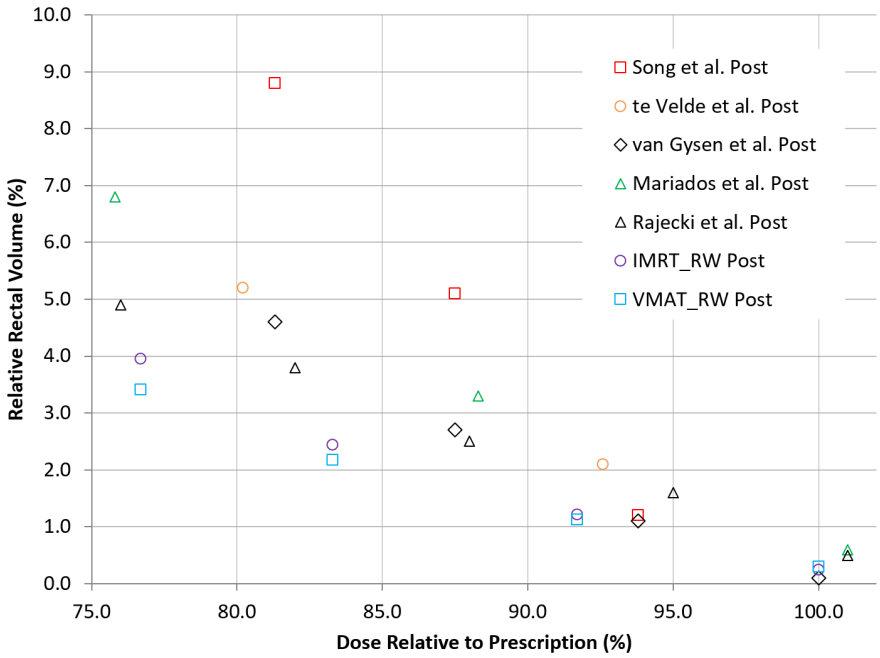

Figure 3.4: Mean volumetric modulated arc therapy and intensity modulated radiotherapy post-SpaceOAR © hydrogel (SOH) rectal dose-volumes achieved in this study with rectal wall compared to other published SOH studies, including Mariados et al.[32] and Rajecki et al.[40]

Most SOH dosimetric studies contoured the rectum from the anus to the rectosigmoid junction[32,33,38–40] with the exception of te Velde et al. which contoured the rectum wall 15 mm superiorly and inferiorly of the caudal or cranial CTV slice for optimization and plan evaluation purposes. As such, the rectum used to generate RW in this retrospective study was also contoured from anus to rectosigmoid junction in order to better compare our study to the current published literature. Mean post-SOH rectal dose-volumes from several studies are presented in Figure 3.4 with the dose relative to the prescription. The RW VMAT and IMRT plans offered the lowest recorded mean rectal dose volumes in this study and were added to Figure 3.2 in comparison. The lowest mean rectal dose-volume metrics are seen with this

retrospective planning study followed by Rajecki et al.,[40] van Gysen et al.,[38] te Velde et al.,[39] Mariados et al.[32] and Song et al.[33] The observable differences in post-SOH rectal dose volumes between published studies can be explained in part due to differences in absolute rectal and PTV volumes. Song et al.[33] had the highest rectal dose volume of dosimetric studies published with dose volumes twice as high for the 80-90% dose range when compared to van Gysen et al.[38] However, patients in Song et al. had a 36% larger average rectum volume and an 8% larger average PTV volume compared to van Gysen et al. The larger rectum and PTV size likely resulted in more overlap between of the PTV and the rectum leading to higher rectum dose volumes. Mean rectal dose volumes reported for the RW optimization structure in this study are slightly lower than those reported in other dosimetric studies and more than 50% lower than van Gysen et al. for the same 80%-90% dose range. However, PTV volumes in this current study were 30% lower on average while rectum volumes were 15% higher, likely leading to lower PTV overlap with the rectum and therefore lower rectal dose volumes.

Bladder dose was evaluated using V60Gy, V55Gy, V50Gy, V46Gy and V37Gy metrics. Each treatment plan passed the clinical objectives, BWV46Gy $< 20\%$ and BWV37Gy $< 40\%$. There were no statistically significant changes in bladder dose pre- to post-SOH in VMAT or IMRT treatment plans ($p > 0.1$) consistent with other studies.[32,33,38] However, VMAT treatment plans resulted in lower bladder dose compared to IMRT treatment plans ($p < 0.007$). Mariados et al. cited a BV70 Gy dose of 11.3% and 11.0% for SOH and non-SOH groups respectively.[32] No statistically significant change in dose between control and SOH treatments was seen by Mariados et al. indicating the modest improvement in urinary QOL observed in this study was not necessarily related to full bladder dose. The prescription equivalent bladder dose-volume for our retrospective study, BV55Gy, was on average 5.4-6.6% with no statistical significance between pre- and post-SOH treatment plans.

Penile bulb has been shown to be an effective analogue to the dose delivered to the tissues surrounding the prostate.[18] Penile bulb dose was evaluated using mean dose to compare between studies with each treatment plan passing clinical objectives, PBV4166cGy $< 50\%$. Hamstra et al.[31] indicated a relationship between the penile bulb dose and erectily dysfunction while reporting a mean PB dose of 14.3 Gy with SOH. Similarly, Mariados et al.[32] observed a pre- to post-SOH decrease in mean PB dose from 22 Gy to 18 Gy. Mean PB dose (Table 3.5) ranged from 12.0 to 14.9% , or an absolute dose of 7.2 to 8.9 Gy. Mean penile bulb dose was found to have no

statistically significant difference between pre- and post-SOH plans ($p > 0.24$) while VMAT treatment techniques yielded lower PB dose with an improvement ranging from 0.5-1.0% ($p < 0.04$). Other studies reported higher pre- and post-SOH mean PB dose while reporting a decrease in mean PB dose from pre- to post-[32] which is inconsistent with the results of this study. The slight increase in mean PB dose seen in this study is attributed to four patients which had an increase of >20% in post-SOH PB dose from pre-SOH plans.

Plan/Metric	Pre_IMRT	CRW_IMRT	RW_IMRT	Pre_VMAT	CRW_VMAT	RW_VMAT
Gradient Measure (cm)	2.49 ± 0.37 (2.04-3.57)	2.39 ± 0.26 (2.11-2.89)	2.44 ± 0.23 (2.18-2.99)	1.65 ± 0.07 (1.52-1.76)	1.72 ± 0.08 (1.63-1.90)	1.66 ± 0.09 (1.52-1.84)
Conformity Index	0.92 ± 0.05 (0.79-0.97)	0.91 ± 0.03 (0.86-0.97)	0.92 ± 0.03 (0.85-0.95)	0.90 ± 0.01 (0.88-0.91)	0.90 ± 0.01 (0.86-0.92)	0.92 ± 0.03 (0.86-0.99)

Table 3.9: Gradient and conformity indices from six treatment plans.

Finally, the gradient measure (GM) and the conformity index (CI) indices were useful indicators of plan quality in addition to the OAR dose (Table 3.4). In Eclipse, GM was defined as the difference between the equivalent sphere radii of the prescription and 50% isodose lines while CI was defined as the volume enclosed by the prescription isodose surface divided by the target volume. VMAT plans had a statistically significant ($p < 0.002$) decrease in GM compared to IMRT while no change in CI was seen between plans. Although VMAT post-SOH treatment plans offered lower bladder dose, mean penile bulb dose and lower GM, IMRT treatment plans were created two times more quickly.

3.5 Conclusions

Rectal dose sparing greater than 25% was achieved in most post- SpaceOAR© Hydrogel treatment plans generated in this planning study. The use of SpaceOAR© Hydrogel significantly reduced rectal dose regardless of optimization structure or treatment technique employed. The rectal wall optimization structure offered a statistically significant reduction in rectal dose compared to the CRW. No statistically significant difference was found between treatment plans planned with use of wall compared to full organ rectum structures as optimization objectives. There was no difference in rectal dose when using VMAT and IMRT treatment techniques, but VMAT offered lower bladder dose, mean penile bulb dose and gradient measure.

Chapter 4

SpaceOAR hydrogel rectal dose reduction prediction model: a decision support tool for clinicians

4.1 Introduction

Prostate is the most common cancer site in Canadian men excluding skin cancers, accounting for 20% of new cases each year and over 10% of cancer deaths in men in 2017.[1] There exist many options for treatment including surgery, external beam radiotherapy (EBRT) and brachytherapy. Many patients choose EBRT as their treatment option, however EBRT results in rectal, urinary and sexual toxicities due to irradiation of organs at risk (OAR) such as the rectum, bladder and penile bulb.[31] The rectum is the dose limiting organ in prostate EBRT due to its proximity to the prostate.[7,71] Products to create space between the rectum and the prostate and thus potentially reduce rectal toxicities during radiotherapy have been suggested. One such product is the SpaceOAR© hydrogel (SOH) which is a polyethylene-glycol based product injected trans-perineally between the prostate and the rectum, producing space between the organs. This additional space allows for sparing of the rectum from high dose, which has resulted in improved quality of life for patients receiving prostate EBRT.[30,32–36]

SOH has been shown to reduce the rectal dose using both intensity modulated radiotherapy (IMRT)[32,33,36,39] and volumetric modulated arc therapy (VMAT) techniques.[34,38,40] However, rectal dose reduction due to SOH has not been shown to be

equal in all patients.[76] Patients with clinical risk factors such as presence of haemorrhoids or previous abdominal surgery have been shown to receive large benefits from SOH.[77] Hutchinson et al. performed a cost effectiveness study to include patient cost due to loss of income in addition to costs incurred due to medical intervention of acute and late side effects.[78] Results indicated SOH incurred an additional $518 cost with 3D-conformal radiotherapy (3D-CRT) while reducing cost by $2640 when treating with high dose stereotactic body radiotherapy (SBRT) or stereotactic ablative radiotherapy (SABR). Additional cost effectiveness models have cited a large range in cost differential of SOH implementation.[78,79] Ensuring optimal management of SOH will allow for the most effective use of resource.

Volume of high dose to the rectum, such as the relative volume receiving 70 Gy (RV70Gy) in 78 Gy RT prescriptions, has been correlated with increased risk of rectal toxicity.[20,54] For 60 Gy in 20 fractions hypofractionated scheme presented in this study, biologically equivalent dose for 70 Gy is 54.4 Gy as such an endpoint of RV55Gy may be used as approximately equivalent for hypofractionated prescription. Several indicators have been correlated to rectal dose-volume and have been used in predictive models. Change in rectal volume from pre-SOH to post-SOH plans has been shown to be proportional to the pre- to post- change in rectal dose.[33] The distance from planning treatment volume (PTV) to rectum has been used to predict the lowest achievable rectum dose in IMRT prostate cancer treatment.[80] Finally, the overlap between the expanded PTV and the rectum has been related to further reduction in rectal dose.[80,81]

The primary aims of this study were to retrospectively determine the pre-SOH CT metrics which were strongly correlated with a change in rectal dose from pre- to post-SOH treatment plans and to create linear models that can be used in nomograms to determine *a priori* patients that would achieve predefined amount of rectal dose sparing. Secondary goal was to minimize the number of contours required on pre-SOH CT for these prediction models in order to create simple and useful decision support tools.

4.2 Methods

Some of the methods described in this study are similar to the methods used in a previous paper.[69] However, different analysis have been applied to the data resulting in unique results and conclusions.

4.2.1 Planning Data Sets

Anonymized CT data set of twenty-two patients with SOH implant between the rectum and the prostate were selected for this institutional ethics board approved retrospective study. Patients on this study received a CT scan 30-60 minutes prior to the fiducial and SOH implant with a comfortably full bladder and empty rectum. Patients were instructed to void and then drink 750 ml of water within a 15 minute window, one hour prior and perform a micro-enema two to three hours prior to the pre-SOH CT scan. SOH was then implanted between the rectum and prostate transperennially via ultrasound guidance followed by implantation of 3-4 gold fiducial markers. A post-SOH CT scan and a pelvic MRI were taken one week post implant with patients following the same bladder and rectum instructions. The MR images (T1 FSPGR and T2 proton weighted) were registered with the post-SOH CT scans via the gold fiducial markers and prostate, and were used to contour structures of interest, in particular the SOH. One patient was removed from the studied data set due to an empty bladder in the pre-SOH CT scan.

4.2.2 Structure Sets

A standardized structure set was used for each patient with the CTV, rectum, bladder, SOH, penile bulb, and femoral heads being contoured. CTV was contoured as the whole prostate gland and 1 cm of the seminal vesicles to emulate patients with intermediate risk disease. PTV was produced by adding margins of 7 mm in all directions with the exception of 5 mm in the posterior direction. The rectum was contoured from the ischial tuberosities to the rectosigmoid junction as a whole organ (rectum) and as a wall structure (3 mm inner wall structure created, RW). A second rectum wall structure was created for plan optimization as per the BC Cancer - Victoria planning guidelines (RW17.5). This is an adapted PROFIT[9] structure which stretches 17.5 mm superiorly and inferiorly of the most extreme PTV slices while maintaining a wall structure. Similarly, three bladder structures were produced, one as a whole organ (bladder), on as a wall structure (BW) and one following BC Cancer - Victoria planning guidelines (BW17.5). SOH and CTV structures were contoured on the post-SOH CT using the fused MR image as a guide. Penile bulb was contoured as the bulbous spongiosum below the GU diaphragm and proximal to the penile shaft. Femoral heads were contoured from the heads of the femur to the area between the greater and lesser trochanters.

4.2.3 Treatment Planning

Treatment planning was completed using Eclipse version 13.6 to produce hypofractionated 60 Gy in 20 fraction single-arc VMAT plans for each CT dataset with final dose calculations being completed by the anisotropic analytical algorithm (AAA, version 11.0.31). Two VMAT treatment plans were created per patient by a single planner, one pre-SOH and one post-SOH. Single-arc VMAT treatment plans were created using inverse optimization (progressive resolution optimizer version 11.0.31) with a series of optimization objectives on various structure contours. Rectal wall (RW) was used as an optimization structure as it has been shown to most effectively reduce the rectal dose when using SOH.[69] Similarly, optimization objectives were placed on PTV, CTV, bladder wall, penile bulb and femoral heads. Treatment plans were deemed optimal once the plan evaluation objectives shown in Table 4.1 were reached with a plan normalization adjustment of less than ±0.5% following the dose calculation. This strict limit on plan normalization adjustment compared to clinical practices (up to 5% adjustment for such hypofractionated prostate plans) was placed to reduce variation between plans due to plan normalization.

Structure	Metric (cGy)	Volume
PTV	V5700	$\geq$ 99 %
	V6300	$\leq$ 1.00 cc
CTV	V6000	$\geq$ 99%
RW17.5	V4600	$\leq$ 30%
	V3700	$\leq$ 50%
BW17.5	V4600	$\leq$ 30%
	V3700	$\leq$ 50%
Lt Femoral head	V4300	$\leq$ 2.5%
Rt Femoral head	V4300	$\leq$ 2.5%
Penile Bulb	V4166	$\leq$ 50%

Table 4.1: Plan evaluation objectives used in VMAT and IMRT treatment planning.

The plan evaluation objectives shown in Table 4.1 were taken from BC Cancer - Victoria planning guideline documentation for hypofractionated, 60 Gy in 20 fractions, prostate radiotherapy. These goals were adopted from the PROFIT[9] and CHHiP[8] studies on hypofractionated prostate radiotherapy. The RW17.5 and BW17.5 structures refer to the secondary wall structure contoured in which both the RW and BW are limited to 17.5 mm superiorly and inferiorly of the final PTV slice.

4.2.4 Metrics of Interest

Several pre-SOH CT geometric descriptors were used as independent metrics in the development of multiple linear regression predictive models. Indepedent metrics used in the models were extracted from Eclipse TPS or RadOnc R package version 1.1.5 using RS dicom file. Rectum, RW, PTV, and CTV volumes were all extracted from Eclipse TPS pre-SOH plan DVH text files. An additional structure was created by a boolean operation between the PTV and the rectum resulting in the volume of rectum in the PTV (RinPTV) in Eclipse TPS prior to file export. Bladder and penile bulb structure volumes were excluded from the process as there was no physical relevance to rectal dose-volume metrics. RinPTV and CTV volumes were also normalized by dividing their volumes by the rectal volume allowing for a relative metric as opposed to an absolute metric. RadOnc R package was a useful tool in accessing further geometric information from structures.[82] Rectum limits were defined using RW creating a rectangular box with dimensions Rx (left/right), Ry (anterior/posterior) and Rz (superior/inferior). A three-dimensional distance comparison was performed through the Hausdorff method which compared two structures, treating them as point clouds. Hausdorff method measures the furthest point between two structures.[83] This technique was employed along each CT slice to return a maximum distance and the mean across all slices was reported as the distance between rectum wall and CTV (RW-toCTV). For this measurement, the height limited rectum wall, RW17.5, was used to ensure consistency in superior/inferior direction. Table 4.2 summarizes the metrics used as independent predictors of the reduction in rectal dose.

Eclipse Software (cc)	**RadOnc R Package (mm)**
Rectum Wall (RW) Volume	Left/Right Rectal Extent (Rx)
Rectum Volume	Anterior/Posterior Rectal Extent (Ry)
PTV Volume	Superior/Inferior Rectal Extent (Rz)
CTV Volume	Distance from RW to CTV (RW to CTV)
Rectum in PTV (RinPTV) Volume	

Table 4.2: Independent metrics used in the predictive models were selected from pre-SOH CT scans using both Eclipse version 13.6 treatment planning software and RadOnc package version 1.1.5.

A number of dependent metrics were chosen for the modeling and quantified. Two rectal dose metrics were measured in pre- and post-SOH plans to determine rectal dose reduction due to SOH implant. A partial integral under the rectal dose volume

histogram (DVH) was used to represent the high dose component to the rectum.

$$HDI(cc) = V_{rectum} \sum_{i=5500\ cGy}^{6000\ cGy} \left(\frac{\Delta D_i}{D_m}\right) V_i \tag{4.1}$$

High dose integral (HDI) was measured from a cumulative DVH where ΔD_i was the bin width (6 cGy for Eclipse TPS DVH text files), D_m was the maximum dose to the organ, V_{rectum} was the rectum volume and V_i was the volume in the corresponding bin. HDI was evaluated for pre- and post-SOH treatment plans from RV55Gy to RV60Gy to represent rectum dose linked to rectal toxicity.[3] Pre-SOH RV55Gy (Pre-RV55), pre- to post-SOH change in HDI (ΔHDI) and change in RV55Gy (ΔRV55) were used as dependent metrics in linear models. Rectal dose reduction metrics are represented in Figure 4.1.

4.2.5 Statistical Analysis

Modeling began by calculating Pearson correlation coefficients to identify anatomical features well correlated to dependent metrics. Independent metrics with high Pearson correlation coefficients were included in multiple linear regression models. Prior to modeling process, any independent metrics indicating dependence were identified and only one of them was selected for modelling purposes. As expected both PTV and CTV as well as rectum and rectum wall volumes were found to be dependent due to contouring methods. CTV volume was used over PTV volume as CTV represents a clinical region of interest while PTV is a geometric volume. Furthermore, contour variations are amplified when a PTV margin is applied. Rectum volume and rectum wall volume were used interchangeably, but separately.

All independent metrics were initially included in the multiple linear regression model of a selected dependent metric and then reduced through use of Akaike information criterion (AIC) and variance inflation factor (VIF). AIC represents the relative quality of the linear regression models with lower values indicating more effective models. A stepwise AIC approach was used in removing independent variables to generate an optimal linear regression model for each dependent metric (ΔHDI, ΔRV55 and Pre-RV55). VIF quantifies the severity of multicolinearity between variables. Independent metrics with large VIF were also removed from the model until VIF was acceptable for all variables (VIF < 5).[84] Independent metrics chosen for multiple linear regression were associated with a beta coefficient, β. These coefficients combined

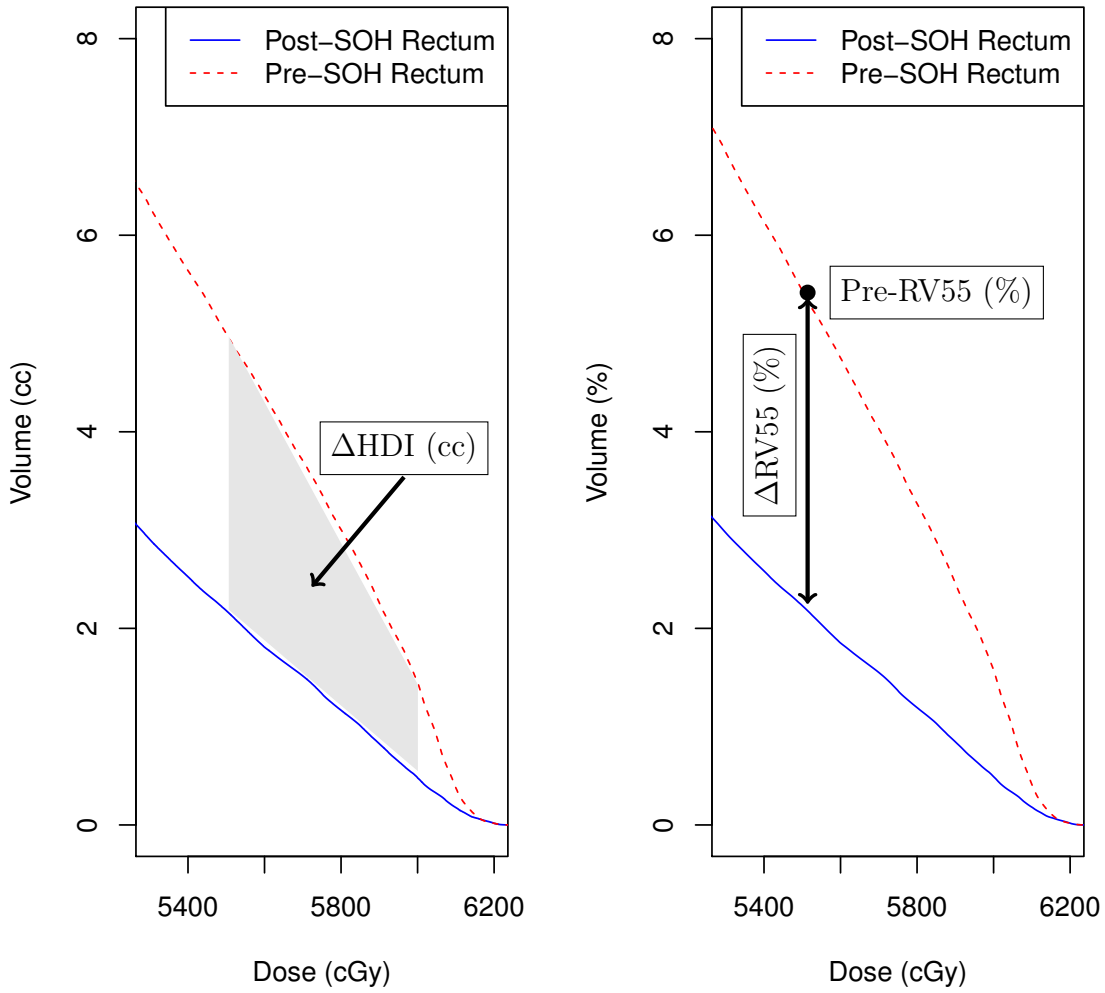

Figure 4.1: A visual representation of rectal dose metrics (ΔHDI, ΔRV55, Pre-RV55) used as depedent metrics in multiple linear regression modelling. Cumulative DVHs are displayed with left and right represented in absolute and relative volumes respectively. This DVH produces rectal dose metrics as follows: ΔHDI = 0.161 cc, ΔRV55 = 3.21% and Pre-RV55=5.44%.

with the metric creates a linear representation of the data as shown below.

$$y = \beta_1 x_1 + \beta_2 x_2 + \beta_3 x_3 + ... \tag{4.2}$$

In this expression, y is the dependent metric, x_i are the independent metrics used

in multiple linear regression models and β_i are the beta coefficients. The relative contributions of each of these independent metrics in describing variance of the data may be described through a structure coefficient, r_s.[85] The structure coefficient describes the contribution of independent metrics to the variance of the dependent metric.

$$r_s = \frac{r_{pears}}{\sqrt{R^2}} \tag{4.3}$$

The structure coefficient is described by dividing Pearson correlation coefficient, r_{pears}, by the square root of R^2 from the model. The squared structure coefficient, r_s^2, will be reported in this study.

Two models were produced per independent predictive metric: an advanced model with metrics defined using RadOnc package (Model 1) and a simpler model using metrics available in Eclipse TPS (Model 2). The selected models were evaluated using leave-one-out cross-validation (LOOCV) techniques reporting mean absolute error (MAE) and relative MAE (%MAE).[86] MAE represents average absolute difference between predicted and actual metrics. %MAE was reported by normalizing MAE by range of dependent metric. R version 3.5.3 was used for statistical analysis. Statistical tests with p-values less than the statistical significance level of $\alpha = 0.01$ were deemed statistically significant.

4.3 Results

Table 4.3 shows the measured min, max, mean and standard deviation of the dependent rectal dose metrics for the 21 patients used to generate predictive models while Table 4.4 summarizes the statistics for the independent pre-SOH CT scan metrics. Table 4.5 summarizes the Pearson correlation coefficients between the dependent metrics (ΔHDI, ΔRV55, Pre-RV55) and the independent variables. Pearson correlation coefficients between dependent metrics and RinPTV volume indicated strong, statistically significant, positive correlation (R>0.68). Normalized RinPTV was also highly correlated with dependent metrics with correlations achieving statistical significance for ΔRV55 and Pre-RV55. RWtoCTV led to a strong, statistically significant, negative correlation with ΔRV55 and Pre-RV55. No other Pearson correlation coefficients showed statistically significant results.

Metric	Mean ± Std. Dev (Min-Max)
ΔHDI (cc)	0.191 ± 0.122 (0.019-0.425)
ΔRV55 (%)	4.5 ± 3.0 (0.8-10.8)
Pre-RV55 (%)	5.9 ± 3.7 (0.8-13.5)

Table 4.3: Statistical summary of the dependent metrics for the 21 patients used to model change in rectal dose after SOH implant.

Metric	Mean ± Std. Dev (Min-Max)
Rectum Vol. (cc)	79.2 ± 32.1 (35.5-149.7)
Rectal Wall Vol. (cc)	35.5 ± 9.7 (20.5-57.8)
CTV Vol. (cc)	39.9 ± 17.2 (24.6-91.5)
Normalized CTV Vol. (%)	62.3 ± 51.7 (19.6-257.7)
RinPTV Vol. (cc)	2.4 ± 1.5 (0.1-5.3)
Normalized RinPTV Vol. (%)	3.4 ± 2.4 (0.2-10.4)
RWtoCTV (cm)	2.18 ± 0.26 (1.71-2.63)
RWtoCTV Cubed (cc)	10.36 ± 4.06 (4.99-18.21)
Rx (mm)	49.9 ± 7.9 (37.5-63.7)
Ry (mm)	65.1 ± 9.5 (46.8-92.2)
Rz (mm)	104.0 ± 15.3 (80.0-137.5)

Table 4.4: Statistical summary of independent geometric variables for the 21 patients extracted from pre-SOH CT scans using Eclipse software and RadOnc R package.

Metrics	Pearson Correlation Coefficients		
	ΔHDI (cc)	**ΔRV55 (%)**	**Pre-RV55 (%)**
Rx (mm)	0.32	-0.21	-0.17
Ry (mm)	0.31	0.12	0.16
Rz (mm)	-0.16	-0.46	-0.42
Rectum Vol. (cc)	0.13	-0.38	-0.33
Rectum Wall Vol. (cc)	0.11	-0.37	-0.32
RinPTV Vol. (cc)	**0.72**	**0.68**	**0.76**
Normalized RinPTV Vol. (%)	0.54	**0.90**	**0.92**
CTV Vol. (cc)	0.24	0.22	0.27
Normalized CTV Vol. (%)	0.00	0.29	0.32
RW to CTV Dist. (cm)	-0.32	**-0.56**	**-0.61**
RW to CTV Dist. Inv. Cubed (cc^{-1})	0.40	0.33	**0.54**

Table 4.5: Pearson correlation coefficients between dependent metrics and independent variables. Bold entries represent statistical significance.

4.3.1 Change in High-Dose Integral (ΔHDI) Models

Change in high-dose integral, ΔHDI, an absolute dose-volume metric, ranged from 0.019 to 0.425 cc. ΔHDI models retained RinPTV and CTV volumes for Model 2

($p < 0.001$, R^2=0.57) with the addition of Rx, Ry and Rz for Model 1 ($p < 0.001$, R^2=0.72). Contributions to the linear model (ie., β and r_s^2) are shown in Table 4.6. RinPTV volume maintains the largest structure coefficient in both models. This dependent rectal dose metric is not commonly used in the clinical setting to evaluate rectal dose reduction, as such the change in RV55Gy (ΔRV55) was also explored as a dependent metric to predict rectal dose reduction.

Metrics	**ΔHDI Models**			
	Model 1		**Model 2**	
	$\boldsymbol{\beta}$	$\mathbf{r_s^2}$	$\boldsymbol{\beta}$	$\mathbf{r_s^2}$
Constant	0.46 ± 0.58	-	0.73 ± 0.51	-
RinPTV Vol. (cc)	0.063 ± 0.012	0.71	0.058 ± 0.013	0.91
CTV Vol. (cc)	0.0012 ± 0.0011	0.08	0.0016 ± 0.0011	0.10
Rx (mm)	0.0064 ± 0.0023	0.14	-	-
Ry (mm)	-0.0016 ± 0.0020	0.13	-	-
Rz (mm)	-0.0016 ± 0.0013	0.03	-	-

Table 4.6: Beta, β_i, and squared structure, r_s^2, coefficients for models predicting change in high-dose integral (ΔHDI) under the rectal DVH.

4.3.2 Change in RV55Gy (ΔRV55) Models

Change in RV55Gy, ΔRV55, a relative dose-volume metric, varied between 0.8 and 10.8% for the 21 patients selected demonstrating large variations in rectal dose sparing using SOH. ΔRV55 was predicted using normalized RinPTV, rectum volume and RWtoCTV for Model 1 ($p < 0.0001$, R^2=0.83) and with only normalized RinPTV volume for Model 2 ($p < 0.0001$, R^2=0.81). Model coefficients are summarized in Table 4.7. The normalization of RinPTV volume produced higher Pearson correlation coefficients compared to RinPTV volume metric resulting in a metric with structure coefficients of about 1.00. Although more clinically relevant, ΔRV55 on its own does not offer enough information regarding pre-SOH rectal dose and must be combined with pre-SOH dose information to become clinically useful.

Metrics	ΔRV55 Models			
	Model 1		Model 2	
	β	r_s^2	β	r_s^2
Constant	0.46 ± 0.58	-	0.73 ± 0.51	-
Normalized RinPTV Vol. (%)	1.25 ± 0.18	0.97	1.10 ± 0.12	1.00
RW to CTV (cm)	2.34 ± 1.68	0.38	-	-
Rectum Vol. (cc)	-0.0077 ± 0.0101	0.18	-	-

Table 4.7: Beta, β_i, and squared structure, r_s^2, coefficients for models predicting change in RV55Gy (ΔRV55).

4.3.3 Pre-SOH RV55 Gy (Pre-RV55) Models

Pre-SOH RV55Gy (Pre-RV55) models may offer insight to relative change in rectal dose, a metric often cited in SOH papers. Pre-RV55 was measured to be 5.9±3.7 % on average and ranged from 0.8 to 13.5% for the 21 patients analyzed. Pre-RV55 was predicted with the use of many metrics, including rectum or RW, CTV and RinPTV volumes (Table 4.8). The distance between RW and CTV was cubed and produced an effective correlation for Model 1 ($p < 0.0001$, $R^2 = 0.87$) but was omitted for Model 2 which only includes RW and RinPTV volumes as predictors ($p < 0.0001$, $R^2 = 0.80$). RinPTV contributed most to models with structure coefficients of 0.66 and 0.71 respectively.

Metrics	Pre-RV55 Models			
	Model 1		Model 2	
	β	r_s^2	β	r_s^2
Constant	-8.66 ± 5.15	-	7.42 ± 1.52	-
RinPTV Vol. (cc)	0.92 ± 0.47	0.66	2.10 ± 0.26	0.71
Rectal Wall Vol. (cc)	-	-	-0.19 ± 0.04	0.13
RW to CTV Inv. Cube (cc^{-1})	48.9 ± 17.3	0.34	-	-
Rectum Vol. (cc)	-0.029 ± 0.01	0.13	-	-
CTV Vol. (cc)	0.072 ± 0.026	0.08	-	-
Ry (mm)	0.098 ± 0.057	0.03	-	-

Table 4.8: Beta, β_i, and squared structure, r_s^2, coefficients for models predicting pre-SOH RV55Gy (Pre-RV55).

4.3.4 Leave-One-Out Cross Validation (LOOCV)

Results from LOOCV analysis resulted in MAE and %MAE for each model as reported in Table 4.9. ΔRV55 models offered lowest %MAE at 9.6% and 11.8% while

ΔHDI models offered highest %MAE at approximately 20%.

Model	MAE	%MAE
ΔHDI Model 1 (cc)	0.085	20.9%
ΔHDI Model 2 (cc)	0.081	20.0%
ΔRV55 Model 1 (%)	1.27	12.9%
ΔRV55 Model 2 (%)	0.96	9.6%
Pre-RV55 Model 1 (%)	2.07	16.3%
Pre-RV55 Model 2 (%)	1.85	14.5%

Table 4.9: Results from leave-one-out cross validation (LOOCV) statistical test to examine effectiveness of chosen models. Mean average error (MAE) and relative mean average error (%MAE) were reported.

4.4 Discussion

This study sought to produce predictive models to inform on effectiveness of SOH implant regarding rectal dose sparing based on data from 21 patients. Metrics quantifying high dose (Pre-RV55, ΔRV55 and ΔHDI) were used as dependent dose metrics in the linear models. Independent pre-SOH volume metrics of interest were selected based on previous studies and Pearson correlation coefficients. Pearson correlation coefficients indicated that volume of RinPTV (absolute and normalized) and RWtoCTV distance (absolute and inverse cubed) provided highest correlation to dependent rectal dose metrics (Table 4.5). These findings are in line with other studies. More specifically, Wang et al.[80] found the overlap between PTV and rectum was related to reduction of rectal dose and the distance from PTV to the rectum was used to predict lowest achievable rectal dose. Mariados et al.[32] indicated the change in rectum volume from pre- to post-SOH plans was shown to be proportional to change in rectal dose. Rectal volume metrics such as rectum or RW volumes and RinPTV were correlated to the change in rectal dose metrics in this retrospective study (Table 4.5).

Stepwise approach of linear regression models using AIC and VIF for model selection retained a variety of independent variables for each dependent metric. Two models were produced for each dependent metric: Model 1 and Model 2. Model 1 represented best fit with metrics available using both RadOnc R package and Eclipse TPS. RadOnc R package metrics require additional computation time making them less clinically practical where decisions must often be made promptly. As such, Model 2 was developed without application of RadOnc metrics using only volumes avail-

able from Eclipse treatment planning software. These models were evaluated with LOOCV which removed a single sample from the model and re-performed the linear regression. A new predicted value was compared to the measured value of the model for all 21 datasets. The difference in measured and predicted was averaged over all datasets, producing a mean absolute error (MAE). Subsequently, the relative mean absolute error (%MAE) was reported. %MAE indicated average percent difference between actual and predicted values. All linear regression models were evaluated in this manner.

Relative MAE was reported to be 9.6-14.6% for ΔRV55 and Pre-RV55 models, increasing to approximately 20% for ΔHDI models. This metric from LOOCV model evaluation represents the uncertainty in the model after predicting a dependent rectal dose reduction metric. Increasing the number of patients within the modeling process should decrease the %MAE as variation from the linear model decreases thus improving the quality of predictive models.

Describing rectal dose information through a single metric is difficult to accomplish. High rectal dose has been associated with increased risk of rectal toxicity,[20,54] and should be encompassed in the metric of interest for rectal dose reduction. RV70Gy is a commonly used metric in prostate radiotherapy plan evaluation for 78 Gy prescription treatments. A 25% decrease in RV70Gy was reported when moving from 3DCRT to IMRT as a treatment technique.[3] This metric has been used in SOH studies to evaluate the effectiveness of SOH implant for rectal dose reduction.[22,32,33] Corresponding relative dose prescription in hypofractionated prescription is approximately RV55Gy. However, a single dose-volume endpoint does not encompass the entire high dose-volume region. As such, a novel metric was designed to represent rectal dose reduction in linear regression models, termed the high dose integral (HDI). It was hypothesized that ΔHDI from pre- to post-SOH may be predicted using pre-SOH anatomical metrics for representation of rectal dose reduction, offering higher correlation compared to a single metric, such as RV55Gy.

HDI corresponded to the integral under rectal DVH from RV55Gy to RV60Gy which encompassed rectal dose region of interest. ΔHDI was found to be strongly and positively correlated to RinPTV volume and as such was used to generate model parameters seen in Table 4.6. ΔHDI prediction model 1 achieved an R^2 of 0.72 while using Rx, Ry and Rz as well as CTV and RinPTV volumes. This ΔHDI model has a statistically significant correlation and %MAE of 20.9%. Several metrics in this model are unavailable in standard Eclipse treatment planning software. Implementation

of these models to the Varian API was considered, but was not pursued. Instead, model 2 was developed to improve clinical applicability even though the model has a smaller but still strong R^2 of 0.57 along with a %MAE of 20.0%. ΔHDI may capture a broader representation of rectal dose reduction due to SOH but it is difficult to interpret clinically. As such, models for RV55Gy, a common metric used in plan evaluation, were also developed.

Prediction of ΔRV55 provides a more intuitive model for rectal dose reduction. ΔRV55 Model 1 and Model 2 presented in Table 4.7 offered R^2 values of 0.83 and 0.81 respectively and achieved statistical significance. RWtoCTV ($r_{pears} = -0.56$) offered a higher correlation compared to inverse cubed metric ($r_{pears} = 0.33$). %MAE for each model was near 10% indicating less variation compared to ΔHDI. ΔRV55 models provided higher R^2 correlation, lower %MAE and lower p-value compared to ΔHDI models. This finding disproved our hypothesis that ΔHDI may be a better predictor of SOH rectal dose sparing compared to a single rectal dose metric. Finally, ΔRV55 is a more intuitive metric making these models more clinically applicable. However, this metric took a single point along rectal DVH while ΔHDI examines the entire high dose region.

Model	P-Value	R-Squared	MAE	%MAE
ΔHDI Model 1 (cc)	$p < 0.001$	0.72	0.085	20.9%
ΔHDI Model 2 (cc)	$p < 0.001$	0.57	0.081	20.0%
ΔRV55 Model 1 (%)	$p < 0.0001$	0.83	1.29	12.9%
ΔRV55 Model 2 (%)	$p < 0.0001$	0.81	0.96	9.6%
Pre-RV55 Model 1 (%)	$p < 0.0001$	0.87	2.07	16.3%
Pre-RV55 Model 2 (%)	$p < 0.0001$	0.80	1.85	14.5%
%ΔRV55 Model (%)	$p < 0.01$	0.31	17.8	17.8%

Table 4.10: Summary of p-value, R squared and MAE from LOOCV for each linear regression model presented.

Percent reduction in RV55 Gy (%ΔRV55) was used in many SOH studies and may provide guidance for clinicians. Pre-RV55 models were produced and combined with ΔRV55 models to produce a model predicting %ΔRV55.

$$\%\Delta RV55 = \frac{\Delta RV55\ Model\ 2}{Pre-RV55\ Model\ 2} \times 100 \tag{4.4}$$

Both ΔRV55 and Pre-RV55 models had R^2 larger than 0.80 as seen in Table 4.10. Combination of ΔRV55 Model 2 and Pre-RV55 Model 2 resulted in a statistically significant model predicting %ΔRV55 but with much weaker correlation ($p < 0.01$,

R^2=0.31). Using LOOCV yielded %MAE= 17.8%. In this model, any predicted values larger than 100% were reallocated a value of 100% reduction. A reduction of 100% occurred in 4/21 patients while a reduction larger than 25% was seen in 20/21 patients. Even though %ΔRV55 model had lower correlation compared to ΔHDI and ΔRV55 models, this model may be more clinically relevant for SOH management.

Producing clinically useful decision support tools for SOH management was a priority when developing these predictive models. Nomograms for each dependent metric (using Model 2) were produced as shown in Figures 4.2 to 4.4 to estimate ΔHDI, ΔRV55 and Pre-RV55 respectively. A workflow diagram (Figure 4.5) was produced as per radiation oncologist guidance to select *a priori* patients that potentially could benefit most dosimetrically from SOH implant and therefore aid in SOH resource management. Limits for the workflow were chosen from Mariados et al.[32] which indicated a mean post-SOH RV70Gy of 3.3%. Pre-RV55 output below this value may not receive significant rectal dose reduction from SOH implant due to already low dose. A similar limit may be placed on %ΔRV55 removing patients below 25% rectal dose reduction, a threshold used to indicate effectiveness of SOH implant in various studies. For the 21 patients in this retrospective study, %ΔRV55 was predicted through the linear model to be 77.6±16.2% with a minimum reduction of 43.7%. All patients were predicted to experience a reduction greater than 25% with 20/21 patients predicted to experience reduction greater than 50%. In measured results, 20/21 experienced reduction of 25% with a minimum reduction of 20% and 18/21 experienced a reduction greater than 50%. As such, the %ΔRV55 model over-predicted relative change in rectal dose. A limit of %ΔRV55 below 25% may not significantly reduce number of patients but does ensure SOH effectiveness. Limits on Pre-RV55 and %ΔRV55 may be adjusted to remove greater or fewer patients. Current limits on Pre-RV55 Model 2 removed 7/21 patients from implant pool while %ΔRV55 removed one additional patient. Overall, suggested workflow limits removed a third of patients in which SOH was deemed least dosimetrically effective.

These models may offer effective SOH management guidelines, however they have many limitations. The maximum ΔRV55 from pre- to post-SOH observed was approximately 10% (Table 4.3) and as such any value predicted above this value may have a large associated error. Limits could be applied to independent geometric variables (Table 4.4), specifically RinPTV, but this would limit the application of the model. For a patient with RinPTV volume=0 cc, many of these models will not be applicable.

Models were built using dosimetric information from plans where a specific PTV margin was applied. Other PTV margins may change RinPTV metrics along with RV55Gy dose. Reducing PTV margins would reduce RinPTV, which subsequently reduces predicted Pre-RV55 and change in rectal dose metrics. Metrics collected in this study were measured using specific guidelines. Varying these guidelines would result in changes to linear regression correlations and coefficients.

Linear regression has been applied in a study by Hwang et al. which produced models correlating hydrogel placement, perirectal space creation and rectum dosimetry for prostate SBRT.[87] This model was used to evaluate hydrogel placement as a learning tool to reduce learning curve seen in hydrogel implant.[88] Models were produced based on post-SOH CT scans with distance from CTV to rectum as a primary metric to predict rectal dosimetric endpoints. The definition of distance between CTV and rectum was different compared to the study presented here but the use of a similar metric between models is significant. A pre-SOH decision model study was completed by van Wijk et al.[76] which produced a virtual spacer implant model. This simulated an implantable rectal spacer (IRS) to help identify patients in which IRS was not beneficial. This study offered a decision support tool which provides cost effectiveness analysis along with toxicity prediction. Models presented here predicted change in rectal dose using nomograms after a single pre-SOH CT scan and contouring of rectum and CTV structures. Implementing these linear models requires an additional CT scan prior to SOH implant. This additional step in patient process increases dose, requires further resources for contouring, CT scan scheduling and may be subject to error from bladder and bowel preparation methods.

Identifying patients that would benefit dosimetrically earlier in the process would aid in decision making for doctors. Applying these models to diagnostic CT scans would improve the workflow of SOH management. Identifying patients for which SOH is most effective during the diagnostic phase would improve the implementation of such a process. Such a task may be performed with radiomics packages available in languages such as R and Python. However, new linear regression models would need to be developed for application with diagnostic CT scans. No RT specific bladder and bowel preparation is completed by patients receiving a diagnostic CT and therefore correlations between anatomical features would differ. Additionally, the lack of specific bowel preparation may reduce correlation with dose as patients perform preparation prior to planning CT and radiotherapy treatment. This causes a change in rectal size greatly affecting relative metrics applied in linear regression models.

4.5 Conclusions

Predictive models were created for change in high dose integral (ΔHDI), change in RV55 Gy (ΔRV55) and pre-SOH RV55 Gy (Pre-RV55). All models reached statistical significance with ΔRV55 and Pre-RV55 models offering an R^2 greater than 0.80 and mean absolute error between 9.6-16.3%. Volumes of rectum in PTV, CTV and rectal wall offered highest correlation with dependent metrics. Distance between rectal wall and CTV contours offered high Pearson correlation but was not included in Eclipse based only models (ie., Model 2). Applying a lower limit of 3.5% on the Pre-RV55 removed a third of patients (7/21). Linear predictive models along with specific limits offer decision support tools for more effective SOH implant management.

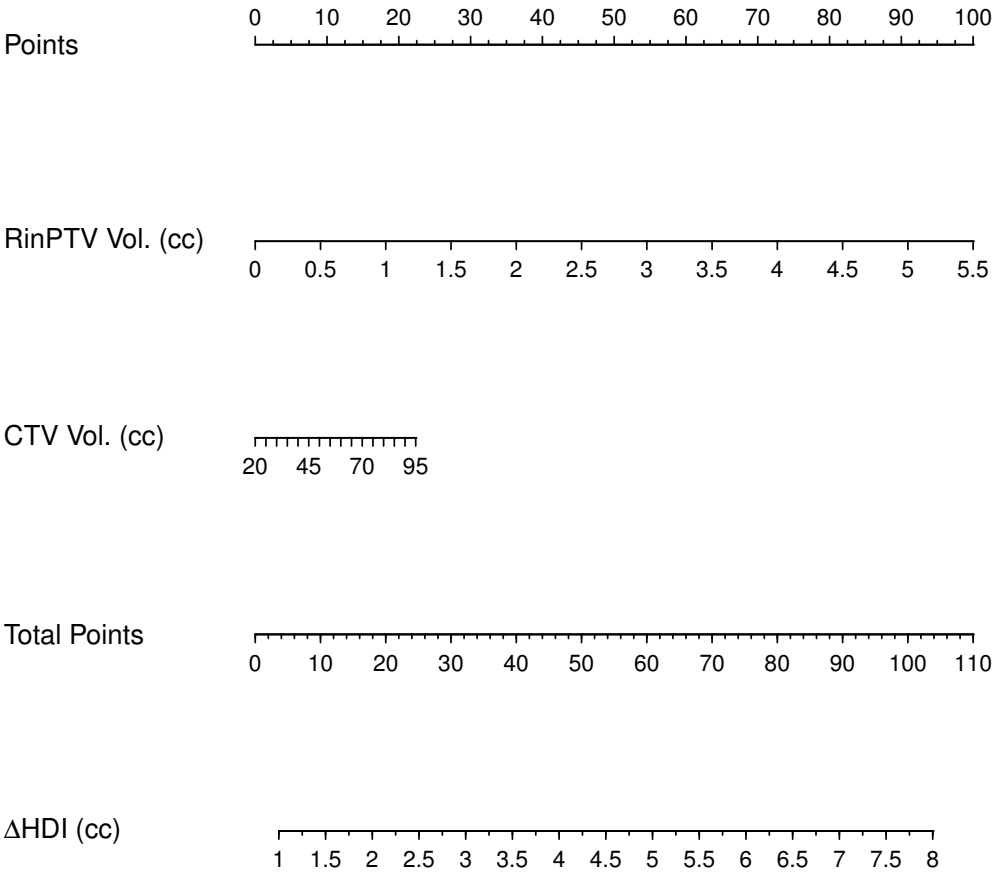

Figure 4.2: Nomogram prepared from change in HDI Model 2. RinPTV and CTV volumes can be used to determine the predicted change in HDI from pre- to post-SOH implant.

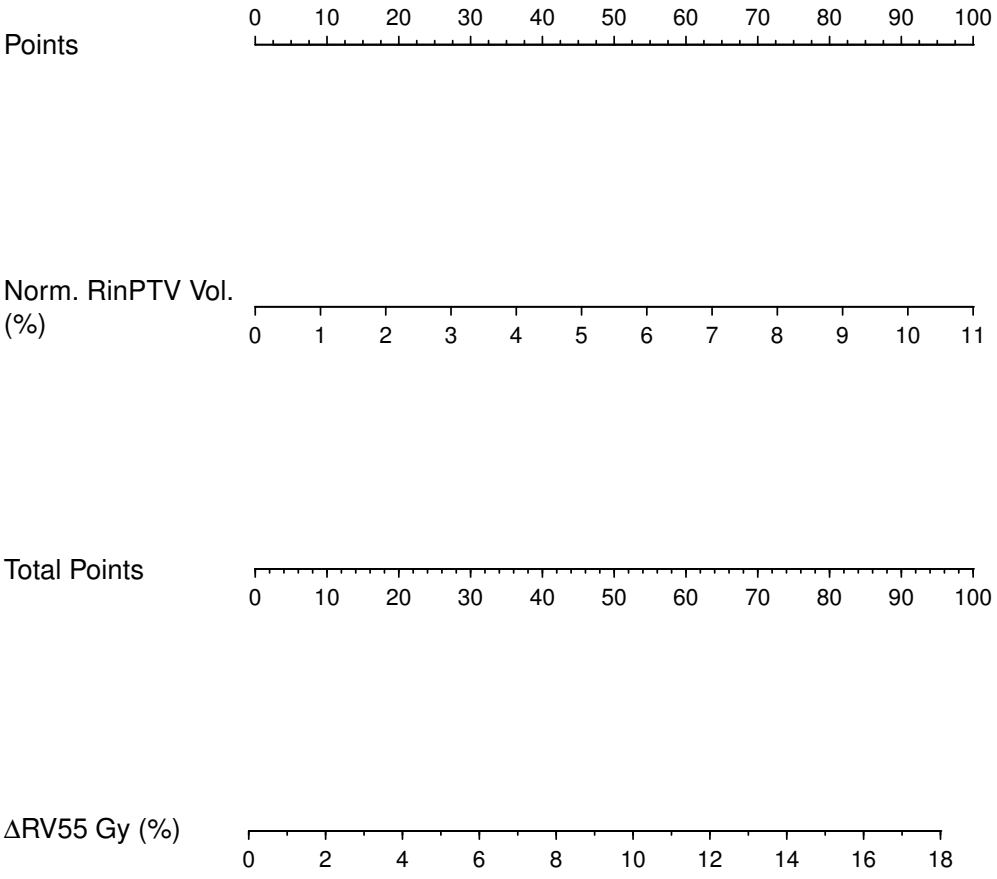

Figure 4.3: Nomogram prepared from change in RV55 Gy Model 2. The points contributed from the normalized RinPTV volume will correlate to the change in RV55 Gy metric as per model.

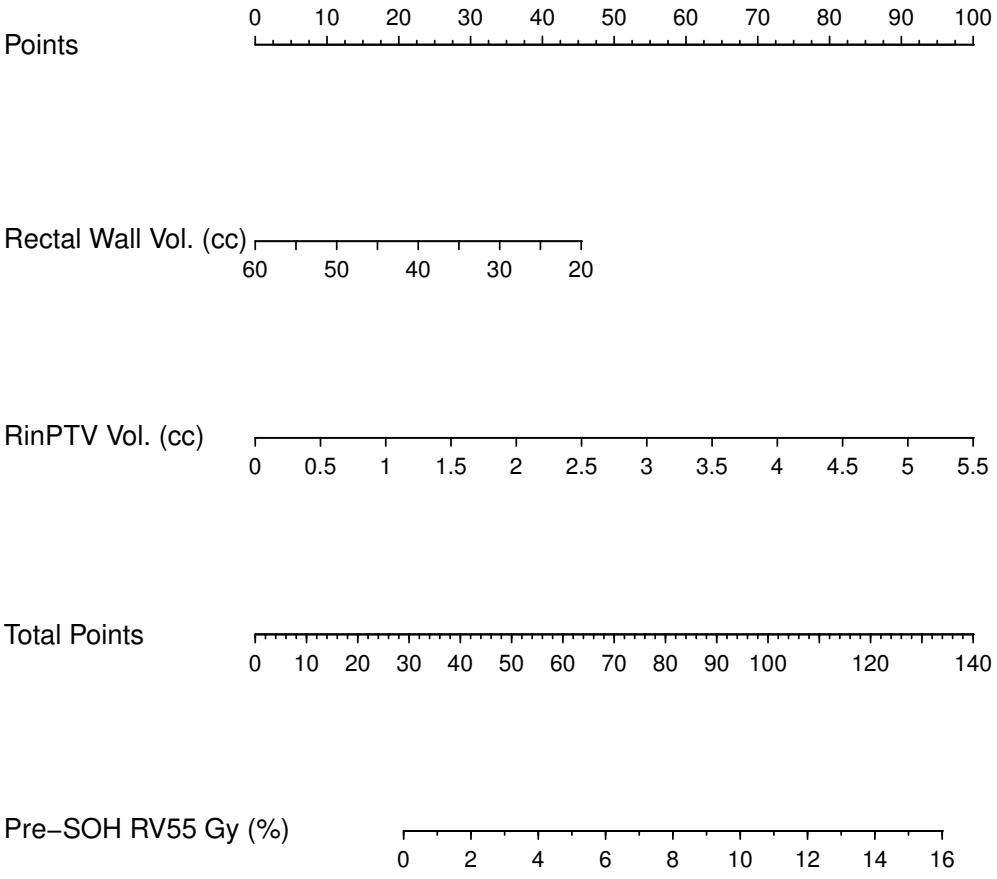

Figure 4.4: Nomogram prepared from pre-SOH RV55 Gy Model 2. Both rectal wall and RinPTV volumes contribute to the model, from which the pre-SOH RV55 Gy metric can be predicted.

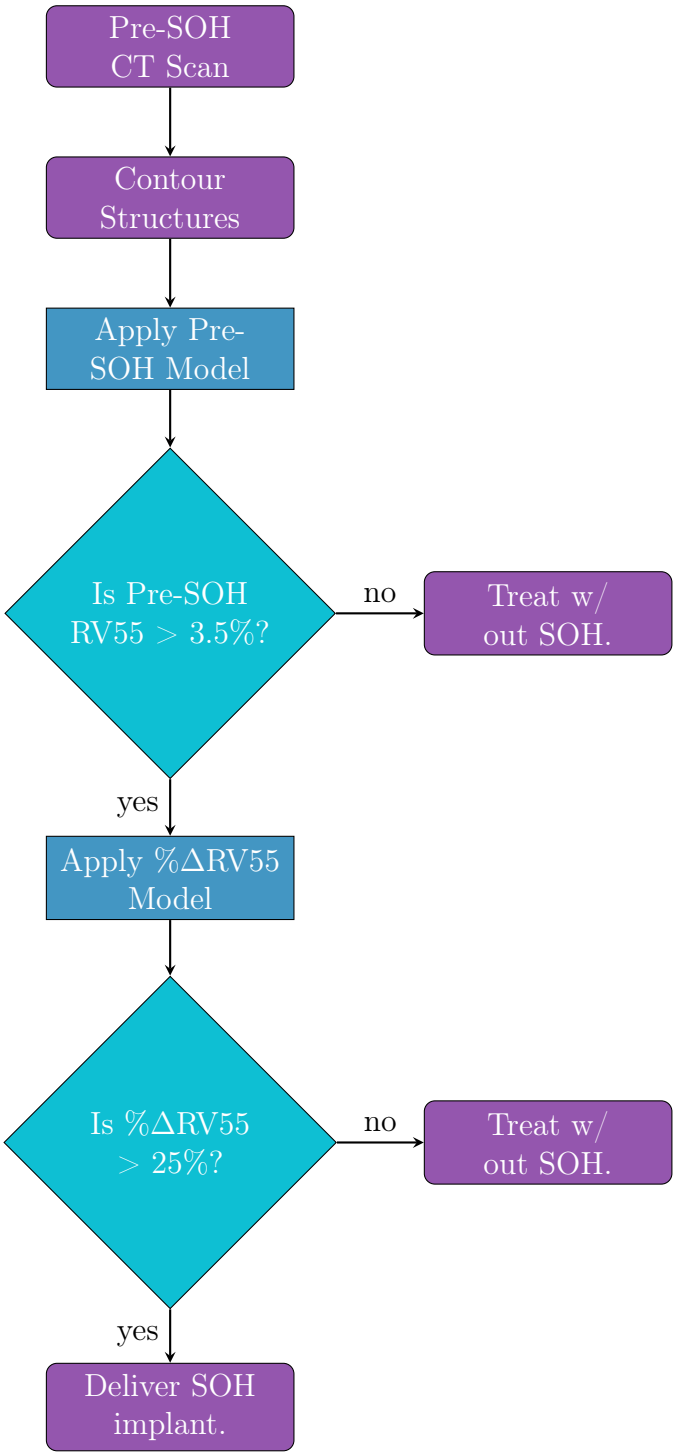

Figure 4.5: Decision making flow chart applying pre-SOH RV55 Gy and %ΔRV55 models. A limit of 3.5% was used for pre-SOH RV55 and a percent reduction of 25% was expected from SOH use.

Chapter 5

Conclusions

The purpose of this research was to examine application of SpaceOAR © hydrogel (SOH) in prostate cancer radiotherapy. Optimal treatment technique and optimization structure for treatment planning were determined. Several models were produced to predict rectal dose reduction based on pre-SOH CT scans. These tools aided in clinical implementation of SOH at BC Cancer - Victoria.

A retrospective planning study evaluating optimal treatment technique and optimization structure was performed on thirteen anonymized CT sets. Six treatment plans per patient were created with a pre- and two post-SOH plans planned for both IMRT and VMAT. Each post-SOH plan applied a different optimization structure, either the rectal wall or composite rectum wall. Rectal dose sparing greater than 25% was achieved in most post-SOH treatment plans generated in this planning study. The use of SOH significantly reduced rectal dose regardless of optimization structure or treatment technique employed. The rectal wall optimization structure offered a statistically significant reduction in rectal dose compared to the CRW. There was no difference in rectal dose when using VMAT and IMRT treatment techniques, but VMAT offered lower bladder dose, mean penile bulb dose and gradient measure. BC Cancer - Victoria now treats all patients receiving SOH are treated with VMAT using RW as an optimization structure.

Rectal dose reduction prediction models were produced using twenty-one anonymized CT scans using linear regression modelling methods. Change in high dose integral (ΔHDI), change in RV55 Gy (ΔRV55) and pre-SOH RV55 Gy (Pre-RV55) were used as dependent metrics for linear modeling. Two models were produced per dependent metric. Model 1 included RadOnc R package and Eclipse metrics while Model 2 used only metrics available in Eclipse TPS. All models reached statistical significance

with ΔRV55 and Pre-RV55 models offering an R^2 greater than 0.80 and mean absolute error between 9.6-16.3%. Rectum in PTV, CTV and rectal wall volumes offered highest correlation with RV55 Gy metrics. Distance between rectal wall and CTV contours offered high Pearson correlation but was not included in Eclipse based only models (ie., Model 2). Several tools were produced to aid in clinical decision making including nomograms for simple Eclipse models and a flowchart indicating decision making process. Applying a lower limit of 3.5% on the Pre-RV55 removed a third of patients (7/21). A test data set to examine the validity of linear models produced would provide further confirmation of clinical application.

These studies have provided guidelines and best practices for application of SOH in a clinical setting with VMAT treatment using rectal wall optimization structure already implemented in BC Cancer - Victoria. Clinical protocols have been developed with more stringent constraints based on this work to maximize rectal sparing. Addition of *a priori* predictive models for rectal dose reduction will aid in ensuring effectiveness of SOH implant in patients. Identifying these patients early will aid in SOH resource management, as such applying these models to diagnostic CT scans would improve the workflow. Further development of models and clinical methods will allow for more effective decision making. Overall, SOH implant reduced rectal dose in 20/21 patients by 25% or more. Finally, many factors have been identified that are able to effectively predict this reduction in rectal dose.

Chapter 6

Appendix

RadOnc package in R was applied for modelling of rectal dose with pre-SOH CT metrics.[82] Documentation has been created by Thompson* to help walk through RadOnc package.[89] The code below is a simplified version of this documentation offering help with simple commands in R. This code was used to extract metrics such as volume, distance between contours and dose metrics. R v3.5.3 was used to determine linear models predicting rectal dose reduction with application of SOH. Sample code for both of these methods has been displayed here.

6.1 Importing DICOM.RT

Importing DICOM.RT into R using RadOnc package allows to extract metrics easily along with a third party software to examine contours without requiring Eclipse. The DICOM.RT files are quite large but may be viewed one at a time in a convenient manner. These can be exported by going to the treatment plan of interest, selecting File → Export → Wizard. The treatment plan or images may be exported. When exporting the entire treatment plan, be sure to select "Include structure set", "Include image slices of 3D volume", "Include reference images", "Generate structure outlines", and "Total plan dose". The dose can be exported in either relative or absolute dose. Finally, select a location by selecting "Change for all objects" to save the file to the location of interest. A new folder can now be created for the DICOM files. These files may now be used in conjunction with the RadOnc R package.

*https://mran.microsoft.com/snapshot/2015-01-16/web/packages/RadOnc/vignettes/RadOnc.pdf

 # Import DICOM.RT image set. Can use this to access 3D CT contours.

dir <- "FILE_DIRECTORY_NAME"

SOH <- read.DICOM.RT(path=paste(dir, "DICOM.RT_FOLDER_NAME", sep=""), verbose=TRUE, modality="CT")

 # Access the structures within DICOM.RT structure set.

soh <- SOH$structures

 # Produce a 3D contour plot as seen in Figure 6.1. This sample code was used to produce a pre-SOH contour plot for patient vi_SPACEOAR_1, and subsequently has a specific file name attached to each organ.

plot(soh[c("rectum pregelct_29sep17", "ctva(i?)", "bladder pregelct_29sep17", "penilebulb(i?)")], col=c("brown","blue","green","purple"))

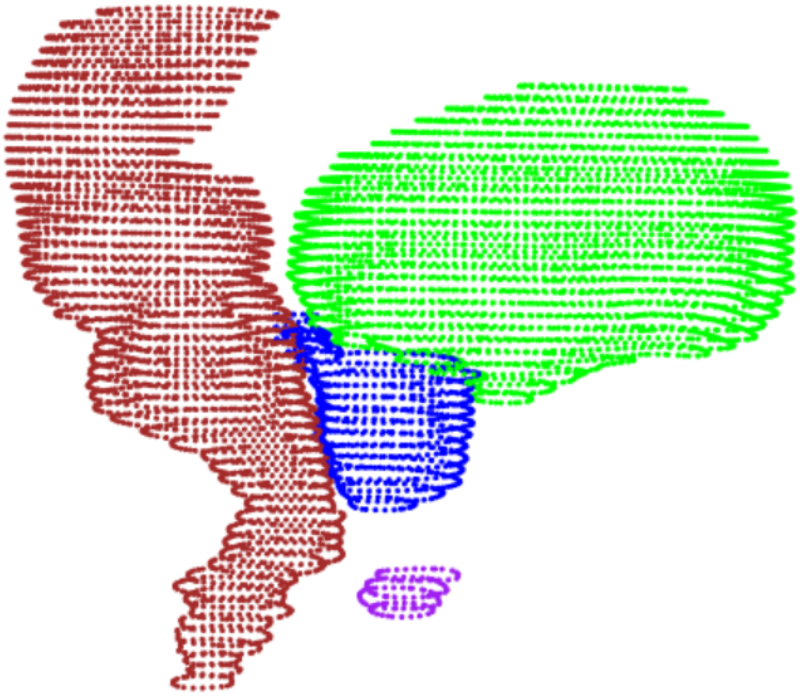

Figure 6.1: A 3D contour plot produced in R using RadOnc package and commands given above. Brown represents rectum, blue represents CTV, green represents bladder and purple represents penile bulb structures. This is a useful tool to visualize OAR in a third party software aside from Eclipse.

 # Pull out range metrics from structures.

r <- range(soh[paste("rectum ",pref,"(i?)", sep="")])

Rx <- r["max","x"] - r["min","x"]

Ry <- r["max","y"] - r["min","y"]

Rz <- r["max","z"] - r["min","z"]

 # Perform Hausdorff distance computation between Rectum, CTV and PTV structures. Note that adding "(i?)" completes string name in R, may gather structures starting with similar names.

d <- compareStructures(soh[c("rwallvicc(i?), "ptva(i?)", "ctva(i?)")], method="hausdorff", hausdorff.method="mean")

rownames(d) <- c("Rectum","PTV","CTV")

colnames(d) <- c("Rectum","PTV","CTV")

patientData$RtoPTV[num] <- d["Rectum","PTV"]

patientData$RtoCTV[num] <- d["Rectum","CTV"]

6.2 Importing DVH

Dose volume histogram (DVH) files may be exported from eclipse as .txt files and subsequently imported to R for analysis. This was done by right clicking on DVH plots in Eclipse and selecting "Export DVH in Tabular Format". This exports currently displayed structures in DVH plot, which can be displayed with relative or absolute dose and volumes. To export all structures, ensure that all structures are displayed in DVH plot of Eclipse prior to saving text file by selecting all the structures of interest under the "Dose Statistics" tab.

 # Import cumulative DVH extracted from Eclipse treatment plan.

dvh <- read.DVH(file = "INSERT_FILE_ NAME_HERE.txt"), type="aria10", verbose=TRUE)

 # Extract volume information from contours of interest. Command "as.numeric" converts from string to double. In this case, "num" is the patient number.

patientData$Rvol[num] <- as.numeric(dvh["Rectum"]$"Volume")

patientData$PTVvol[num] <- as.numeric(dvh["CTVa(i?)"]$"Volume")

patientData$Rinvol[num] <- as.numeric(dvh["RinPTV(i?)"]$"Volume")

 # Extract DVH metrics from imported DVH. This can be done through volume or dose metrics. Volume metrics can be placed in relative or absolute dose while dose metrics are relative and return a relative prescription.

```
patientData$PI_RV37[num] <- dvh["Rectum"]$"V37Gy"
patientData$PI_RV46[num] <- dvh["Rectum"]$"V46Gy"
patientData$PI_RV50[num] <- dvh["Rectum"]$"V50Gy"
patientData$PI_RV55[num] <- dvh["Rectum"]$"V55Gy"
patientData$PI_RV60[num] <- dvh["Rectum"]$"V60Gy"

dvh["Rectum"]$"D50%"
dvh["Rectum"]$"V4600cGy"
dvh["Rectum"]$"V91.66%"
```

6.3 Linear Modelling

This section reviews simple linear modelling along with how to apply Pearson correlation, AIC and VIF tests to examine validity of modelling. Additionally, a script has been included to perfrom normality tests such as qq plots and residuals to determine if fit meets required assumptions.

 # Change in HDI models were produced using linear regression modelling. Pearson correlations, Aikake information criterion (AIC) and variation inflation factor (VIF) were used to determine best models. Data was stored in H:/ drive excel file at BC Cancer - Victoria and can be imported using csv file.

```
# Read in CSV file of data frame.
pd <- read.table("INSERT_FILE_NAME_HERE", header=TRUE)

# Call necessary statistical packages.
library(Hmisc)

# Examine Pearson correlation to see which independent variables offer significant correlation.
pearsCor <- rcor(pd, type="pearson")
```

```
# Produce a linear fit predicting initial variable using independent metrics.
fit <- lm(Pl.6_Rku ~ Rinvol + CTVvol, data=pd)

# Evaluate VIF, AIC and summary of fit to examine if statistically significant.
vif(fit)
AIC(fit)
sum <- summary(fit)

# Apply AIC to step through fits and determine optimal independent variables for fit. This fit call includes all variables in given data frame.
fit <- lm(Pl.6_Rku ~ . , data=pd)
step <- stepAIC(fit)

# Linear models were tested for normality of distribution along with plotting fitted against actual data. This includes a residuals vs fitted plot, normality of the residuals, a QQ plot, and fitted vs actual plots. Additionally, this script pulls out the fitted R-squared value and prints it on the plot. Additionally, the following script prints out information from LOOCV, fit summary, and VIF.
library(car)
library(MASS)
library(ggplot2)
library(broom)
library(caret)

par(mfrow=c(2,2))

ft = fit
sum = summary(ft)

#Measuring fit using LOOCV methods. This will return MAE evaluating fit.
tr<-train(eval(sum$call[[2]]), data=pd, trControl=trainControl(method="LOOCV"))

#Write fit summary and vif to csv file.
write.csv(tidy(fit),"fit.csv")
write.csv(tr$results,"loocv.csv")
```

```
    #Multicolinearity check:
    if (grepl(toString(sum$call[[2]]),"+") == TRUE){
        #Compare if there is any multicolinearity between variables.
        vif = vif(ft)
        write.csv(vif,"vif.csv")
    }

    #Plot Residuals vs Fitted:
    plot(fitted(ft),residuals(ft), main = "Residuals vs Fitted", ylab = "Residuals" ,
xlab = "Fitted")
    abline(0,0,lty = "dashed",col="red")

    #Normality of Residuals:
    #Examining the residuals, ensuring that the plot is normally distributed.
    sresid <- studres(ft)
    hist(sresid, freq=FALSE, main = "Dist. of Studentized Residuals")
    xfit <- seq(min(sresid),max(sresid),length=40)
    yfit <- dnorm(xfit)
    lines(xfit,yfit, col = "blue")

    #Continue with normality by looking at the qq plot.
    #Looking for a linear trend in this section.
    qqPlot(ft, main = "QQ Plot")

    #Fitted vs Actual plot:
    plot(pd$Response, fitted(ft), col = "blue", pch = 16, cex = 0.7, main = "Reduc-
tion of Eff. Vol.", ylab = "Predicted", xlab = "Measure")
    testfit = lm(pd$Response   fitted(ft))
    abline(tidy(testfit)[[1,2]],tidy(testfit)[[2,2]])

    text(0.8*max(pd$Response), 1.4*min(fitted(ft)),paste("R-sq.=",
round(eval(summary(testfit)[[8]]), digits = 4),sep=""))
```

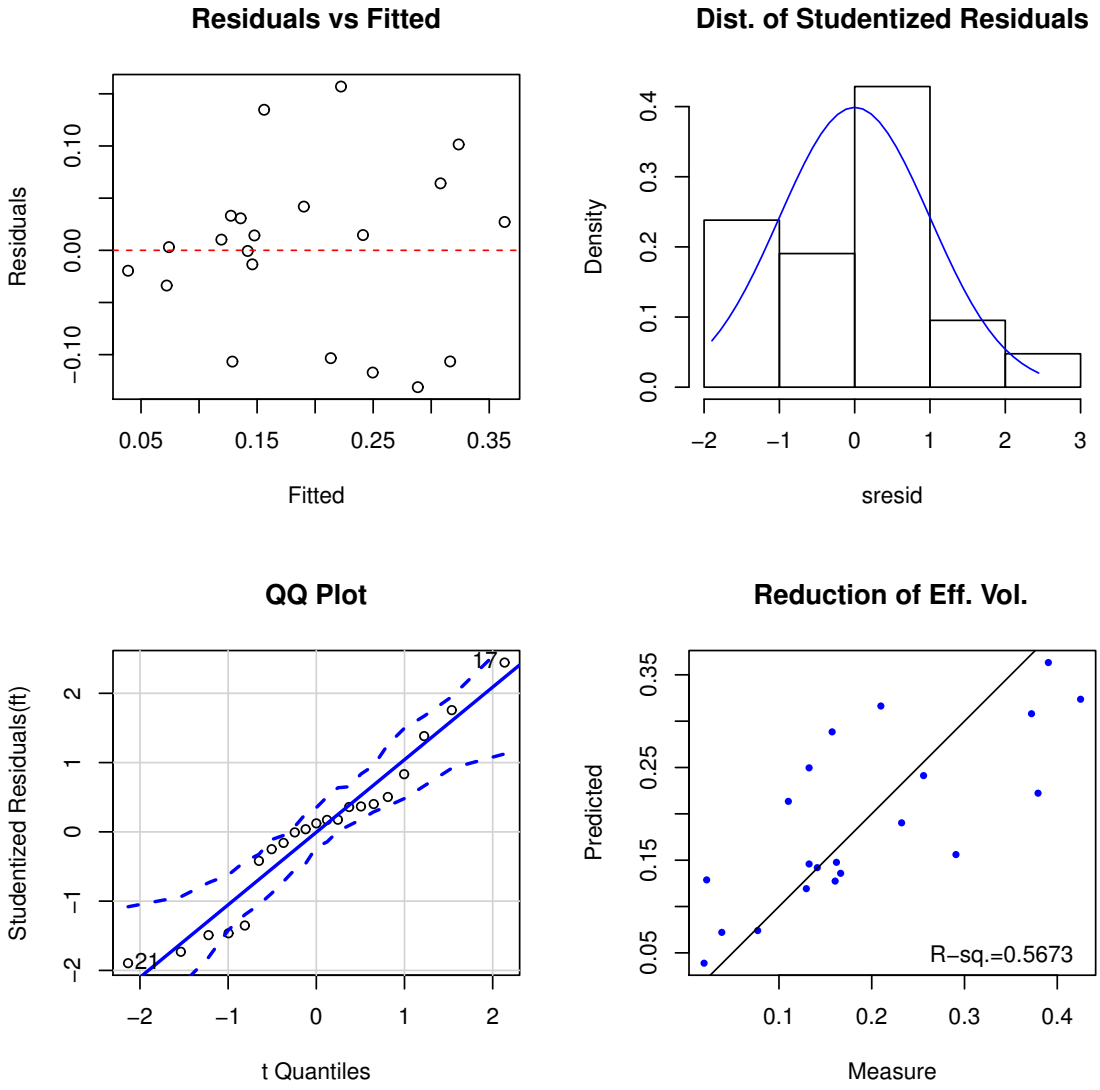

Figure 6.2: Sample of script used to evaluate model normality and fit as seen in Appendix 6.3. Evaluating fit of change in HDI Model 2 described in Chapter 4.

Bibliography

[1] Smith, L.; Bryan, S.; De, P.; Rahal, R.; Shaw, A.; Turner, D.; Manitoba, C.; Hannah Weir, M. K.; Woods, R.; Dixon, M. *Members of the Canadian Cancer Statistics Advisory Committee Project management*; 2018.

[2] Baskar, R.; Lee, K. A.; Yeo, R.; Yeoh, K. W. Cancer and radiation therapy: Current advances and future directions. 2012; http://www.ncbi.nlm.nih.gov/pubmed/22408567 http://www.pubmedcentral.nih.gov/articlerender.fcgi?artid=PMC3298009.

[3] Luo, C.; Yang, C.; Narayan, S.; Stern, R.; of . . . , J. P. I. J.; 2006, U. Use of benchmark doseâvolume histograms for selection of the optimal technique between three-dimensional conformal radiation therapy and intensity-modulated. *Int. J. Radiation Oncology Biol. Phys* **2006**, *66*, 1253–1262, DOI: 10.1016/j.ijrobp.2006.06.010.

[4] Wolff, D.; Stieler, F.; Welzel, G.; Lorenz, F.; Abo-Madyan, Y.; Mai, S.; Herskind, C.; Polednik, M.; Steil, V.; Wenz, F.; Lohr, F. Volumetric modulated arc therapy (VMAT) vs. serial tomotherapy, step-and-shoot IMRT and 3D-conformal RT for treatment of prostate cancer. *Radiotherapy and Oncology* **2009**, *93*, 226–233, DOI: 10.1016/j.radonc.2009.08.011.

[5] Gianfaldoni, S.; Gianfaldoni, R.; Wollina, U.; Lotti, J.; Tchernev, G.; Lotti, T. An Overview on Radiotherapy: From Its History to Its Current Applications in Dermatology. *Open Access Macedonian Journal of Medical Sciences* **2017**, *5*, 521, DOI: 10.3889/oamjms.2017.122.

[6] Joiner, M.; van der Kogel, A. *Basic Clinical Radiobiology*, fourth edi ed.; Hodder Arnold, 2009; DOI: 10.1783/147118901101195272.

[7] Brenner, D. Fractionation and late rectal toxicity. *Int. J. Radiation Oncology Biol. Phys* **2004**, *60*, 1013–1015, DOI: 10.1016/j.ijrobp.2004.04.014.

[8] Dearnaley, D. et al. Conventional versus hypofractionated high-dose intensity-modulated radiotherapy for prostate cancer: 5-year outcomes of the randomised, non-inferiority, phase 3 CHHiP trial. *The Lancet Oncology* **2016**, *17*, 1047–1060, DOI: 10.1016/S1470-2045(16)30102-4.

[9] Catton, C. N. et al. Randomized Trial of a Hypofractionated Radiation Regimen for the Treatment of Localized Prostate Cancer. *Journal of Clinical Oncology* **2017**, *35*, 1884–1890, DOI: 10.1200/JCO.2016.71.7397.

[10] GALVIN, J. Implementing IMRT in clinical practice: a joint document of the American Society for Therapeutic Radiology and Oncology and the American Association of Physicists in Medicine. *International Journal of Radiation Oncology*Biology*Physics* **2004**, *58*, 1616–1634, DOI: 10.1016/s0360-3016(03)02431-3.

[11] Otto, K. Volumetric modulated arc therapy: IMRT in a single gantry arc. *Medical physics* **2008**, *35*, 310–7, DOI: 10.1118/1.2818738.

[12] Quan, E. M.; Li, X.; Li, Y.; Wang, X.; Kudchadker, R. J.; Johnson, J. L.; Kuban, D. A.; Lee, A. K.; Zhang, X. A comprehensive comparison of IMRT and VMAT plan quality for prostate cancer treatment. *International Journal of Radiation Oncology Biology Physics* **2012**, *83*, 1169–1178, DOI: 10.1016/j.ijrobp.2011.09.015.

[13] Verellen, D.; Ridder, M. D.; Linthout, N.; Tournel, K.; Soete, G.; Storme, G. Innovations in image-guided radiotherapy. *Nature Reviews Cancer* **2007**, *7*, 949–960, DOI: 10.1038/nrc2288.

[14] Lawrence, E. O.; Livingston, M. S. The production of high speed light ions without the use of high voltages. *Physical Review* **1932**, *40*, 19–35, DOI: 10.1103/PhysRev.40.19.

[15] Bentzen, S. M.; Constine, L. S.; Deasy, J. O.; Eisbruch, A.; Jackson, A.; Marks, L. B.; Ten Haken, R. K.; Yorke, E. D. Quantitative Analyses of Normal Tissue Effects in the Clinic (QUANTEC): an introduction to the scientific

issues. *International journal of radiation oncology, biology, physics* **2010**, *76*, S3–9, DOI: 10.1016/j.ijrobp.2009.09.040.

[16] D'Amico, A. V.; Whittington, R.; Malkowicz, S. B.; Schultz, D.; Blank, K.; Broderick, G. A.; Tomaszewski, J. E.; Renshaw, A. A.; Kaplan, I.; Beard, C. J.; Wein, A. Biochemical Outcome After Radical Prostatectomy, External Beam Radiation Therapy, or Interstitial Radiation Therapy for Clinically Localized Prostate Cancer. *JAMA* **1998**, *280*, 969, DOI: 10.1001/jama.280.11.969.

[17] Zelefsky, M. J.; Levin, E. J.; Hunt, M.; Yamada, Y.; Shippy, A. M.; Jackson, A.; Amols, H. I. Incidence of late rectal and urinary toxicities after three-dimensional conformal radiotherapy and intensity-modulated radiothaerapy for localized prostate cancer. *Int. J. Radiation Oncology Biol. Phys* **2008**, *70*, 1124–1129, DOI: 10.1016/j.ijrobp.2007.11.044.

[18] Roach, M.; Nam, J.; Gagliardi, G.; El Naqa, I.; Deasy, J. O.; Marks, L. B. Radiation dose-volume effects and the penile bulb. *Int. J. Radiation Oncology Biol. Phys* **2010**, *76*, S130–S134, DOI: 10.1016/j.ijrobp.2009.04.094.

[19] Donovan, J. L. et al. Patient-Reported Outcomes after Monitoring, Surgery, or Radiotherapy for Prostate Cancer. *New England Journal of Medicine* **2016**, *375*, 1425–1437, DOI: 10.1056/NEJMoa1606221.

[20] Huang, E. H.; Pollack, A.; Levy, L.; Starkschall, G.; Dong, L.; Rosen, I.; Kuban, D. A. Late rectal toxicity: dose-volume effects of conformal radiotherapy for prostate cancer. *Int. J. Radiation Oncology Biol. Phys* **2002**, *54*, 1314–1321, DOI: 10.1016/S0360-3016(02)03742-2.

[21] Michalski, J. M.; Gay, H.; Jackson, A.; Tucker, S. L.; Deasy, J. O. Radiation Dose-Volume Effects in Radiation-Induced Rectal Injury. *International Journal of Radiation Oncology Biology Physics* **2010**, *76*, S123–S129, DOI: 10.1016/j.ijrobp.2009.03.078.

[22] Mok, G.; Benz, E.; Vallee, J.-P.; Miralbell, R.; Zilli, T. Optimization of Radiation Therapy Techniques for Prostate Cancer With Prostate-Rectum Spacers: A Systematic Review. *Int. J. Radiation Oncology Biol. Phys* **2014**, *90*, 278–288, DOI: 10.1016/J.IJROBP.2014.06.044.

[23] Ng, M.; Brown, E.; Williams, A.; Chao, M.; Lawrentschuk, N.; Chee, R. Fiducial markers and spacers in prostate radiotherapy: Current applications. *BJU International* **2014**, *113*, 13–20, DOI: 10.1111/bju.12624.

[24] Dubouloz, A.; Rouzaud, M.; Tsvang, L.; Verbakel, W.; Björkqvist, M.; Linthout, N.; Lencart, J.; Pérez-Moreno, J. M.; Ozen, Z.; Escude, L.; Zilli, T.; Miralbell, R. Urethra-sparing stereotactic body radiotherapy for prostate cancer: how much can the rectal wall dose be reduced with or without an endorectal balloon? *Radiation Oncology* **2018**, *13*, 114, DOI: 10.1186/s13014-018-1059-1.

[25] Susil, R. C.; McNutt, T. R.; DeWeese, T. L.; Song, D. Effects of prostate-rectum separation on rectal dose from external beam radiotherapy. *International journal of radiation oncology, biology, physics* **2010**, *76*, 1251–8, DOI: 10.1016/j.ijrobp.2009.07.1679.

[26] Wolf, F.; Gaisberger, C.; Ziegler, I.; Krenn, E.; Scherer, P.; Hruby, S.; Schätz, T.; Forstner, R.; Holzinger, J.; Vaszi, A.; Kametriser, G.; Steininger, P.; Deutschmann, H.; Sedlmayer, F. Comparison of two different rectal spacers in prostate cancer external beam radiotherapy in terms of rectal sparing and volume consistency. *Radiotherapy and Oncology* **2015**, *116*, 221–225, DOI: 10.1016/j.radonc.2015.07.027.

[27] Inc., A. SpaceOAR Hydrogel. 2019; https://www.spaceoar.com/what-is-spaceoar-hydrogel/how-does-spaceoar-hydrogel-work/, [Online; accessed June 12, 2019].

[28] Montoya, J.; Gross, E.; Karsh, L. *How I Do It: Hydrogel spacer placement in men scheduled to undergo prostate radiotherapy*; 2018; Vol. 25.

[29] Berlin, A.; Di Tomasso, A.; Ballantyne, H.; Patterson, S.; Lam, T.; Sundaramurthy, A.; Helou, J.; Bayley, A.; Chung, P.; Chung, P. Use of hydrogel spacer for improved rectal dose-sparing in patients undergoing radical radiotherapy for localized prostate cancer: First Canadian experience. *Canadian Urological Association Journal* **2017**, *11*, 373–5, DOI: 10.5489/cuaj.4681.

[30] Hamstra, D. A. et al. Continued Benefit to Rectal Separation for Prostate Radiation Therapy: Final Results of a Phase III Trial. *Int. J. Radiation Oncology Biol. Phys* **2017**, *97*, 976–985, DOI: 10.1016/J.IJROBP.2016.12.024.

[31] Hamstra, D. A. et al. Sexual quality of life following prostate intensity modulated radiation therapy (IMRT) with a rectal/prostate spacer: Secondary analysis of a phase 3 trial. *Practical Radiation Oncology* **2018**, *8*, 7–15, DOI: 10.1016/j.prro.2017.07.008.

[32] Mariados, N. et al. Hydrogel Spacer Prospective Multicenter Randomized Controlled Pivotal Trial: Dosimetric and Clinical Effects of Perirectal Spacer Application in Men Undergoing Prostate Image Guided Intensity Modulated Radiation Therapy. *Int. J. Radiation Oncology Biol. Phys* **2015**, *92*, 971–977, DOI: 10.1016/J.IJROBP.2015.04.030.

[33] Song, D.; Herfarth, K.; Uhl, M.; of ..., M. E. I. J.; 2013, U. A multi-institutional clinical trial of rectal dose reduction via injected polyethyleneglycol hydrogel during intensity modulated radiation therapy for prostate cancer. *Int. J. Radiation Oncology Biol. Phys* **2013**, *87*, 81–87, DOI: 10.1016/j.ijrobp.2012.12.019.

[34] Pinkawa, M.; Berneking, V.; König, L.; Frank, D.; Bretgeld, M.; Eble, M. J.; Michael Pinkawa MPinkawa, M. Hydrogel injection reduces rectal toxicity after radiotherapy for localized prostate cancer. *Strahlentherapie und Onkologie* **2017**, *193*, 22–28, DOI: 10.1007/s00066-016-1040-6.

[35] Uhl, M.; Herfarth, K.; Eble, M. J.; Pinkawa, M.; van Triest, B.; Kalisvaart, R.; Weber, D. C.; Miralbell, R.; Song, D. Y.; DeWeese, T. L. Absorbable hydrogel spacer use in men undergoing prostate cancer radiotherapy: 12 month toxicity and proctoscopy results of a prospective multicenter phase II trial. *Radiation Oncology* **2014**, *9*, 96, DOI: 10.1186/1748-717X-9-96.

[36] Whalley, D.; Hruby, G.; Alfieri, F.; Kneebone, A.; Eade, T. SpaceOAR Hydrogel in Dose-escalated Prostate Cancer Radiotherapy: Rectal Dosimetry and Late Toxicity. *Clinical Oncology* **2016**, *28*, 148–154, DOI: 10.1016/j.clon.2016.05.005.

[37] Heikkila, V.-P.; Phil, L. PEG spacer gel and adaptive planning vs single plan in external prostate radiotherapy-clinical dosimetry evaluation. *British Hournal of Radiology* **2015**, *88*, DOI: 10.1259/bjr.20150421.

[38] Van Gysen, K.; Kneebone, A.; Alfieri, F.; Guo, L.; Eade, T. Feasibility of and rectal dosimetry improvement with the use of SpaceOAR® hydrogel for dose-escalated prostate cancer radiotherapy. *Radiation Oncology* **2014**, *58*, 511–516, DOI: 10.1111/1754-9485.12152.

[39] te Velde, B. L.; Westhuyzen, J.; Awad, N.; Wood, M.; Shakespeare, T. P. Can a peri-rectal hydrogel spaceOAR programme for prostate cancer intensity-modulated radiotherapy be successfully implemented in a regional setting? *Journal of Medical Imaging and Radiation Oncology* **2017**, *61*, 528–533, DOI: 10.1111/1754-9485.12580.

[40] Rajecki, M.; Thurber, A.; Catalfamo, F.; Duff, M.; Shah, D. SU-E-T-284: Dose Plan Optimization When Using Hydrogel Prostate-Rectum Spacer: A Single Institution Experience. *Medical Physics* **2015**, *42*, 3398–3398, DOI: 10.1118/1.4924646.

[41] Salvat, F.; Fernández-Varea, J. M. Overview of physical interaction models for photon and electron transport used in Monte Carlo codes. *Metrologia* **2009**, *46*, S112–S138, DOI: 10.1088/0026-1394/46/2/S08.

[42] Podgorsak, E. *Radiation Physics for Medical Physicists*; Springer, Cham, 2018; pp 165–187, DOI: 10.1007/978-3-319-25382-4_6␣229.

[43] Nikjoo, H.; Uehara, S.; Emfietzoglou, D. *Alpha-, Beta- and Gamma-ray Spectroscopy: Volume 1. Edited by Kai Siegbahn. Published by North-Holland Publishing Company, Amsterdam, 1965, p.37*; CRC Press, 2012.

[44] Bushberg, J. T.; Seibert, J. A.; Leidholdt, A. M.; Boone, J. M. *The Essential Physics of Medical Imaging*; Lippincott Williams & Wilkins, 2011.

[45] Paetkau, O.; Parsons, Z.; Paetkau, M. Computerized tomography platform using beta rays. *American Journal of Physics* **2017**, *85*, 896–900, DOI: 10.1119/1.5008267.

[46] Nissman, D. B.; Dale, B. M. *Text-Atlas of Skeletal Age Determination*; 2013; pp 149–154, DOI: 10.1002/9781118692202.ch17.

[47] Ho, H. et al. A Prospective Analysis of Hydrogel Rectal Spacing and Rectal Toxicity in the Treatment of Prostate Cancer SpaceOAR The Use of TraceIT ®

as a Fiducial Marker in Bladder Radiotherapy. *Journal of Medical Imaging and Radiation Oncology* **2015**, *87*, 3–4.

[48] Chao, M.; Lim Joon, D.; Khoo, V.; Lawrentschuk, N. The use of hydrogel spacer in men undergoing high-dose prostate cancer radiotherapy: results of a prospective phase 2 clinical trial. *World Journal of Urology* **2018**, DOI: 10.1007/s00345-018-2502-5.

[49] Pinkawa, M.; Escobar Corral, N.; Caffaro, M.; Piroth, M. D.; Holy, R.; Djukic, V.; Otto, G.; Schoth, F.; Eble, M. J. Application of a spacer gel to optimize three-dimensional conformal and intensity modulated radiotherapy for prostate cancer. *Radiotherapy and Oncology* **2011**, *100*, 436–441, DOI: 10.1016/j.radonc.2011.09.005.

[50] Augmenix Inc, *De Novo Classification Request for SpaceOAR System*; 2014; pp 1–10.

[51] Mihai Grumezescu, A. *Elsevier*; 2017; p 372.

[52] Augmenix Inc, *SpaceOAR® System Product Code SO-2101 INSTRUCTIONS FOR USE*; pp 1–2.

[53] of Chicago Medicine, U. Overview of the Male Anatomy. 2018; http://healthlibrary.uchospitals.edu/content/adult-diseases-and-conditions-v0/overview-of-the-male-anatomy/.

[54] Vargas, C.; Martinez, A.; Kestin, L. L.; Yan, D. I.; Grills, I.; Brabbins, D. S.; Lockman, D. M.; Liang, J.; Gustafson, G. S.; Chen, P. Y.; Vicini, F. A.; Wong, J. W. Dose-volume analysis of predictors for chronic rectal toxicity after treatment of prostate cancer with adaptive image-guided radiotherapy. *Int. J. Radiation Oncology Biol. Phys* **2005**, *62*, 1297–1308, DOI: 10.1016/j.ijrobp.2004.12.052.

[55] Jackson, A.; Skwarchuk, M. W.; Zelefsky, M. J.; Cowen, D. M.; Venkatraman, E. S.; Levegrun, S.; Burman, C. M.; Kutcher, G. J.; Fuks, Z.; Liebel, S. A.; Ling, C. C. Late rectal bleeding after conformal radiotherapy of prostate cancer (II): volume effects and dose-volume histograms. *International Journal of Radiation Oncology Biology Physics* **2001**, *49*, 685–698, DOI: 10.1016/S0360-3016(00)01414-0.

[56] Fiorino, C.; Valdagni, R.; Rancati, T.; Sanguineti, G. Dose-volume effects for normal tissues in external radiotherapy: Pelvis. *Radiotherapy and Oncology* **2009**, *93*, 153–167, DOI: 10.1016/j.radonc.2009.08.004.

[57] Emami, B. Tolerance of Normal Tissue to Therapeutic Radiation. *Reports of Radiotherapy & Oncology* **2013**, *1*, 35–48, DOI: 10.1118/1.4736403.

[58] Viswanathan, A. N.; Yorke, E. D.; Marks, L. B.; Eifel, P. J.; Shipley, W. U. Radiation Dose-Volume Effects of the Urinary Bladder. *International Journal of Radiation Oncology Biology Physics* **2010**, *76*, S116–S122, DOI: 10.1016/j.ijrobp.2009.02.090.

[59] Zelefsky, M. J.; Aschkenasy, E.; Kelsen, S.; Leibel, S. A. Tolerance and early outcome results of postprostatectomy three-dimensional conformal radiotherapy. *Int. J. Radiation Oncology Biol. Phys* **1997**, *39*, 327–333, DOI: 10.1016/S0360-3016(97)00056-4.

[60] Fisch, B. M.; Pickett, B.; Weinberg, V.; Roach, M. Dose of radiation received by the bulb of the penis correlates with risk of impotence after three-dimensional conformal radiotherapy for prostate cancer. *Urology* **2001**, *57*, 955–959, DOI: 10.1016/S0090-4295(01)00940-2.

[61] Brown, M. W.; Brooks, J. P.; Albert, P. S.; Poggi, M. M. An analysis of erectile function after intensity modulated radiation therapy for localized prostate carcinoma. *Prostate Cancer and Prostatic Diseases* **2007**, *10*, 189–193, DOI: 10.1038/sj.pcan.4500938.

[62] Mangar, S. A.; Sydes, M. R.; Tucker, H. L.; Coffey, J.; Sohaib, S. A.; Gianolini, S.; Webb, S.; Khoo, V. S.; Dearnaley, D. P. Evaluating the relationship between erectile dysfunction and dose received by the penile bulb: Using data from a randomised controlled trial of conformal radiotherapy in prostate cancer (MRC RT01, ISRCTN47772397). *Radiotherapy and Oncology* **2006**, *80*, 355–362, DOI: 10.1016/j.radonc.2006.07.037.

[63] Roach, M.; Winter, K.; Michalski, J. M.; Cox, J. D.; Purdy, J. A.; Bosch, W.; Lin, X.; Shipley, W. S. Penile bulb dose and impotence after three-dimensional conformal radiotherapy for prostate cancer on RTOG 9406: Findings from a prospective, multi-institutional, phase I/II dose-escalation study. *International*

Journal of Radiation Oncology Biology Physics **2004**, *60*, 1351–1356, DOI: 10.1016/j.ijrobp.2004.05.026.

[64] Grigsby, P. W.; Roberts, H. L.; Perez, C. A. Femoral neck fracture following groin irradiation. *International Journal of Radiation Oncology, Biology, Physics* **1995**, *32*, 63–67, DOI: 10.1016/0360-3016(95)00546-B.

[65] Bedford, J. A.; Khoo, V. S.; Webb, S.; Dearnaley, D. P. Optimization of coplanar six-field techniques for conformal radiotherapy of the prostate. *Int. J. Radiation Oncology Biol. Phys* **2000**, *46*, 231–238.

[66] Ahuja, R. K.; Orlin, J. B. Inverse Optimization. *Operations Research* **2003**, *49*, 771–783, DOI: 10.1287/opre.49.5.771.10607.

[67] Eclipse Photon and Electron Algorithms Reference Guide. Varian Medical Systems: 3100 Hansen Way Palo Alto, CA 94304-1038 United States of America, 2015.

[68] Van Esch, A.; Tillikainen, L.; Pyykkonen, J.; Tenhunen, M.; Helminen, H.; Siljamäki, S.; Alakuijala, J.; Paiusco, M.; Iori, M.; Huyskens, D. P. Testing of the analytical anisotropic algorithm for photon dose calculation. *Medical Physics* **2006**, *33*, 4130–4148, DOI: 10.1118/1.2358333.

[69] Paetkau, O.; Gagne, I. M.; Pai, H. H.; Lam, J.; Goulart, J.; Alexander, A. Maximizing rectal dose sparing with hydrogel: A retrospective planning study. *Journal of Applied Clinical Medical Physics* **2019**, *20*, 91–98, DOI: 10.1002/acm2.12566.

[70] Pinkawa, M.; Klotz, J.; Djukic, V.; Schubert, C.; Escobar-Corral, N.; Caffaro, M.; Piroth, M. D.; Holy, R.; Eble, M. J. Learning Curve in the Application of a Hydrogel Spacer to Protect the Rectal Wall During Radiotherapy of Localized Prostate Cancer. *Urology* **2013**, *82*, 963–968, DOI: 10.1016/J.UROLOGY.2013.07.014.

[71] Padmanabhan, R.; Pinkawa, M.; Song, D. Y. Hydrogel spacers in prostate radiotherapy: a promising approach to decrease rectal toxicity. *Future Oncology* **2017**, *13*, 2697–2708, DOI: 10.2217/fon-2017-0073.

[72] Kopp, R. W.; Duff, M.; Catalfamo, F.; Shah, D.; Rajecki, M.; Ahmad, K. VMAT vs. 7-Field-IMRT: Assessing the dosimetric parameters of prostate cancer treatment with a 292-patient sample. *Medical Dosimetry* **2011**, *36*, 365–372, DOI: 10.1016/j.meddos.2010.09.004.

[73] Palma, D.; Vollans, E.; James, K.; Nakano, S.; Moiseenko, V.; Shaffer, R.; McKenzie, M.; Morris, J.; Otto, K. Volumetric Modulated Arc Therapy for Delivery of Prostate Radiotherapy: Comparison With Intensity-Modulated Radiotherapy and Three-Dimensional Conformal Radiotherapy. *International Journal of Radiation Oncology Biology Physics* **2008**, *72*, 996–1001, DOI: 10.1016/j.ijrobp.2008.02.047.

[74] Morgan, S. C. et al. Hypofractionated Radiation Therapy for Localized Prostate Cancer: Executive Summary of an ASTRO, ASCO, and AUA Evidence-Based Guideline. *Practical radiation oncology* **2018**, *0*, 1–7, DOI: 10.1016/j.prro.2018.08.002.

[75] Taussky, D.; Austen, L.; Toi, A.; Yeung, I.; Williams, T.; Pearson, S.; McLean, M.; Pond, G.; Crook, J. Sequential evaluation of prostate edema after permanent seed prostate brachytherapy using CT-MRI fusion. *Int. J. Radiation Oncology Biol. Phys* **2005**, *62*, 974–980, DOI: 10.1016/J.IJROBP.2004.12.012.

[76] van Wijk, Y.; Vanneste, B. G.; Walsh, S.; van der Meer, S.; Ramaekers, B.; van Elmpt, W.; Pinkawa, M.; Lambin, P. Development of a virtual spacer to support the decision for the placement of an implantable rectum spacer for prostate cancer radiotherapy: Comparison of dose, toxicity and cost-effectiveness. *Radiotherapy and Oncology* **2017**, *125*, 107–112, DOI: 10.1016/j.radonc.2017.07.026.

[77] Vanneste, B. G.; Hoffmann, A. L.; van Lin, E. N.; Van De Voorde, L.; Pinkawa, M.; Lambin, P. Who will benefit most from hydrogel rectum spacer implantation in prostate cancer radiotherapy? A model-based approach for patient selection. *Radiotherapy and Oncology* **2016**, *121*, 118–123, DOI: 10.1016/j.radonc.2016.08.026.

[78] Hutchinson, R. C.; Sundaram, V.; Folkert, M.; Lotan, Y. Decision analysis model evaluating the cost of a temporary hydrogel rectal spacer before prostate radiation therapy to reduce the incidence of rectal complications. *Uro-*

logic Oncology: Seminars and Original Investigations **2016**, *34*, 19–26, DOI: 10.1016/j.urolonc.2016.02.024.

[79] Vanneste, B. G.; Pijls-Johannesma, M.; Van De Voorde, L.; Van Lin, E. N.; Van De Beek, K.; Van Loon, J.; Ramaekers, B. L.; Lambin, P. Spacers in radiotherapy treatment of prostate cancer: Is reduction of toxicity cost-effective? *Radiotherapy and Oncology* **2015**, *114*, 276–281, DOI: 10.1016/j.radonc.2015.01.005.

[80] Wang, Y.; Zolnay, A.; Incrocci, L.; Joosten, H.; McNutt, T.; Heijmen, B.; Petit, S. A quality control model that uses PTV-rectal distances to predict the lowest achievable rectum dose, improves IMRT planning for patients with prostate cancer. *Radiotherapy and Oncology* **2013**, *107*, 352–357, DOI: 10.1016/j.radonc.2013.05.032.

[81] Petit, S. F.; Wu, B.; Kazhdan, M.; Dekker, A.; Simari, P.; Kumar, R.; Taylor, R.; Herman, J. M.; McNutt, T. Increased organ sparing using shape-based treatment plan optimization for intensity modulated radiation therapy of pancreatic adenocarcinoma. *Radiotherapy and Oncology* **2012**, *102*, 38–44, DOI: 10.1016/j.radonc.2011.05.025.

[82] Thompson, R. F. RadOnc: An R Package for Analysis of Dose-Volume Histogram and Three-Dimensional Structural Data. *J Radiat Oncol Inform* **2014**, *6*, 98–110, DOI: 10.5166/jroi-6-1-25.

[83] Huttenlocher, D. P.; Klanderman, G. A.; Rucklidge, W. J. Comparing Images Using the Hausdorff Distance. *IEEE Transactions on Pattern Analysis and Machine Intelligence* **1993**, *15*, 850–863, DOI: https://doi.org/10.1109/34.232073.

[84] James, G.; Witten, D.; Hastie, T.; Tibshirani, R. *An Introduction to Statistical Learning with Applications in R*; 2013.

[85] Ziglari, L. Interpreting Multiple Regression Results: β Weights and Structure Coefficients. *General Linear Model Journal* **2018**, *43*, 13–22, DOI: 10.31523/glmj.043002.002.

[86] Zeitoune, G.; Nadal, J.; Batista, L. A.; Metsavaht, L.; Moraes, A. P.; Leporace, G. Prediction of mild anatomical leg length discrepancy based on gait kinematics and linear regression model. *Gait and Posture* **2019**, *67*, 117–121, DOI: 10.1016/j.gaitpost.2018.09.027.

[87] Hwang, M. E.; Black, P. J.; Elliston, C. D.; Wolthuis, B. A.; Smith, D. R.; Wu, C. C.; Wenske, S.; Deutsch, I. A novel model to correlate hydrogel spacer placement, perirectal space creation, and rectum dosimetry in prostate stereotactic body radiotherapy. *Radiation Oncology* **2018**, *13*, 192, DOI: 10.1186/s13014-018-1135-6.

[88] Pinkawa, M.; Klotz, J.; Djukic, V.; Schubert, C.; Escobar-Corral, N.; Caffaro, M.; Piroth, M. D.; Holy, R.; Eble, M. J. Learning curve in the application of a hydrogel spacer to protect the rectal wall during radiotherapy of localized prostate cancer. Urology. 2013; pp 963–968, DOI: 10.1016/j.urology.2013.07.014.

[89] Thompson, R. F. *Radiation Oncology (RadOnc) Tools*; 2014.